

Title:

**Results of GEANT simulations and comparison
with first experiments at DANCE**

Author(s):

R. Reifarth, T.A. Bredeweg, J.C. Browne, E.I. Esch,
U. Greife, R.C. Haight, J.M. O'Donnell,
A. Kronenberg, R.S. Rundberg, J.L. Ullmann,
D.J. Vieira, J.B. Wilhelmy, J.M. Wouters

Submitted to:

<http://lib-www.lanl.gov/cgi-bin/getfile?00852234.pdf>

Results of GEANT simulations and comparison with first experiments at DANCE

On how a not-quite 4π array works

R. Reifarth^a, T.A. Bredeweg^a, J.C. Browne^a, E.I. Esch^a, U. Greife^b, R.C. Haight^a,
J.M. O'Donnell^a, A. Kronenberg^a, R.S. Rundberg^a, J.L. Ullmann^a, D.J. Vieira^a,
J.B. Wilhelmy^a, J.M. Wouters^a

^a *Los Alamos National Laboratory, Los Alamos, New Mexico, 87545, USA*

^b *Colorado School of Mines, Golden, Colorado, 80401, USA*

Abstract: This report describes intensive Monte Carlo simulations carried out to be compared with the results of the first run cycle with DANCE (Detector for Advanced Neutron Capture Experiments). The experimental results were gained during the commissioning phase 2002/2003 with only a part of the array. Based on the results of these simulations the most important items to be improved before the next experiments will be addressed.

Table of Contents

Table of Contents.....	1
List of Figures.....	2
List of Tables	5
1 Introduction.....	6
2 Computational Approach	6
3 141 crystals & high threshold	8
3.1 Calibration sources.....	11
3.1.1 Source: ^{60}Co	12
3.1.2 Source: ^{22}Na	14
3.1.3 Source: ^{88}Y	16
3.2 Mono-energetic γ -rays	18
3.3 Au(n, γ)	21
3.3.1 Au cascades.....	21
3.3.2 Neutrons on Au.....	22
4 159 crystals & low threshold	27
4.1 Calibration sources.....	27
4.1.1 Source: ^{60}Co	28
4.1.2 Source: ^{22}Na	29
4.1.3 Source: ^{88}Y	32
4.2 Mono-energetic γ -rays	34
4.3 Au(n, γ)	39
4.3.1 Au cascades.....	39
4.3.2 Neutrons on Au.....	42
5 Neutron reactions with surrounding material	46
6 Conclusions.....	58
References.....	58

List of Figures

Figure 1: Views of the simulated setup: from left / right (relative to beam direction). Each color corresponds to a different crystal type (A – green, B – dark blue, C – yellow, D - red). The missing crystals allowing the beam pipe (light blue) to be seen were either not connected or not in place during the runs carried out during the commissioning phase 2002/2003. 9

Figure 2: Views of the simulated setup: from downstream / upstream (relative to beam direction). Each color corresponds to a different crystal type (A – green, B – dark blue, C – yellow, D - red). The missing crystals allowing the beam pipe (light blue) to be seen were either not connected or not in place during the runs carried out during the commissioning phase 2002/2003. 9

Figure 3: Detailed view of the beam pipe crossing for neutron beam and sample changer (light blue). Some of the BaF₂ crystals are shown too in order to see the relative size. Each color corresponds to a different crystal type (A – green, B – dark blue, C – yellow, D - red). 10

Figure 4: Decay scheme of ⁶⁰Co according to the Table of Isotopes [5]. 12

Figure 5: Experimental and simulated data for ⁶⁰Co, no ⁶LiH. 13

Figure 6: Experimental and simulated data for ⁶⁰Co, ⁶LiH. 13

Figure 7: Decay scheme of ²²Na according to the Table of Isotopes [5]. 14

Figure 8: Experimental and simulated data for ²²Na, no ⁶LiH absorber. 14

Figure 9: Experimental and simulated data for ²²Na, ⁶LiH absorber. 15

Figure 10: Decay scheme of ⁸⁸Y according to the Table of Isotopes [5]. 16

Figure 11: Experimental and simulated data for ⁸⁸Y, no ⁶LiH. 17

Figure 12: Experimental and simulated data for ⁸⁸Y, ⁶LiH. 17

Figure 13: Energy deposit summed over all crystals for γ -energies from 0.5 MeV to 10 MeV. Spectra with (red) and without (black) the ⁶LiH absorber for 141 crystals and high detector threshold are shown. 18

Figure 14: Percentage of counts above a given threshold energy for the spectra shown in Figure 13. Spectra with (red) and without (black) the ⁶LiH absorber for 141 crystals and high detector threshold are shown. The curves are normalized to the number of emitted γ -rays, which means, the value at E = 0 MeV reflects the total efficiency of the array. 19

Figure 15: Number of clusters for mono-energetic γ -rays of different energies with (red) and without (black) ⁶LiH- absorber. 10⁶ γ -rays have been simulated for each spectrum. 20

Figure 16: Left: Response of the DANCE array with 141 crystals and high single detector thresholds to theoretical gold capture cascades. Right: Percentage of counts above a given threshold energy for the spectra on the left. The curves are normalized to the number of emitted γ -cascades, which means, the value at E = 0 MeV reflects the total efficiency of the array. 22

Figure 17: Response of the DANCE array with 141 crystals and high detector threshold to neutron reactions on a gold sample. The red line corresponds to events due to captures on a gold sample, the black curve to events due to neutrons scattered at the gold sample. The neutron energy 10 ..100 keV. The left picture shows the results without ⁶LiH absorber, while the right picture corresponds to the standard ⁶LiH absorber in place. 23

Figure 18: Left: Number of clusters for capture-events (red) and for scattered events (black) for neutron energies between 0.1 and 1 keV. Right: Corresponding percentage of counts for at least a given number of clusters. 24

Figure 19: Left: Number of clusters for capture-events (red) and for scattered events (black) for neutron energies between 1 and 10 keV. Right: Corresponding percentage of counts for at least a given number of clusters. 24

Figure 20: Left: Number of clusters for capture-events (red) and for scattered events (black) for neutron energies between 10 and 100 keV. Right: Corresponding percentage of counts for at least a given number of clusters.....	25
Figure 21: Left: Number of clusters for capture-events (red) and for scattered events (black) for neutron energies between 0.1 and 1 keV. The y-axis is expanded in order to increase the visibility. Right: Same as left, but without y-axis expansion and logarithmic y-axes.....	25
Figure 22: Percentage of counts equals or above a given number of clusters for the spectra shown in Figure 21. The numbers are normalized to the total number of detected events, respectively.	26
Figure 23: Response of the DANCE array with 141 and 159 crystals as well as low and high single detector thresholds to decay cascades of ^{60}Co . Additionally a configuration with 162 crystals is included.....	28
Figure 24: Response of the DANCE array with 159 crystals and low single detector thresholds with and without ^6LiH to decay cascades of ^{60}Co	29
Figure 25: Response of the DANCE array with 141 and 159 crystals as well as low and high single detector thresholds to decay cascades of ^{22}Na . Additionally a configuration with 162 crystals is included.....	30
Figure 26: Response of the DANCE array with 159 crystals and low single detector thresholds with and without ^6LiH to decay cascades of ^{22}Na	31
Figure 27: Response of the DANCE array with 141 and 159 crystals as well as low and high single detector thresholds to decay cascades of ^{88}Y . Additionally a configuration with 162 crystals is included.....	32
Figure 28: Response of the DANCE array with 159 crystals and low single detector thresholds with and without ^6LiH to decay cascades of ^{88}Y	33
Figure 29: Energy deposit summed over all crystals for γ -energies from 0.5 MeV to 10 MeV. All spectra are without ^6LiH absorber. The different colors correspond to spectra with 159 crystals with low threshold (black), 159 crystals with high threshold (red) and 141 crystals with high threshold (blue).....	34
Figure 30: Percentage of counts above a given threshold energy for the spectra shown in Figure 29. The curves are normalized to the number of emitted γ -rays, which means, the value at $E = 0$ MeV reflects the total efficiency of the array.	35
Figure 31: Energy deposit summed over all crystals for γ -energies from 0.5 MeV to 10 MeV. Spectra with (red) and without (black) the ^6LiH absorber for 159 crystals and low detector threshold are shown.	36
Figure 32: Percentage of counts above a given threshold energy for the spectra shown in Figure 31. The curves are normalized to the number of emitted γ -rays, which means, the value at $E = 0$ MeV reflects the total efficiency of the array.	37
Figure 33: Number of clusters for mono-energetic g-rays of different energies with (red) and without (black) ^6LiH - absorber.	38
Figure 34: Left: Response of the DANCE array with 141 and 159 crystals as well as low and high single detector thresholds to theoretical gold capture cascades. Right: Percentage of counts above a given threshold energy for the spectra on the left. The curves are normalized to the number of emitted γ -cascades, which means, the value at $E = 0$ MeV reflects the total efficiency of the array.	39
Figure 35: Beam pipe cross (light blue) as well as supporting pieces (red) as simulated. The surrounding DANCE ball is not shown. The sample position is in the middle of the cross. Neutrons are traveling horizontally.	40
Figure 36: Left: Response of the DANCE array with 159 crystals and low single detector thresholds to theoretical gold capture cascades with and without additional supports for the beam pipe crossing. Right: Percentage of counts above a given threshold energy for the spectra on the left. The curves are normalized to the number of emitted γ -cascades, which means, the value at $E = 0$ MeV reflects the total efficiency of the array.....	40

Figure 37: Left: Response of the DANCE array with 159 and 162 crystals with and without beam pipe to theoretical gold capture cascades. Right: Percentage of counts above a given threshold energy for the spectra on the left. The curves are normalized to the number of emitted γ -cascades, which means, the value at $E = 0$ MeV reflects the total efficiency of the array.	41
Figure 38: Left: Response of the DANCE array with 159 crystals and low single detector thresholds to theoretical gold capture cascades. Right: Percentage of counts above a given threshold energy for the spectra on the left. The curves are normalized to the number of emitted γ -cascades, which means, the value at $E = 0$ MeV reflects the total efficiency of the array.	41
Figure 39: Response of the DANCE array with 159 crystals and low detector threshold to neutron reactions on a gold sample. The red line corresponds to events due to captures on a gold sample, the black curve to events due to neutrons scattered at the gold sample. The neutron energy 10 ..100 keV. The left picture shows the results without ^6LiH absorber, while the right picture corresponds to the standard ^6LiH absorber in place.	42
Figure 40: Left: Number of clusters for capture-events (red) and for scattered events (black) for neutron energies between 0.1 and 1 keV. Right: Corresponding percentage of counts for at least a given number of clusters.	43
Figure 41: Left: Number of clusters for capture-events (red) and for scattered events (black) for neutron energies between 1 and 10 keV. Right: Corresponding percentage of counts for at least a given number of clusters.	43
Figure 42: Left: Number of clusters for capture-events (red) and for scattered events (black) for neutron energies between 10 and 100 keV. Right: Corresponding percentage of counts for at least a given number of clusters.	44
Figure 43: Left: Number of clusters for capture-events (red) and for scattered events (black) for neutron energies between 0.1 and 1 keV. The y-axis is expanded in order to increase the visibility. Right: Same as left, but without y-axis expansion and logarithmic y-axes.	44
Figure 44: Percentage of counts equals or above a given number of clusters for the spectra shown in Figure 43. The numbers are normalized to the total number of detected events, respectively.	45
Figure 45: Schematic view of the simulated setup. The neutrons are coming from the left in both pictures. The left part shows a side view (side walls are not drawn) and the right part a view from the top. The light blue corresponds to 5% BPE walls, dark blue to the concrete floor and black to the lead shielding at the end of the beam pipe. The red rectangles mark the 3 different positions of the aluminum windows. The size of the windows is not to scale.	46
Figure 46: Background caused by 10^6 neutrons per energy interval, emitted 1 m downstream of the center of the crystal ball. The different peaks correspond to neutron captures on even, odd Ba isotopes, H, B (from right). The surrounding housing consists of 5% BPE.	47
Figure 47: Background caused by 10^6 neutrons per energy interval, emitted 1 m downstream of the center of the crystal ball. The different peaks correspond to neutron captures on even, odd Ba isotopes, H, B (from right). The surrounding housing consists of 30% BPE.	48
Figure 48: Comparison between a 3.18 mm (1/8 inch) aluminum window (blue) positioned 1 m upstream of the sample with neutron capture events (black) as well as neutron scatter events (red) on a 0.002 mm gold sample in the center of the crystal ball. $\text{Al}(n,x)$ means that all reactions which eventually deposit energy in the BaF_2 crystals are included. These reactions are mainly $\text{Al}(n,\gamma)$ and $\text{Al}(n,n)$	49
Figure 49: Comparison between 3.18 mm (1/8 inch) aluminum window (blue) positioned 1.5 m upstream of the sample with neutron capture events (black) as well as neutron scatter events (red) on a 0.002 mm gold sample in the center of the crystal ball.	50
Figure 50: Comparison between a 0.25 mm (10 mil) aluminum window (blue) positioned 1 m downstream of the sample with neutron capture events (black) as well as neutron scatter events (red) on a 0.002 mm gold sample in the center of the crystal ball.	51

Figure 51: Schematic view of the simulated setup. The neutrons are coming from the left in both pictures. The left part shows a side view (side walls are not drawn) and the right part a view from the top. The light blue corresponds to 5% BPE walls, dark blue to the concrete floor and black to the lead collimator at the end of the beam pipe. The red rectangles mark the 4 different positions of the aluminum windows. The size of the windows is not on scale for visibility reasons. 52

Figure 52: Background caused by 10^6 neutrons per energy interval, emitted 1 m downstream of the center of the crystal ball. The different peaks correspond to neutron captures on even, odd Ba isotopes, H, B (from right). The surrounding housing consists of 5% BPE. The ball is asymmetrically positioned inside the shed. 53

Figure 53: Comparison between a 3.18 mm (1/8 inch) aluminum window (blue) positioned 1 m upstream of the sample with neutron capture events (black) as well as neutron scatter events (red) on a 0.002 mm gold sample in the center of the crystal ball. The ball is asymmetrically positioned inside the shed. 54

Figure 54: Comparison between a 3.18 mm (1/8 inch) aluminum window (blue) positioned 0.8 m upstream of the sample with neutron capture events (black) as well as neutron scatter events (red) on a 0.002 mm gold sample in the center of the crystal ball. The ball is asymmetrically positioned inside the shed. 55

Figure 55: Comparison between a 3.18 mm (1/8 inch) aluminum window (blue) positioned 0.7 m upstream of the sample with neutron capture events (black) as well as neutron scatter events (red) on a 0.002 mm gold sample in the center of the crystal ball. The ball is asymmetrically positioned inside the shed. 56

Figure 56: Comparison between a 0.25 mm (10 mil) aluminum window (blue) positioned 1 m downstream of the sample with neutron capture events (black) as well as neutron scatter events (red) on a 0.002 mm gold sample in the center of the crystal ball. The ball is asymmetrically positioned inside the shed. 57

List of Tables

Table 1: Total efficiency and part of events with cluster multiplicity 2 or higher as a function of energy. All the numbers are relative to the total number of emitted γ -rays. 20

Table 2: Ratio of events from scattered neutrons and capture events on the sample for different setups. The last column is for events with total deposited energy above 1 MeV only, while all other ratios correspond to the total number of detected events. 23

Table 3: Total efficiency and part of events with cluster multiplicity 2 or higher as a function of energy. All the numbers are relative to the total number of emitted γ -rays. 38

Table 4: Ratio of events from scattered neutrons and capture events on the sample for different setups. The last column is for events with $E_{\text{tot}} > 1$ MeV only, while all other ratios correspond to the total number of detected events. 42

1 Introduction

The first part of this report (Chapter 3) describes extensive simulations carried out to describe and understand the results of the first run cycle with DANCE (Detector for Advanced Neutron Capture Experiments). The DANCE array is a 159-element 4π barium fluoride array designed to study neutron capture on small quantities of radioactive material. It is located on a 20 meter neutron flight path, which views an "upper tier" water moderator at the Manuel J. Lujan Jr. Neutron Scattering Center at the Los Alamos Neutron Science Center (LANSCE) [1].

During the first commissioning phase of this project from November 2002 until January 2003 only 141 crystals were available. Therefore a comparison with former simulations [2-4] can not be done directly, and a new set of simulations turned out to be necessary. The discussed setup is as close as possible to the setup used during the beam cycle 2002/2003.

The second part (Chapter 4) is intended to predict the effect of possible improvements during the shutdown phase. In particular, the number of crystals and the energy threshold per detector will be different from the commissioning phase.

2 Calculational Approach

The detector response to neutrons and gamma rays was studied using the Monte Carlo code GEANT 3.21. The inner radius of a closed sphere in the following simulations is 17 cm and the crystals have a length of 15 cm. The crystals are supported by a spherical structure out of aluminum with an inner radius of 49.7 cm and an outer radius of 53.5 cm (1.5 inches thickness). Each crystal is wrapped by a PVC housing of 0.7 mm thickness and glued to a photo multiplier tube (PMT). The crystal-PMT unit was then put into an aluminum housing in a way that there is no aluminum between the crystals or between crystals and sample, but the PMT is surrounded by aluminum. Using this Al-housing the crystals were finally mounted to the surrounding supporting structure. The supporting structure as well as the aluminum housings were included in the simulations, while due to restrictions in the number of defined volumes only a simplified PMT could be included. The simplification was that the material of the PMT (mainly Co, Ni contained in the magnetic shielding) was mixed into the material of the Al-housings. In order to make the simulations as realistic as possible the beam pipe including the cross for the sample changer were included in the simulations.

The following parameters have been used for the ${}^6\text{LiH}$ moderator:

- density: 0.85 g/cm^3
- isotopic abundance of ${}^6\text{Li}$: 100 %
- chemical composition: ${}^6\text{LiH}$

The threshold behavior, the energy resolution and the air gap between the crystals were optimized in order to fit the measured calibration source spectra. The finally used set was:

- 1 mm PVC around the crystals, which accounts also for the sometimes increased thickness due to electrical tape and the very thin reflection material.
- 3 mm additional air gaps between the crystals.
- The beam pipe was made of aluminum alloy with an inner radius of 2.1825 cm and an outer radius of 2.5 cm.
- The energy threshold for crystals 1 .. 95 was set to 250 keV and 500 keV for the other crystals. Furthermore an additional Gaussian distribution with a full-width-half-maximum of 150 keV was added to the threshold on a event by event basis in order to

emulate the baseline fluctuations. These assumptions result in a different shape of the total energy spectrum close to the threshold. The edge will not be sharp, but rather flat.

3 141 crystals & high threshold

All the experimental data shown in this report were taken under the following conditions. Only 148 crystals were delivered and mounted. Data were taken from 141 crystals, since one of the Acqiris modules used for the data acquisition could not be operated reliably. Furthermore, the threshold per detector was set to 50 mV in order to avoid triggers on the 60 Hz oscillations discovered on the output of the photo multipliers. This threshold corresponds to photon energies between 300 and 500 keV. Due to differences in gain as well as threshold levels, the effective energy threshold observed in the single detector spectra was between 300 and 500 keV.

Even in the final version, the detector will have 159 crystals and not 162 needed to cover the full solid angle. Two crystals are needed to be left out for the neutron beam pipe consisting of aluminum alloy and another one for the sample changer. Figure 1 and Figure 2 illustrate the conditions as they were simulated. The simulations were as close to the experiment as possible. Therefore the 7 mounted crystals that were not connected were included in the simulations as passive detectors but were not drawn in the figures in order to increase the visibility of the interior of the ball. Furthermore 4 supporting structure pieces were included. These pieces are welded onto the cross of the beam line inside the ball in order to increase the mechanical stability. They can be seen in the left part of Figure 1 and detailed in Figure 3.

The DANCE array is divided into two halves, left-hand side and right-hand side according to the neutron flight direction. Almost all of the missing crystals were left out at the equatorial ring joining the two halves, which can be seen at Figure 2.

Previous GEANT simulations [2-4] have shown that the background due to neutrons, which are scattered at the sample and eventually captured in the surrounding material can be significantly reduced by a spherical ${}^6\text{LiH}$ shell between sample and BaF_2 detectors. Some runs carried out during the commissioning phase had a ${}^6\text{LiH}$ moderator with an inner radius of 10.5 cm and an outer radius of 16.5 cm in place. Therefore most of the simulations described here were done both with and without such a moderator.

In a first attempt many parameters included in the simulations have been varied in order to describe the results of calibration carried out with a set of γ -ray sources. These sources were ${}^{22}\text{Na}$, ${}^{88}\text{Y}$ and ${}^{60}\text{Co}$. A set of parameters containing the detector threshold (see above), the energy resolution of the BaF_2 crystals and the distance between the crystals and the center of the ball were optimized to fit the measured spectra as good as possible. Afterwards the response of the detector array to single mono-energetic γ -rays as well as γ -ray cascades predicted by theory following a neutron capture on gold could be simulated with the same set of parameters and eventually the response to neutrons including scattering at the sample could be investigated.

During the runs carried out with neutrons a large background due to capture on hydrogen was discovered. In order to figure out, where this background comes from, especially where the neutrons creating this background are generated, a set of simulations including the walls of the detector cave made of Borated Polyethylene (5%) and aluminum windows up- and downstream of the DANCE array has been carried out.

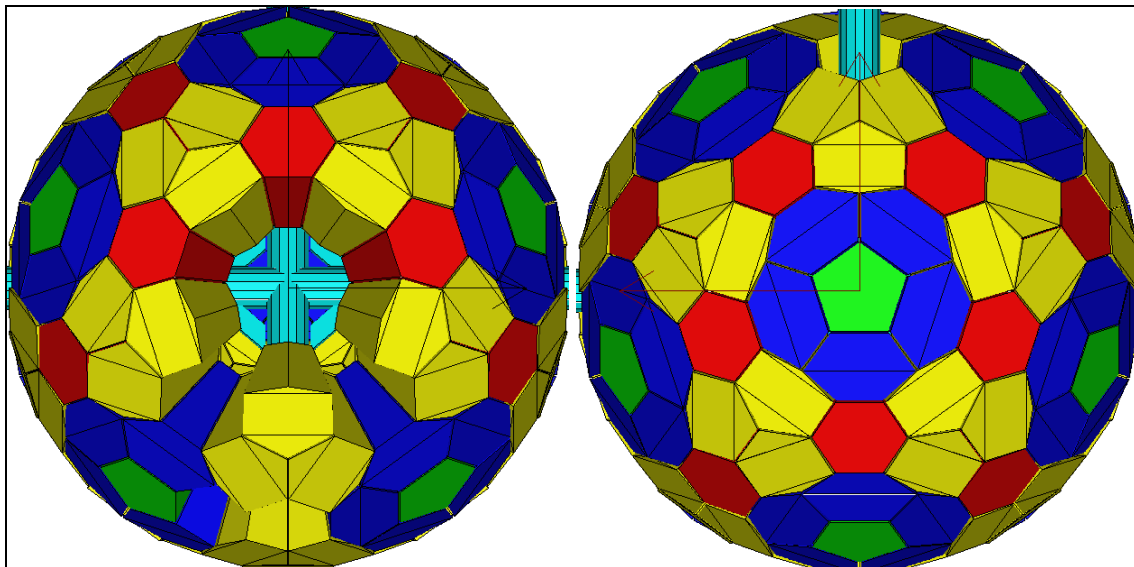


Figure 1: Views of the simulated setup: from left / right (relative to beam direction). Each color corresponds to a different crystal type (A – green, B – dark blue, C – yellow, D - red). The missing crystals allowing the beam pipe (light blue) to be seen were either not connected or not in place during the runs carried out during the commissioning phase 2002/2003.

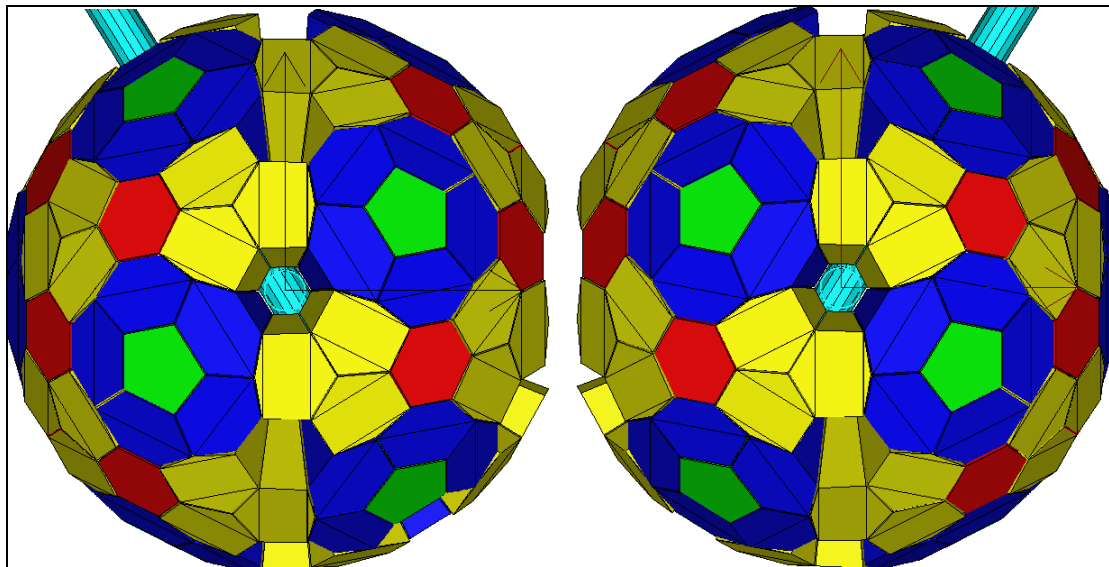


Figure 2: Views of the simulated setup: from downstream / upstream (relative to beam direction). Each color corresponds to a different crystal type (A – green, B – dark blue, C – yellow, D - red). The missing crystals allowing the beam pipe (light blue) to be seen were either not connected or not in place during the runs carried out during the commissioning phase 2002/2003.

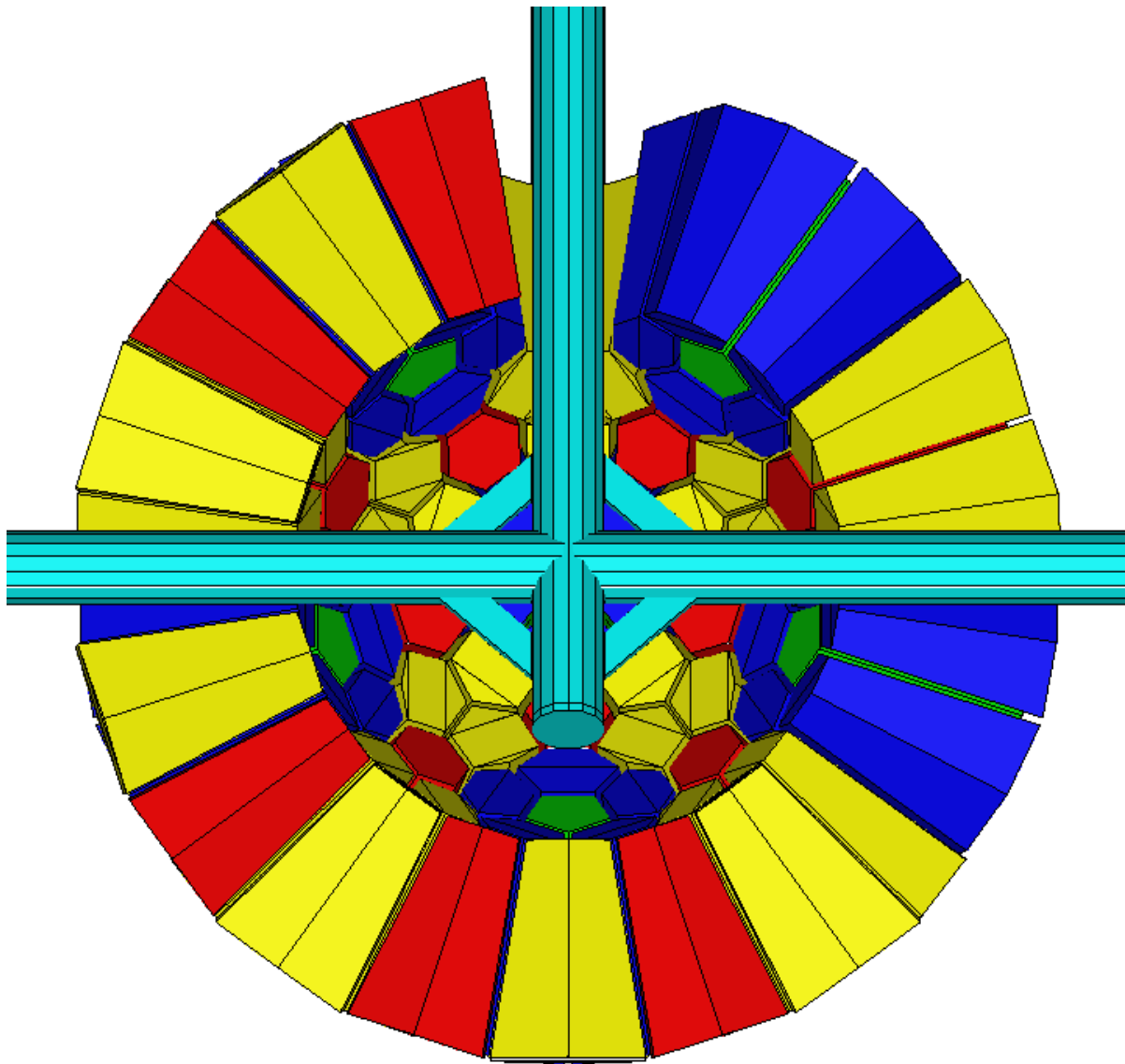


Figure 3: Detailed view of the beam pipe crossing for neutron beam and sample changer (light blue). Some of the BaF_2 crystals are shown too in order to see the relative size. Each color corresponds to a different crystal type (A – green, B – dark blue, C – yellow, D - red).

3.1 Calibration sources

Experimental data exist for the common gamma-calibration sources ^{22}Na , ^{60}Co , ^{88}Y , and ^{137}Cs . Each of them was used because the energy as well as the multiplicity of the emitted γ -rays is different, hence it helps to fully understand the behavior of the detector. Within this chapter only ^{22}Na , ^{60}Co , ^{88}Y will be discussed. The ^{137}Cs data will be ignored, since the threshold applied during these runs was very close to the energy of the emitted gamma (662 keV) and not much can be learned.

In order to get an energy resolution comparable to the experimental data, all the simulated energy spectra contain 10000 channels and range from 0 to 100 MeV, which corresponds to an energy resolution of 10 keV/channel.

For each different run 10^6 decays were simulated. The decay properties were included, the electron emitted during the ^{60}Co decay was neglected. The angular correlation between the emitted photons are neglected, except for the 511 keV annihilation radiation following the β^+ decay of ^{22}Na .

3.1.1 Source: ^{60}Co

Figure 4 shows the decay probabilities of ^{60}Co . Only the most abundant branch of the ^{60}Ni deexcitation emitting a 1173 keV photon in coincidence with a 1332 keV photon was considered. This means, the γ -multiplicity was always 2.

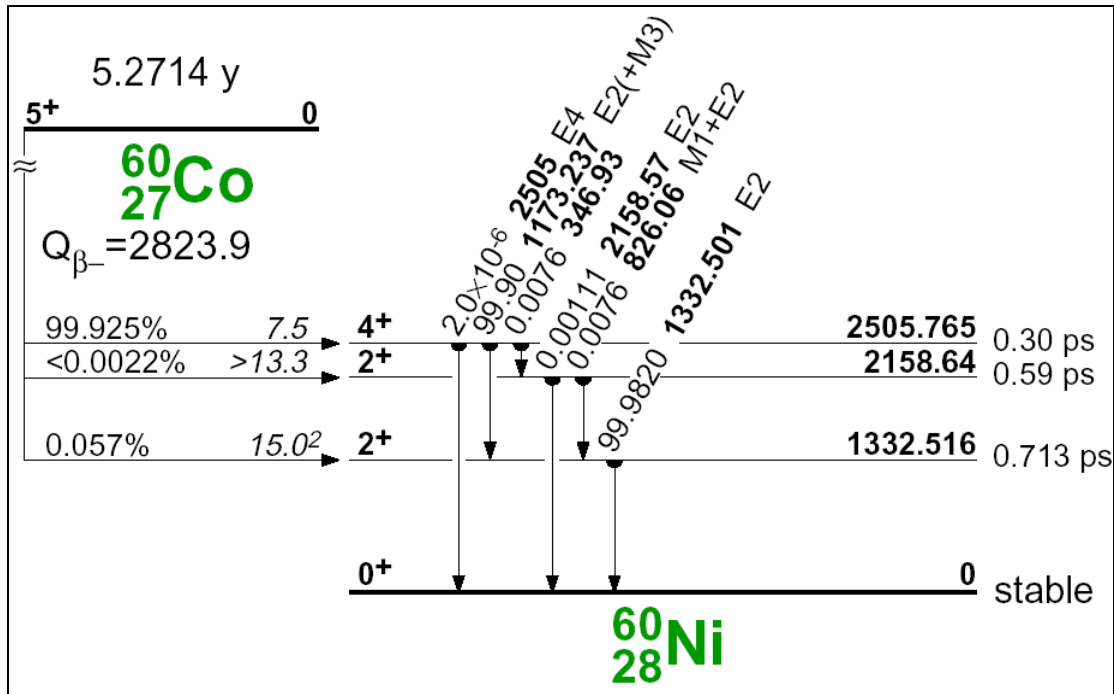


Figure 4: Decay scheme of ^{60}Co according to the Table of Isotopes [5].

Figure 5 and Figure 6 show the comparison of experiment and simulation for the setup during the commissioning phase with and without the ^6LiH moderator. The best agreement between experiment and simulation could be found for ^{60}Co . It was not possible to find a set of parameters where the agreement was as good for all three calibration sources. One of the reasons is probably that the threshold behavior is not correctly reproduced. In the case of ^{60}Co both emitted photons are well above the threshold, therefore the ratios of the three peaks are well reproduced. The simulations show, however, discrepancies if a part of the energy is lost due to Compton scattering or pair production.

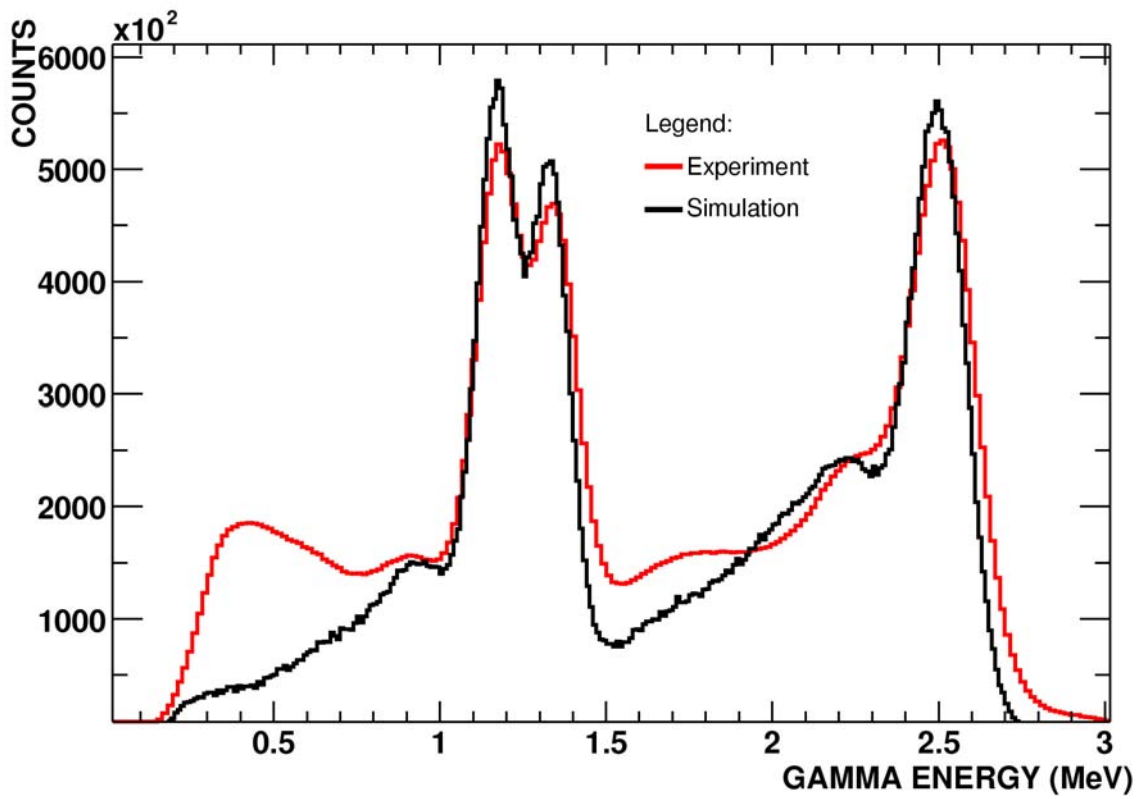


Figure 5: Experimental and simulated data for ^{60}Co , no ^6LiH .

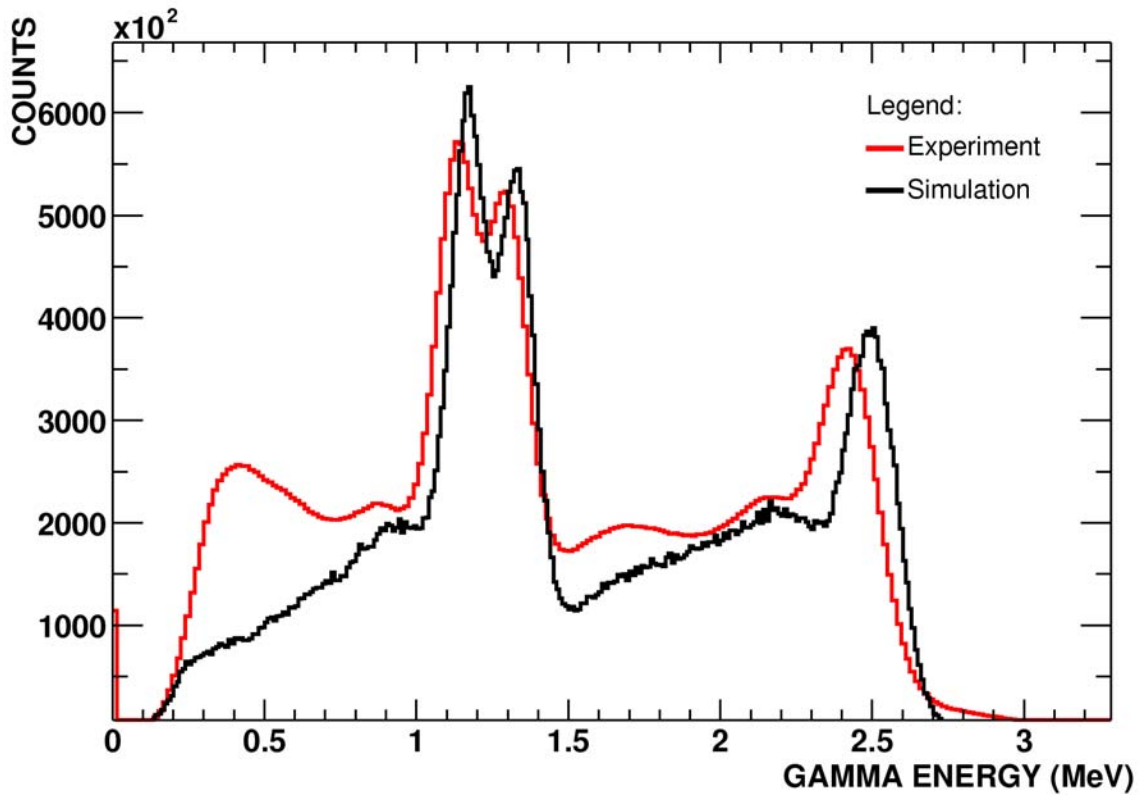


Figure 6: Experimental and simulated data for ^{60}Co , ^6LiH .

3.1.2 Source: ^{22}Na

Figure 7 shows the decay probabilities of ^{22}Na . 90.5 % of the ^{22}Na decays are β^+ and 9.5% are electron capture (EC). Therefore the γ -multiplicity of the decay is 3 for 90.5% of the decays (2x 511 keV and 1x 1275 keV) and 1 otherwise. Figure 8 and Figure 9 show the comparison of experiment and simulation for the setup during the commissioning phase with and without the ^6LiH moderator.

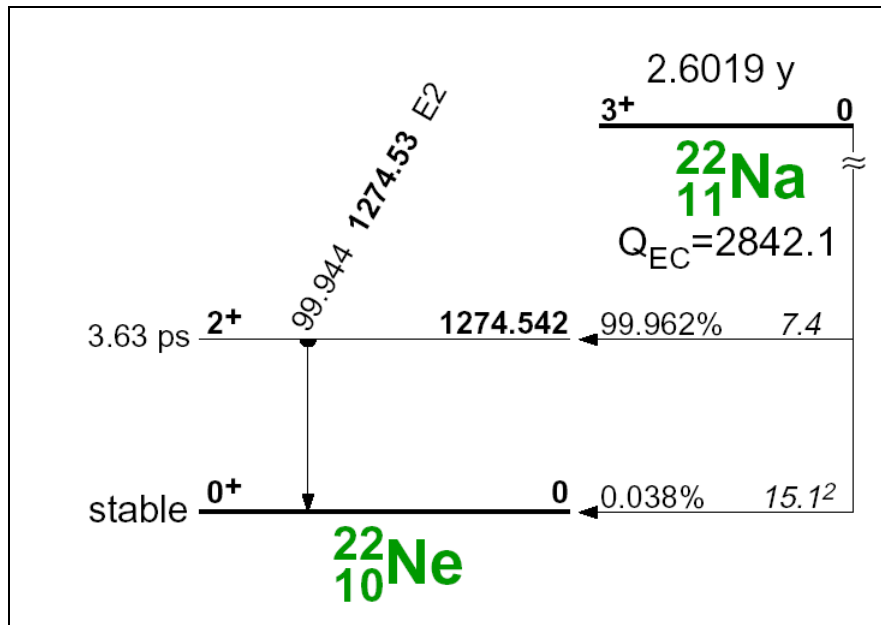


Figure 7: Decay scheme of ^{22}Na according to the Table of Isotopes [5].

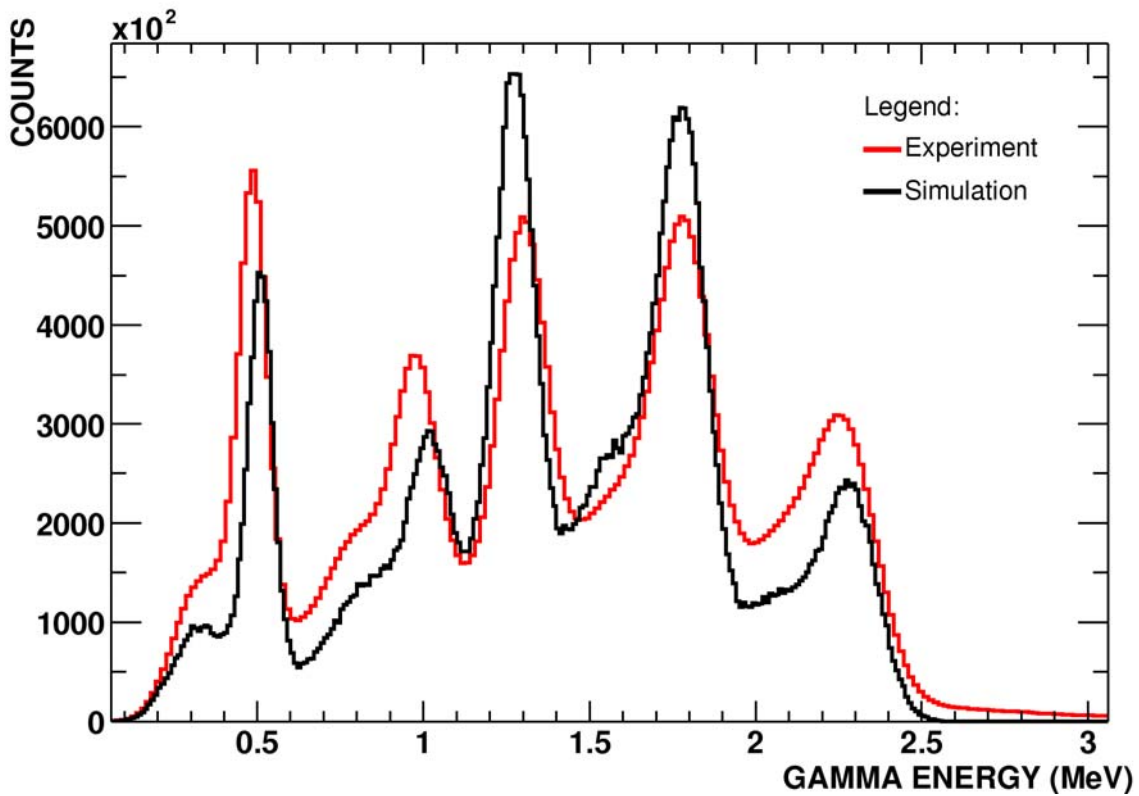


Figure 8: Experimental and simulated data for ^{22}Na , no ^6LiH absorber.

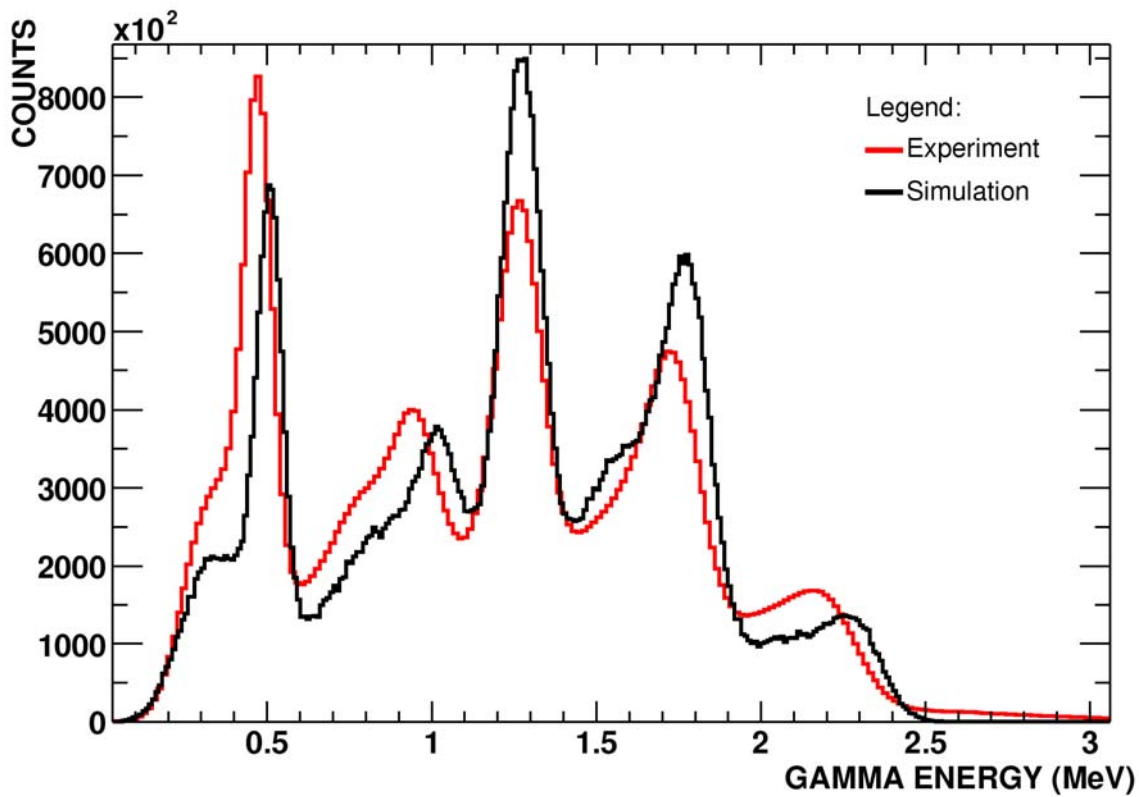


Figure 9: Experimental and simulated data for ^{22}Na , ^6LiH absorber.

Especially the peak efficiency for the 511 keV annihilation radiation depends on the single detector threshold. Therefore the content ratio of the different peaks depends on the threshold behavior too. Only with the high threshold described previously the agreement shown here could be achieved. The peak ratios are reproduced within about 10%, higher accuracy would demand detailed knowledge about threshold behavior and baseline oscillation for *each* detector. These parameters are also a function of time – depending on the status of neighboring experiments in the Lujan Center the oscillations are changing in amplitude. Therefore a better agreement was not the goal of this investigation.

Figure 9 shows also a discrepancy between simulation and experiment as far as the energy calibration is concerned. The experimental data shown here contain only a linear energy calibration, while it is known that a quadratic calibration is needed for BaF_2 arrays. This will be applied in future experiments. Furthermore, the energy calibration is not stable for a certain time after turning on the high voltage power supply of the photo multiplier tubes. For approximately one hour the temperature of the tubes will rise and therefore the number of electrons emitted per incident photon is changing.

3.1.3 Source: ^{88}Y

Figure 10 shows the decay probabilities of ^{88}Y . Only 0.2 % of the ^{88}Y decays are β^+ and 99.8 % are electron capture (EC). Therefore the β^+ was neglected during the simulations. Furthermore only the most abundant branch of the ^{88}Sr deexcitation emitting a 898 keV photon in coincidence with a 1836 keV photon was considered. This means, the γ -multiplicity was always 2.

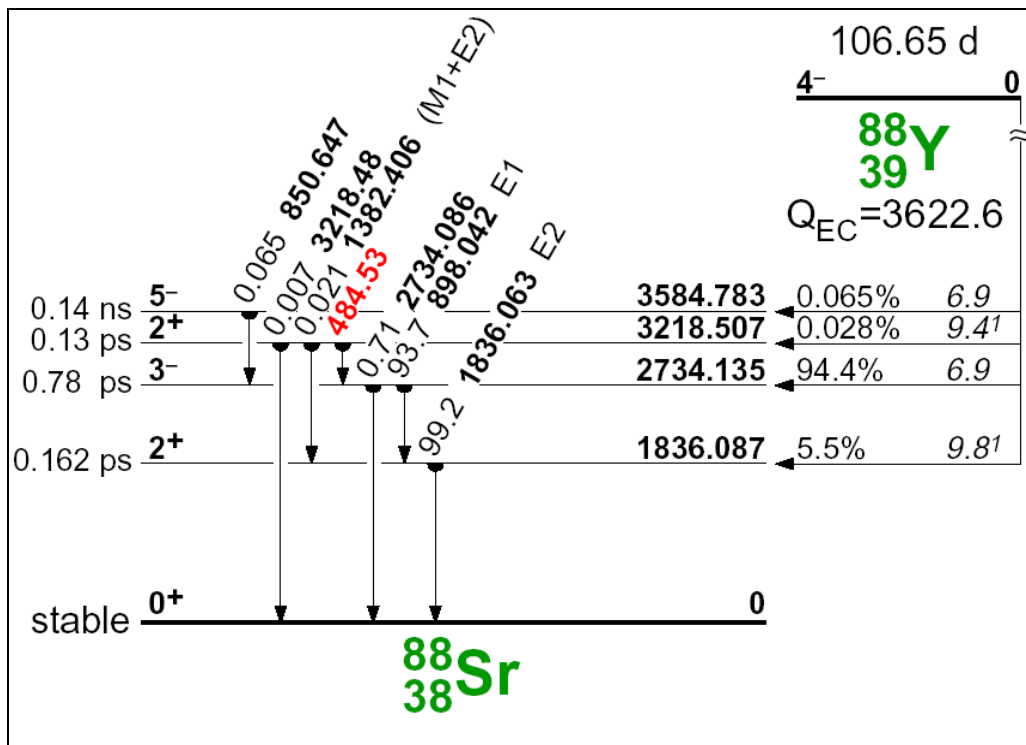


Figure 10: Decay scheme of ^{88}Y according to the Table of Isotopes [5].

Figure 11 and Figure 12 show the comparison of experiment and simulation for the setup during the commissioning phase with and without the ^6LiH moderator. Even though the same set of parameters has been applied for all three calibration sources, the experimental peak ratios for ^{88}Y are not well reproduced by the simulation. If normalized at the single gamma peaks, the experimental full energy peak is about 25% below the simulated one.

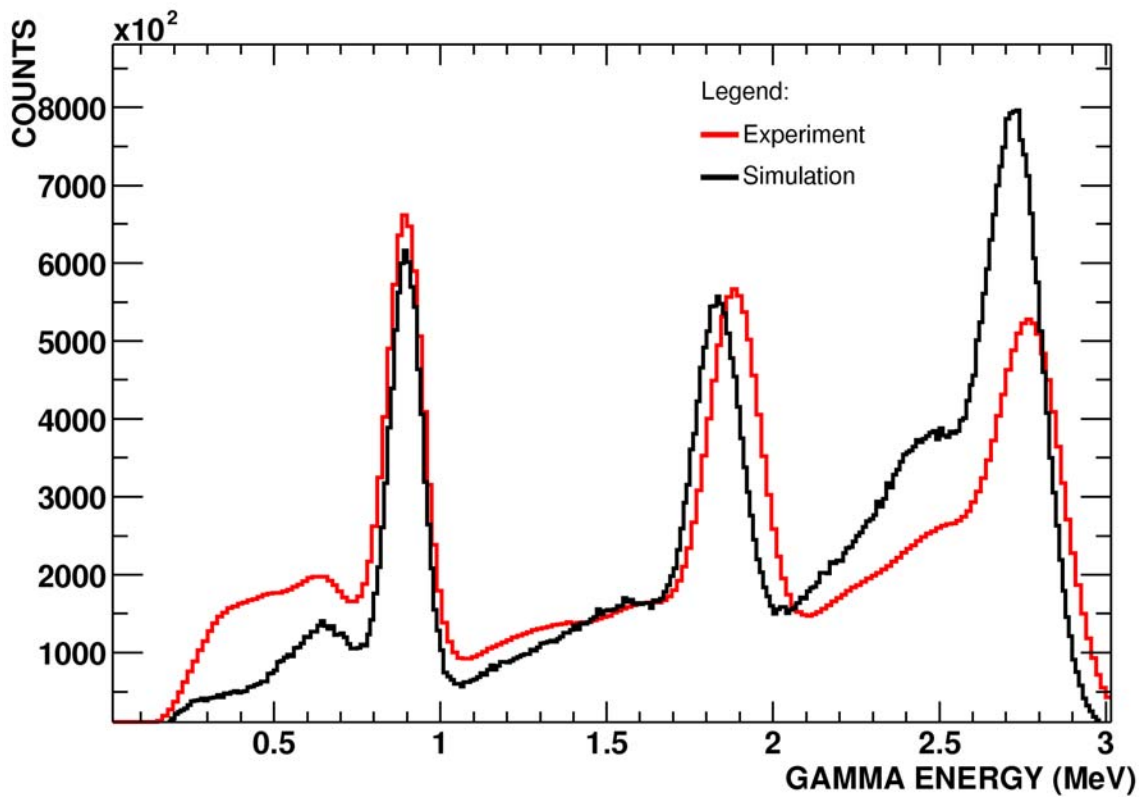


Figure 11: Experimental and simulated data for ^{88}Y , no ^6LiH

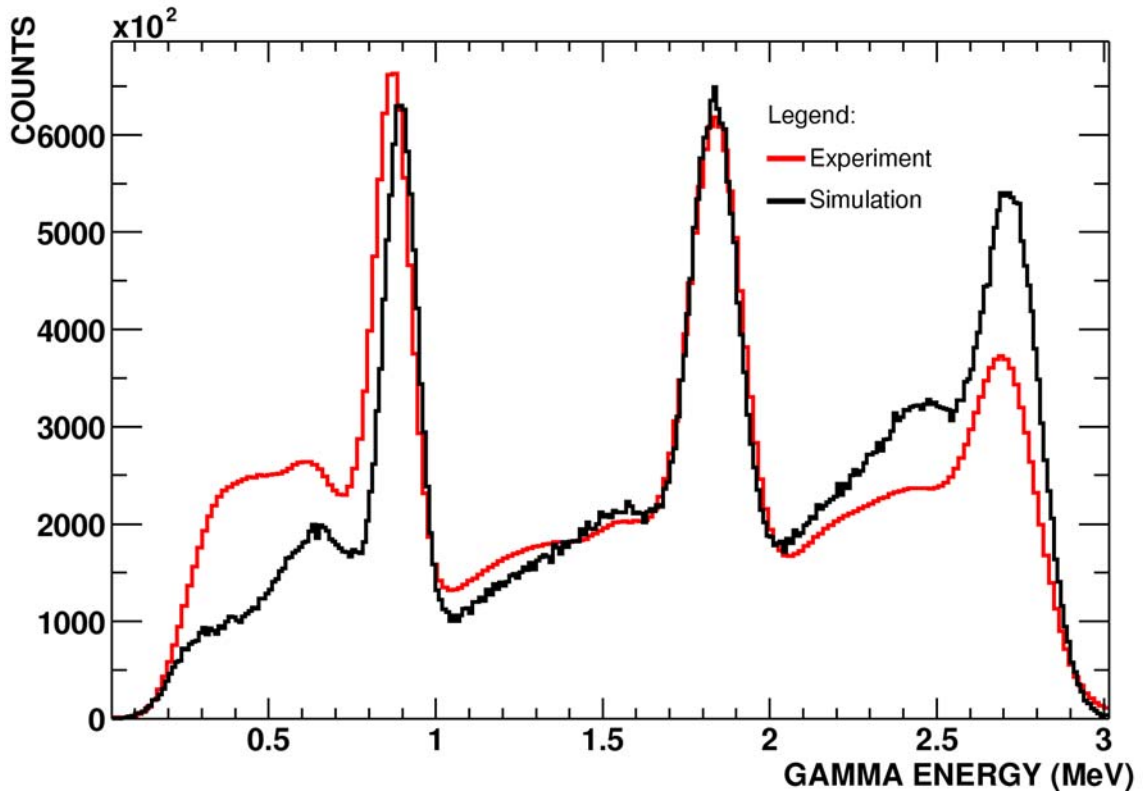


Figure 12: Experimental and simulated data for ^{88}Y , ^6LiH

3.2 Mono-energetic γ -rays

With the same parameters for threshold and energy resolution as in the previous chapter, the response to mono-energetic γ -rays of different energies has been simulated. Each spectrum shown in Figure 13 and Figure 14 correspond to 10^6 γ -rays, started isotropically in the center of the DANCE array. Figure 13 shows the total energy deposited in the BaF_2 crystals as a function of the primary γ -ray energy with and without the ${}^6\text{LiH}$ moderator in place. The ${}^6\text{LiH}$ moderator slightly reduces the full energy peak. The absorption effect of the ${}^6\text{LiH}$ shell on the γ -rays can be seen in Figure 14, which shows the integral of all counts above a given energy threshold.

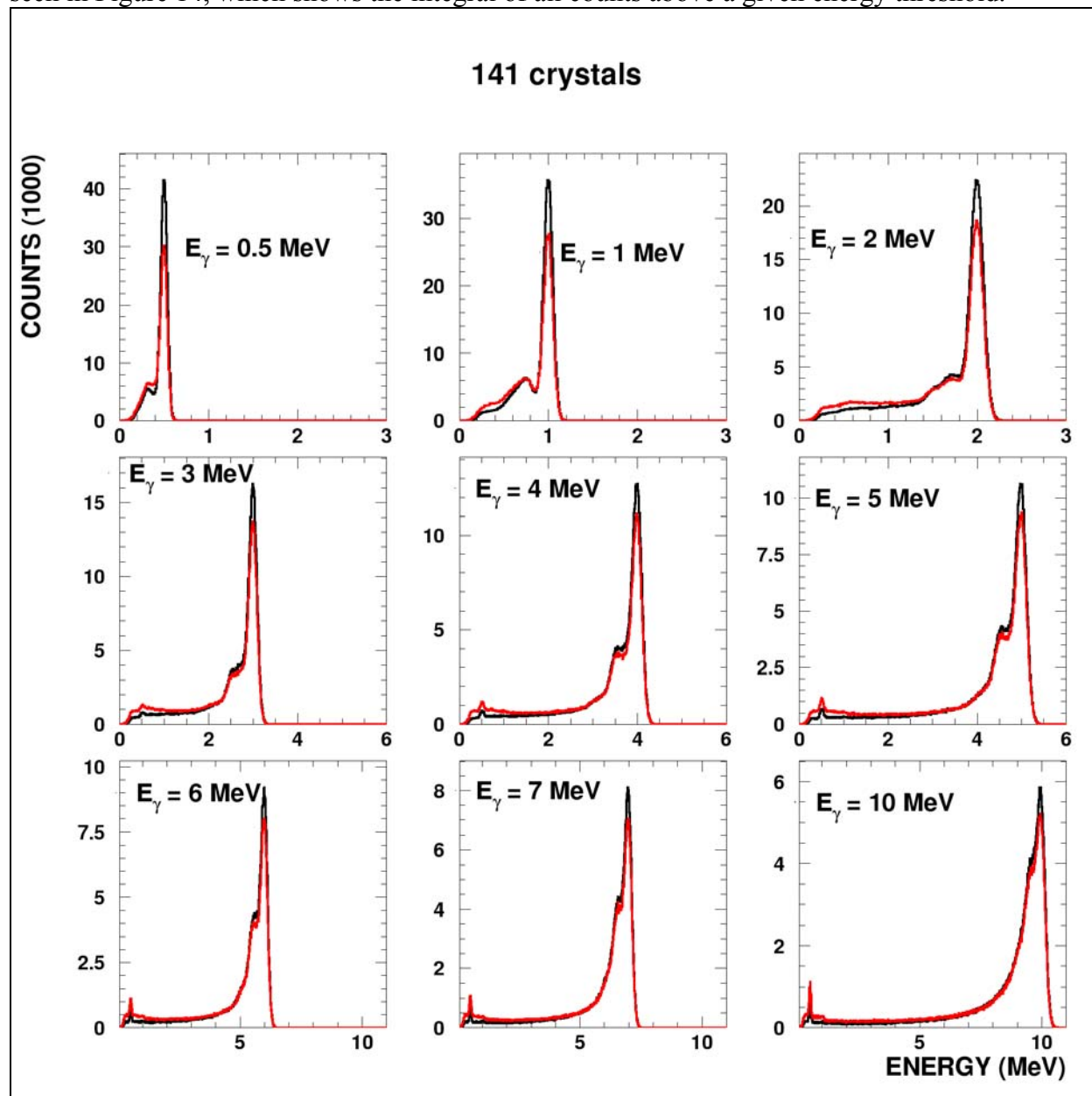


Figure 13: Energy deposit summed over all crystals for γ -energies from 0.5 MeV to 10 MeV. Spectra with (red) and without (black) the ${}^6\text{LiH}$ absorber for 141 crystals and high detector threshold are shown.

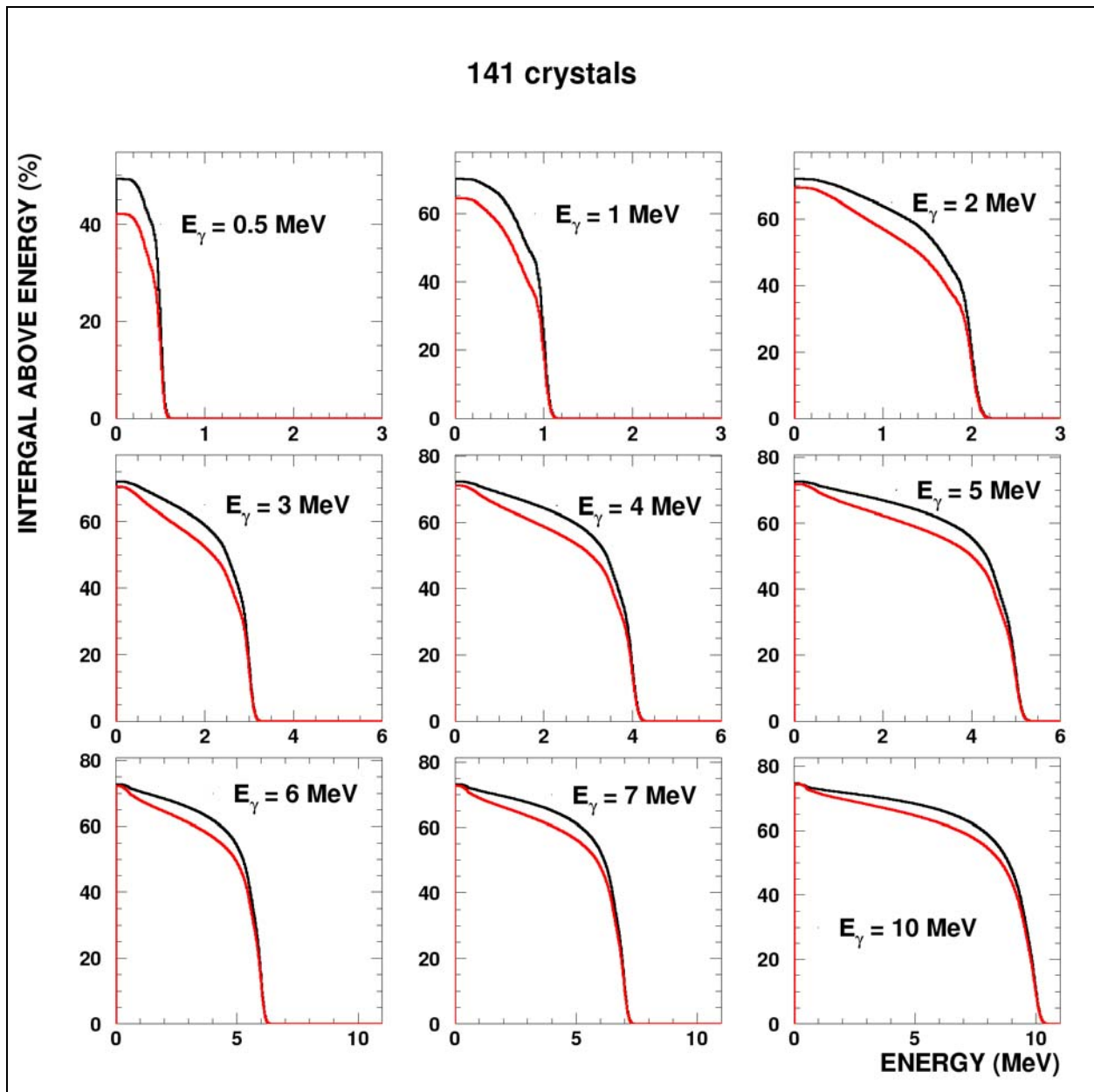


Figure 14: Percentage of counts above a given threshold energy for the spectra shown in Figure 13. Spectra with (red) and without (black) the ${}^6\text{LiH}$ absorber for 141 crystals and high detector threshold are shown. The curves are normalized to the number of emitted γ -rays, which means, the value at $E = 0$ MeV reflects the total efficiency of the array.

According to previous simulations, mono-energetic γ -rays of 500 keV have a probability of 25 % for depositing energy in more than one crystal. This effect is called cross talking. If one defines a cluster as a number of adjacent crystals which have a energy deposition above the single detector threshold, one finds that the number of cluster per event is much closer to the original γ -ray multiplicity than the number of fired crystals. This fact is illustrated in Figure 15, showing the cluster multiplicity for single photons of different energies. Even for the highest energies the probability for creating more than 1 cluster is below 25 %.

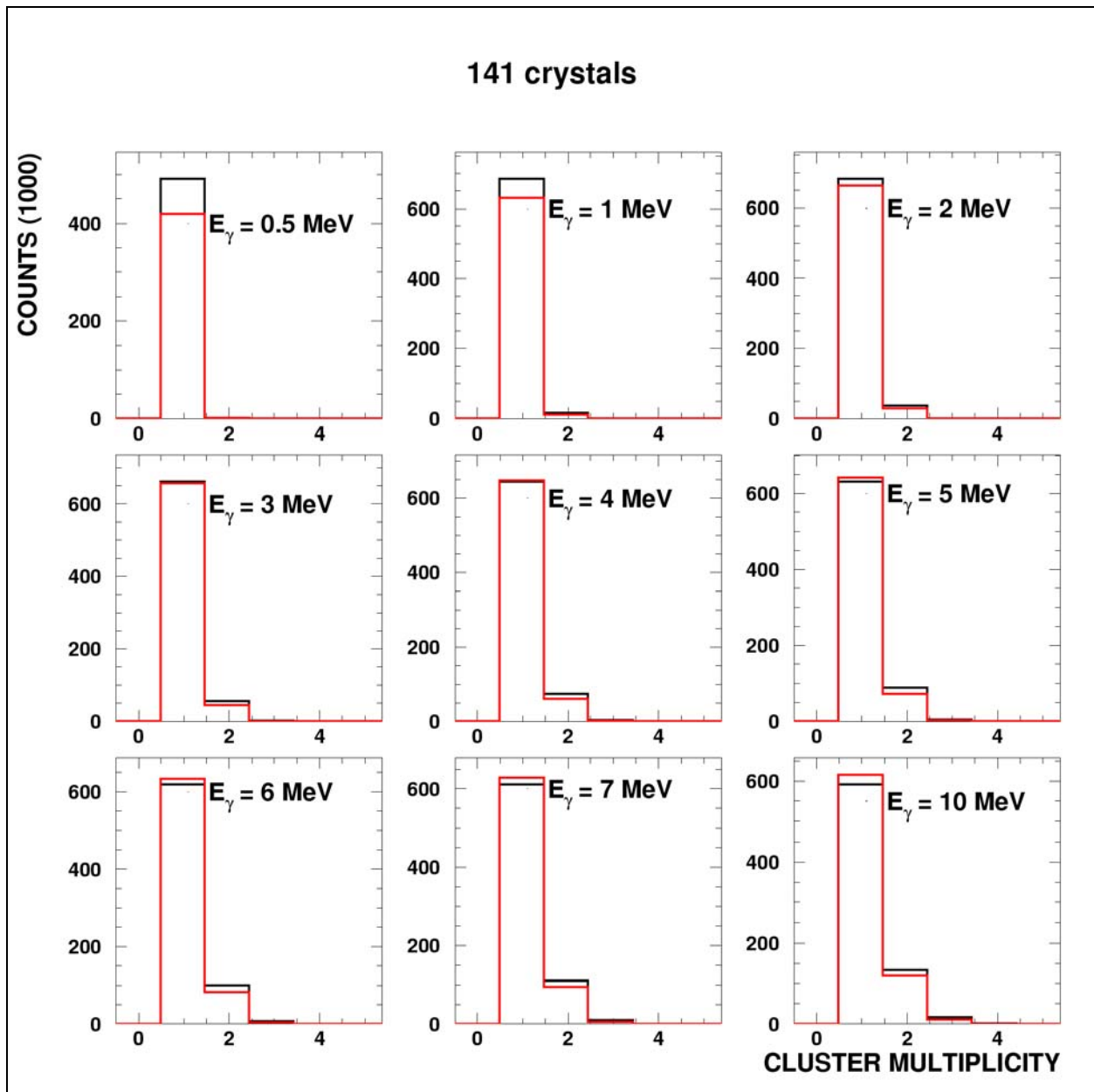


Figure 15: Number of clusters for mono-energetic γ -rays of different energies with (red) and without (black) ${}^6\text{LiH}$ -absorber. 10^6 γ -rays have been simulated for each spectrum.

Crystal made of BaF_2 suffer from the disadvantage of containing Ra, a chemical homologue of Ba ($t_{1/2} = 1600$ a). Radium and its daughter decays produce an intrinsic background of about 200 counts/s/crystal. This background tends to form only one cluster, while neutron capture events usually emit several γ -rays and form more than 1 cluster. Furthermore single γ -rays emitted during the decay of the sample material tends to create only 1 cluster. Both background components might therefore be significantly reduced by applying a cluster multiplicity threshold. Table 1 contains total efficiency information for the 2 setups discussed in this chapter – 141 crystals with and without ${}^6\text{LiH}$ ball – integrated over all cluster multiplicities as well as only for cluster multiplicity 2 and above.

Table 1: Total efficiency and part of events with cluster multiplicity 2 or higher as a function of energy. All the numbers are relative to the total number of emitted γ -rays.

E_γ (MeV)	total efficiency (%)		part (%) above cluster multiplicity 1	
	without ${}^6\text{LiH}$	with ${}^6\text{LiH}$	without ${}^6\text{LiH}$	with ${}^6\text{LiH}$
0.5	~400	~450	~10	~10
1	~600	~650	~10	~10
2	~600	~650	~10	~10
3	~600	~650	~10	~10
4	~600	~650	~10	~10
5	~600	~650	~10	~10
6	~600	~650	~10	~10
7	~600	~650	~10	~10
10	~600	~650	~10	~10

0.5	49.2	42.1	0.4	0.3
1	70.0	64.3	2.3	1.8
2	71.9	69.3	5.2	4.3
3	71.9	70.4	8.1	6.6
4	72.2	71.1	10.7	8.8
5	72.5	71.7	12.9	10.6
6	72.7	72.2	14.9	12.2
7	73.2	72.8	16.5	13.8
8	73.2	72.8	16.5	13.8
9	73.6	73.5	17.9	15.1
10	74.4	74.6	20.4	17.5

An important background component during the commissioning phase was the 2.2 MeV photon following a neutron capture on hydrogen. According to Table 1 one would reduce the detection efficiency for a 2 MeV photon from 72 % to 5 % by applying a cluster multiplicity cut. This would mean, the number of detected events would be reduced by a factor of 15. The reduction for true capture events is much less (see chapter 3.3.2, Figure 18), since usually several gammas are emitted.

3.3 $Au(n, \gamma)$

3.3.1 Au cascades

After understanding the response of the array to mono-energetic γ -rays the response to cascades following a thermal neutron capture on gold was investigated. The cascades used for the simulation are theoretical cascades, which include nuclear structure information [6, 7]. Figure 16 shows the results for 141 crystals with and without ${}^6\text{LiH}$. 10^6 cascades were emitted in the center of the crystal ball for each run. One criterion for choosing ${}^6\text{LiH}$ as the material of the neutron moderator inside the DANCE array was the low atomic number of the involved nuclei, which means a low interaction probability of the capture γ -rays on their way to the BaF_2 crystals. The left part of Figure 16 shows that the finite interaction probability in the absorber results in a 25% reduction in counts in the peak.

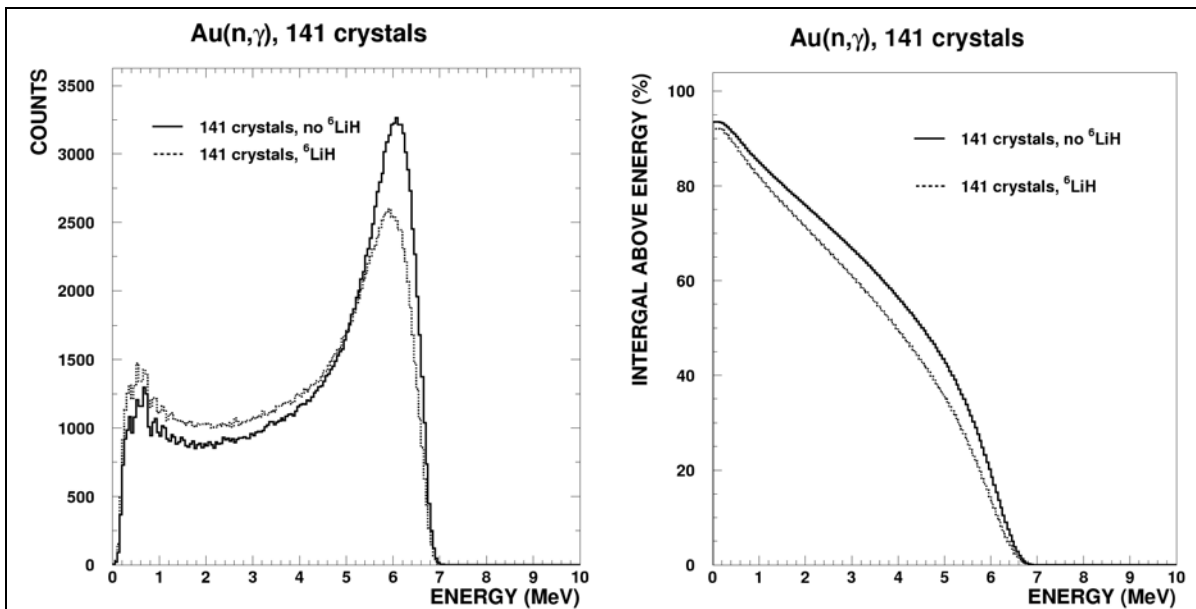


Figure 16: Left: Response of the DANCE array with 141 crystals and high single detector thresholds to theoretical gold capture cascades. Right: Percentage of counts above a given threshold energy for the spectra on the left. The curves are normalized to the number of emitted γ -cascades, which means, the value at $E = 0$ MeV reflects the total efficiency of the array.

3.3.2 Neutrons on Au

The reason for the simulations discussed in the section is to show the advantage of using the ^6LiH moderator. In the last section a 25 % decrease of the peak to tail ratio was shown. Figure 17 corresponds to 10^7 simulated neutrons emitted 20 m away from the center of the ball. The gold sample in the ball hit by the neutrons was 1 cm in diameter and 0.2 mm thick. The emitted neutron spectrum was a typical $1/E$ moderated spallation spectrum. The simulations have been carried out for neutrons energies from 1 eV up to 100 MeV. The left part of Figure 17 shows the result for neutrons between 10 and 100 keV without the ^6LiH moderator in place, while the right part shows result for the same setup with ^6LiH moderator in place. This energy region is especially interesting for nuclear astrophysics, stockpile stewardship and advanced reactor concepts. Obviously the signal to background ratio increased significantly, even though the full energy peak of gold is broadened due to partial absorption of the emitted capture photons.

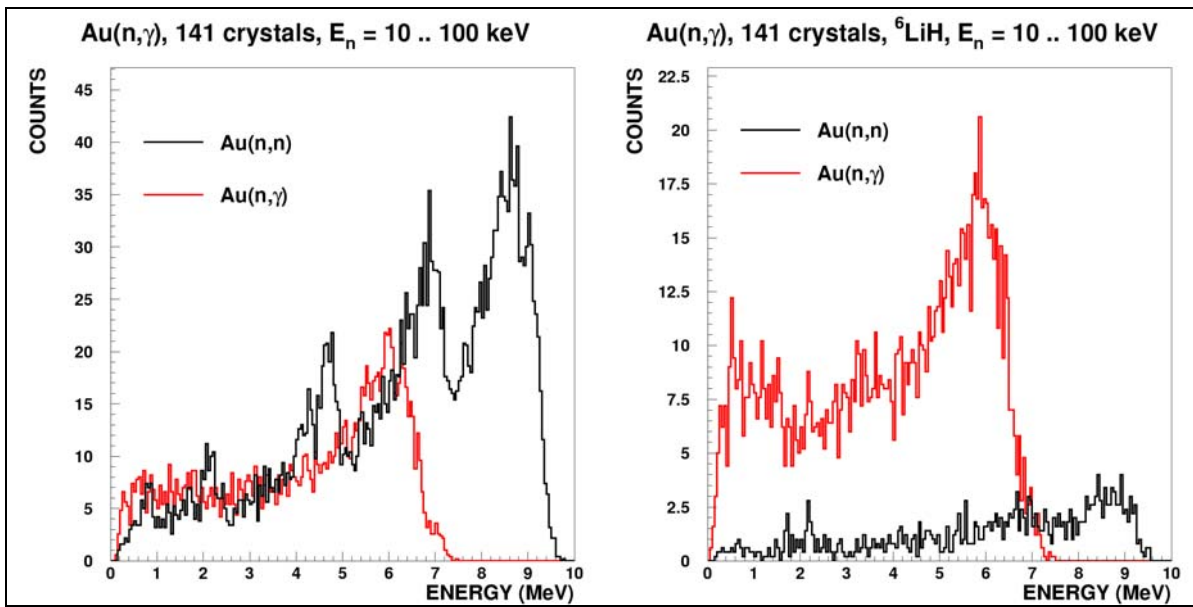


Figure 17: Response of the DANCE array with 141 crystals and high detector threshold to neutron reactions on a gold sample. The red line corresponds to events due to captures on a gold sample, the black curve to events due to neutrons scattered at the gold sample. The neutron energy 10 ..100 keV. The left picture shows the results without ⁶LiH absorber, while the right picture corresponds to the standard ⁶LiH absorber in place.

Table 2 contains the ratio of events due to neutron scatter on the sample to events to neutron capture. For lower energies a significant background reduction is to be expected, while for neutron energies of 100 keV or above the reduction is not as strong anymore. The reduction factor varies from 100 to 4 depending on the neutron energy.

Table 2: Ratio of events from scattered neutrons and capture events on the sample for different setups. The last column is for events with total deposited energy above 1 MeV only, while all other ratios correspond to the total number of detected events.

Setup	Ratio between scattered and captured events for different neutron energy regions.			
	0.1 .. 1 keV	1 ..10 keV	10 .. 100 keV	0.1 .. 1 MeV
141 crystals, high threshold, no ⁶ LiH	0.47	1.2	2.2	2.7
141 crystals, high threshold, ⁶ LiH	0.0035	0.025	0.20	0.66
141 crystals, ratio without/with ⁶ LiH	134	48	11	4.1

Another possibility of increasing the signal to scatter-background ratio is to take advantage of the high granularity of the detector. As mentioned in section 3.2, a cluster multiplicity cut would reduce background due to internal decays as well as from single γ -rays significantly. Figure 18 to Figure 22 illustrate that this holds true even for events due to scattered neutrons, which are eventually captured in the BaF₂ crystals. Since all the photons after a neutron capture in one of the crystals are emitted within this crystal, such an event tends to form only one big cluster, rather than 2 or more small cluster like capture events on the sample. The right part of Figure 18 shows that applying a cluster multiplicity threshold of 2 would reduce the number of background events by 50 %, while more than 80 % of the sample-captures would still be counted.

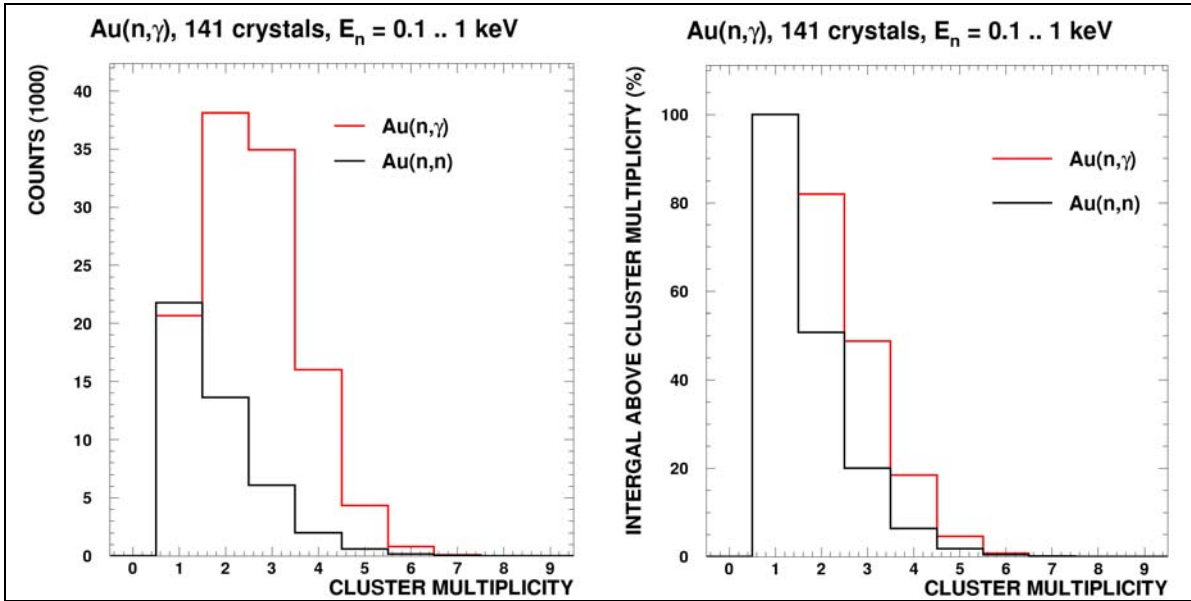


Figure 18: Left: Number of clusters for capture-events (red) and for scattered events (black) for neutron energies between 0.1 and 1 keV. Right: Corresponding percentage of counts for at least a given number of clusters.

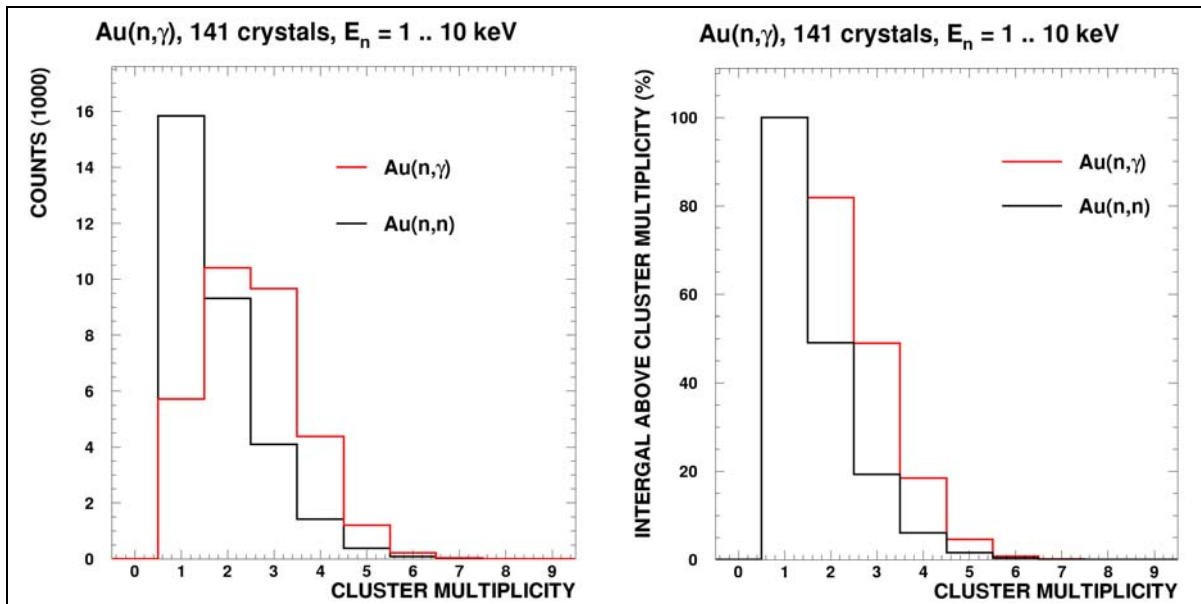


Figure 19: Left: Number of clusters for capture-events (red) and for scattered events (black) for neutron energies between 1 and 10 keV. Right: Corresponding percentage of counts for at least a given number of clusters.

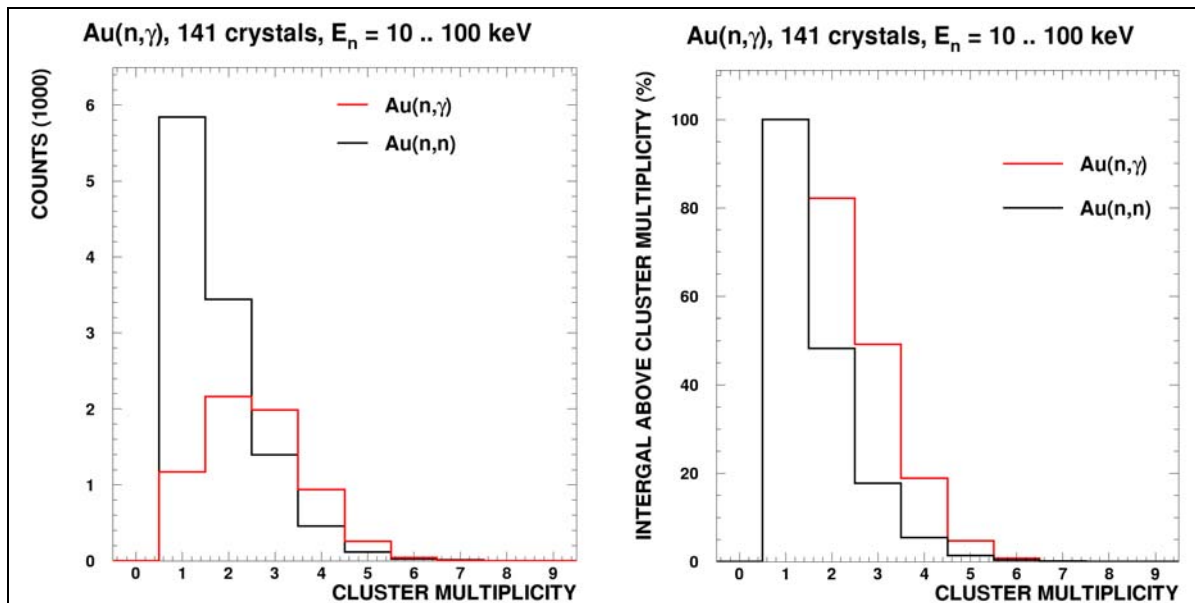


Figure 20: Left: Number of clusters for capture-events (**red**) and for scattered events (**black**) for neutron energies between 10 and 100 keV. Right: Corresponding percentage of counts for at least a given number of clusters.

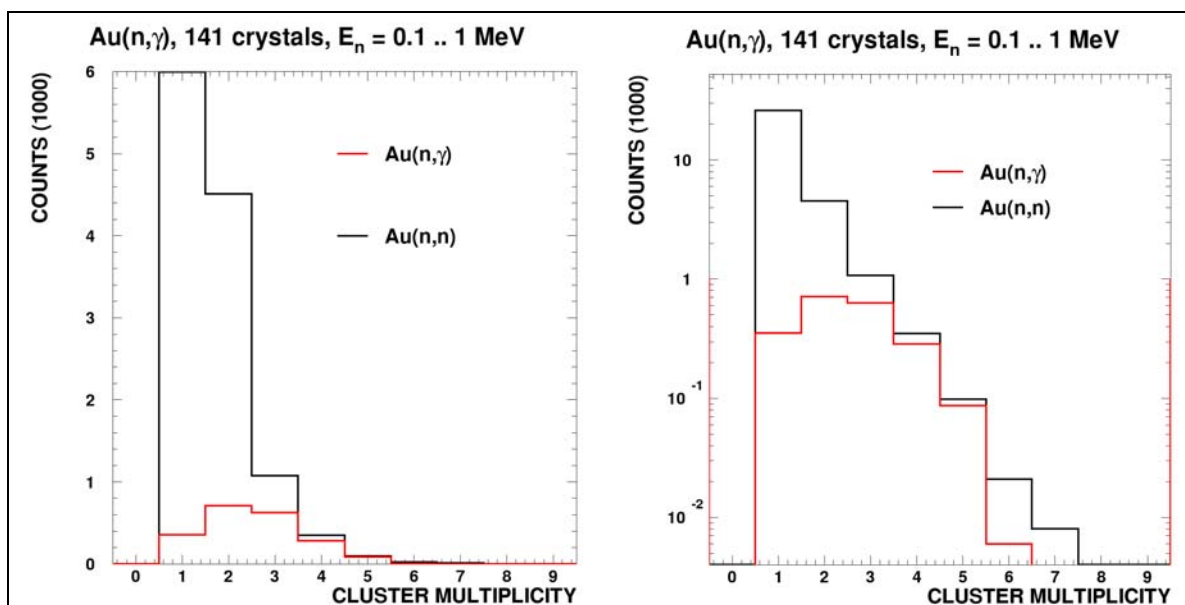


Figure 21: Left: Number of clusters for capture-events (**red**) and for scattered events (**black**) for neutron energies between 0.1 and 1 keV. The y-axis is expanded in order to increase the visibility. Right: Same as left, but without y-axis expansion and logarithmic y-axes.

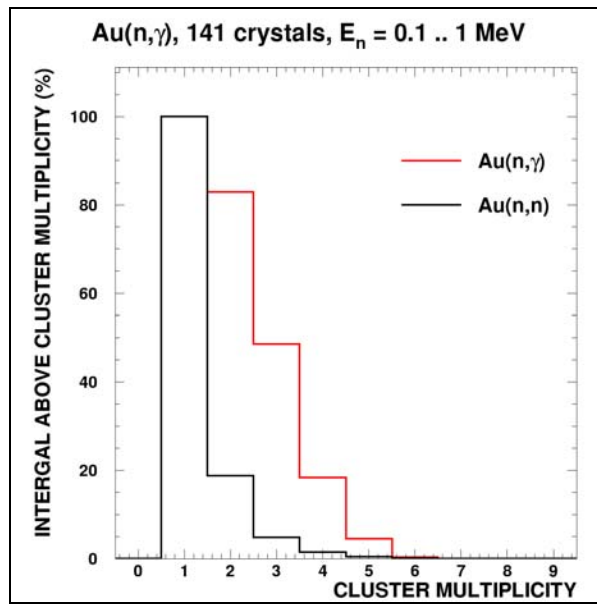


Figure 22: Percentage of counts equals or above a given number of clusters for the spectra shown in Figure 21. The numbers are normalized to the total number of detected events, respectively.

4 159 crystals & low threshold

The setup described in the previous chapter was a preliminary setup used during the commissioning phase of the run cycle 2002/2003. The final setup of DANCE will consist of 159 BaF₂ crystals. The beam pipe crossings as well as the supporting pieces were included in the simulations (for details see Figure 3). During similar experiments at the Karlsruhe BaF₂ ball the energy threshold per single detector is typically 50 keV. As it will turn out during this chapter, the energy detection threshold for a single crystal is very crucial for the shape of the measured spectra as well as for the total and especially the peak efficiency of the DANCE array. In order to show this effect all the simulations with γ -rays have been carried out with the high threshold setup described in chapter 2 and applied for the entire previous chapter as well as with a general 50 keV threshold – from now on referred to as low threshold.

All the parameters except number of crystals and the threshold behavior used during the next sections were identical to the parameter set used during the previous chapter.

During section 5 the cause of the 2.2 MeV background component observed during the commissioning phase of the run cycle 2002/2003 will be investigated under the same conditions.

4.1 Calibration sources

In order to show the different steps of improvement, the number of crystals and the threshold behavior were changed separately. The following sections contain figures comparing the results of the 4 setups:

- 141 crystals and high threshold - the setup during the commissioning phase,
- 159 crystals and high threshold - the setup, which will be the least improvement for the next run cycle, and
- 159 crystals and low - the desired setup for runs with low systematic uncertainties.
- 162 crystals (4π) and low threshold – an idealized setup in order to show the potential of so far not foreseen improvements.

The last configuration still includes the standard beam pipe, but the gaps between the crystals were reduced to 0 mm.

Furthermore all simulations have been carried out with and without the ⁶LiH ball, in order to show the effects on photons as well as on scattered neutrons.

As in section 3.1, all the simulated energy spectra contain 10000 channels and range from 0 to 100 MeV, which corresponds to an energy resolution of 10 keV/channel.

For each different run 10^6 decays were simulated. The electron emitted during the ⁶⁰Co decay was neglected as was the kinetic energy of the positron in the decay of ²²Na. The angular correlation between the emitted particles are neglected, except for the 511 keV annihilation radiation following the β^+ decay of ²²Na.

4.1.1 Source: ^{60}Co

Figure 23 contains the comparison of three realistic configurations as well as the idealized setup with 162 crystals. All simulations are without the ^6LiH ball.

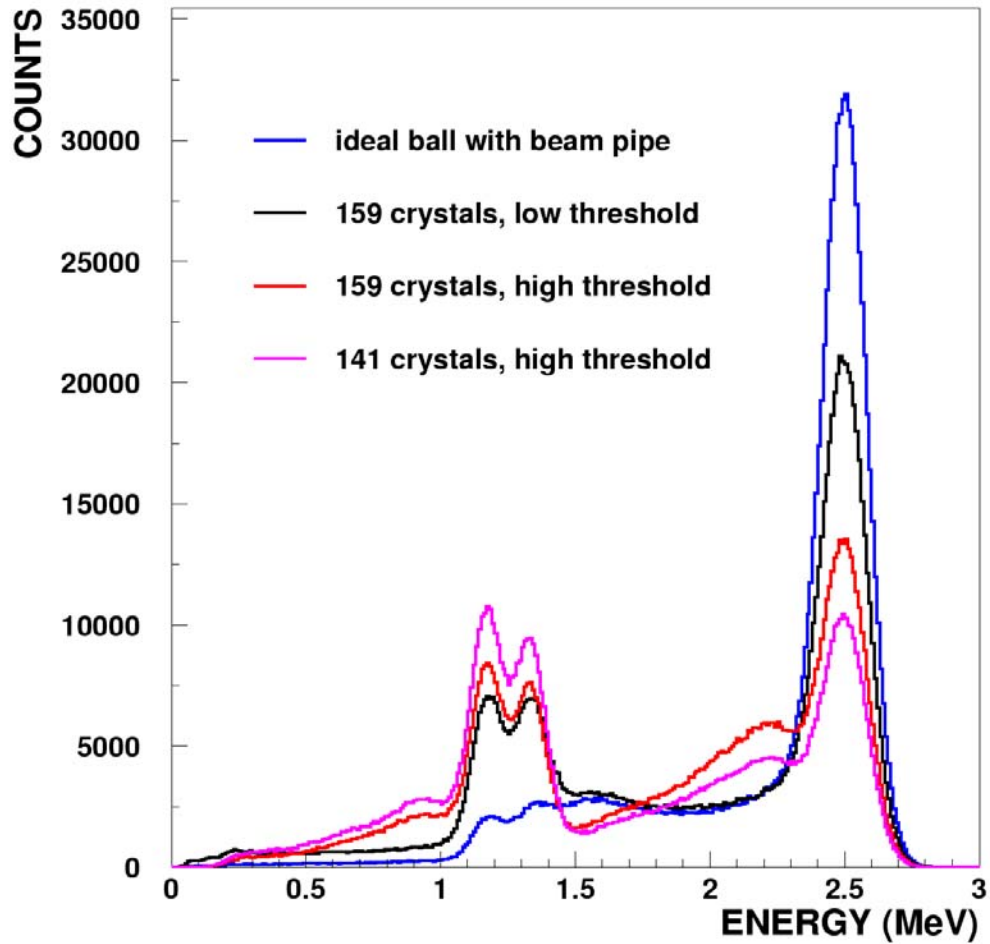


Figure 23: Response of the DANCE array with 141 and 159 crystals as well as low and high single detector thresholds to decay cascades of ^{60}Co . Additionally a configuration with 162 crystals is included.

Figure 24 shows the comparison of the setup with 159 crystals and low threshold with and without the ^6LiH moderator. The effect of the ^6LiH moderator on the full energy peak is about 40 % reduction.

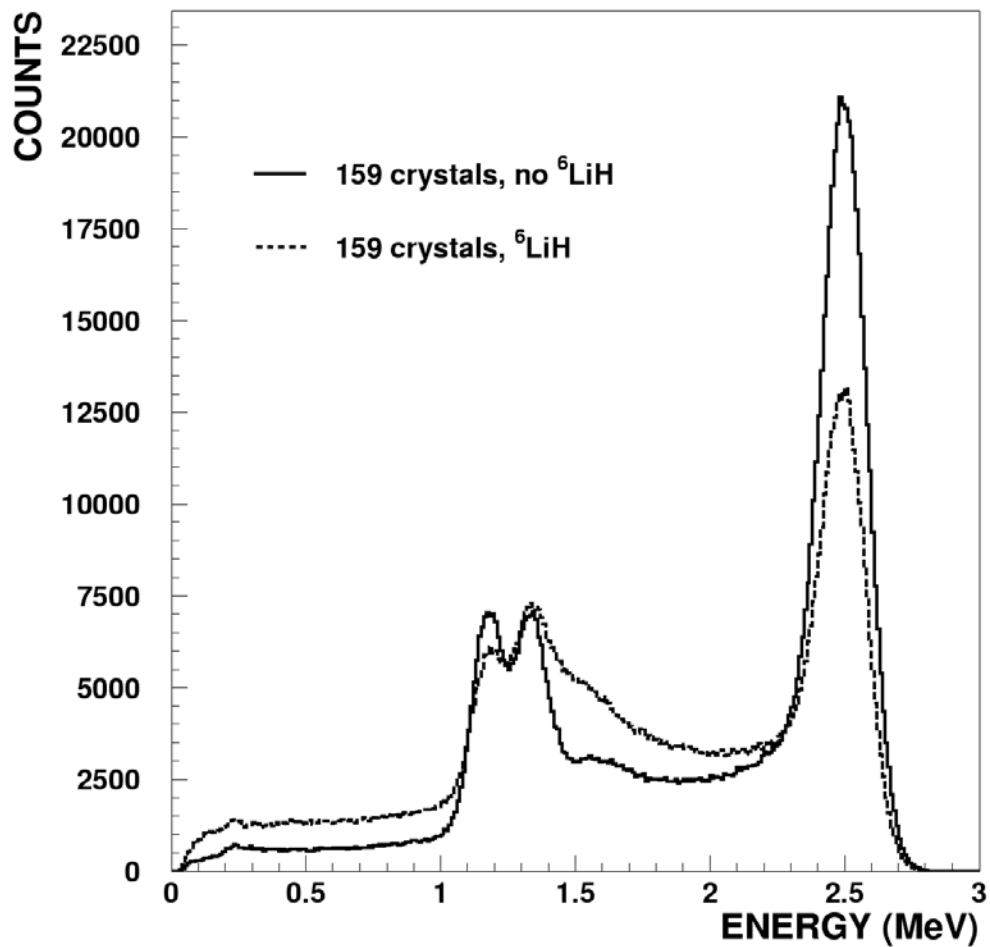


Figure 24: Response of the DANCE array with 159 crystals and low single detector thresholds with and without ${}^6\text{LiH}$ to decay cascades of ${}^{60}\text{Co}$.

4.1.2 Source: ${}^{22}\text{Na}$

Figure 25 contains the comparison of three realistic configurations as well as the idealized setup with 162 crystals. All simulations are without the ${}^6\text{LiH}$ ball. For interpreting the results it is important to remember that the positron and hence the two 511 keV annihilation photons are emitted only in 90.5 % of the decays.

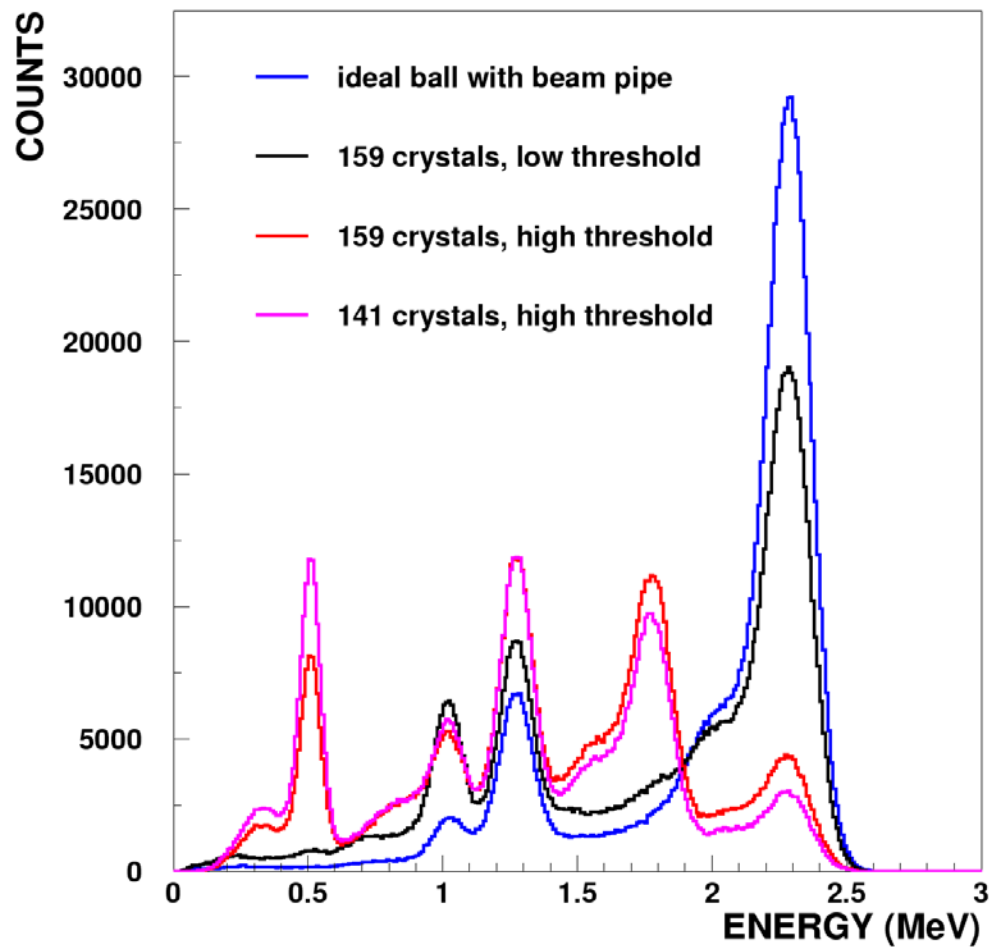


Figure 25: Response of the DANCE array with 141 and 159 crystals as well as low and high single detector thresholds to decay cascades of ^{22}Na . Additionally a configuration with 162 crystals is included.

Figure 26 shows the comparison of the setup with 159 crystals and low threshold with and without the ${}^6\text{LiH}$ moderator. The effect of the ${}^6\text{LiH}$ moderator on the full energy peak is about a factor of 2.

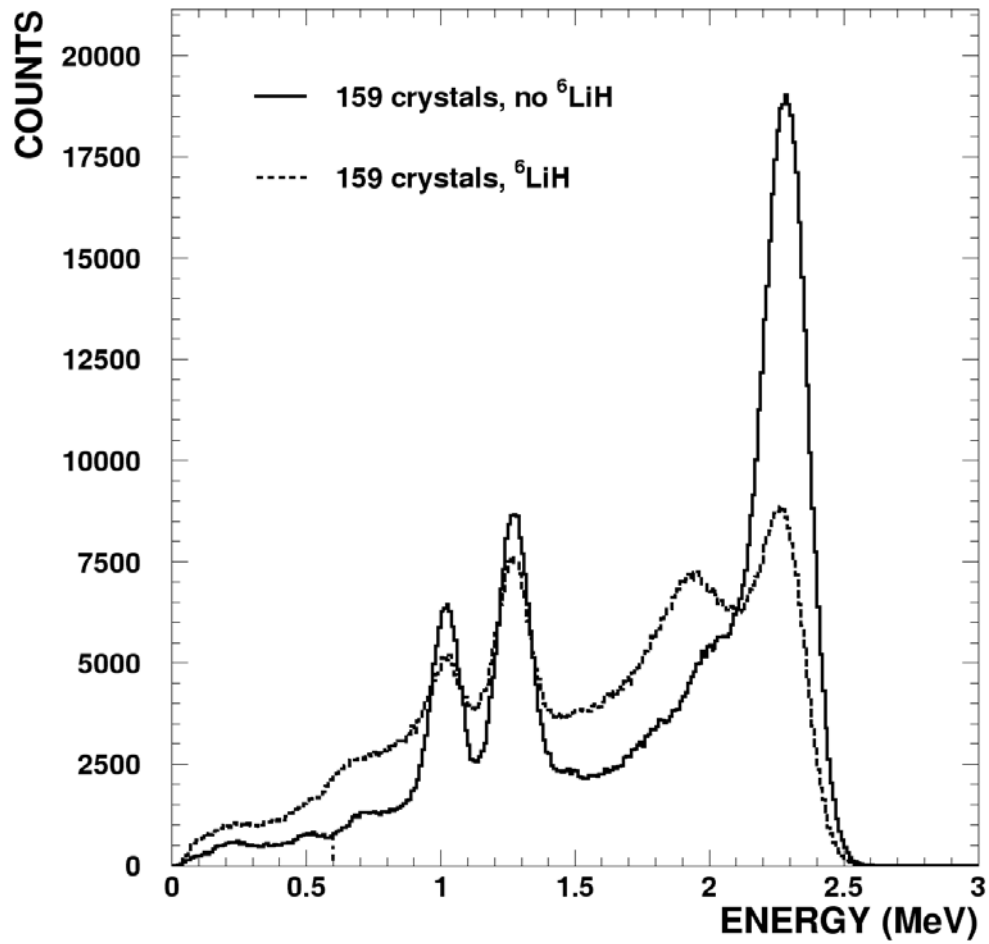


Figure 26: Response of the DANCE array with 159 crystals and low single detector thresholds with and without ${}^6\text{LiH}$ to decay cascades of ${}^{22}\text{Na}$.

4.1.3 Source: ^{88}Y

Figure 27 contains the comparison of three realistic configurations as well as the idealized setup with 162 crystals. All simulations are without the ^6LiH ball.

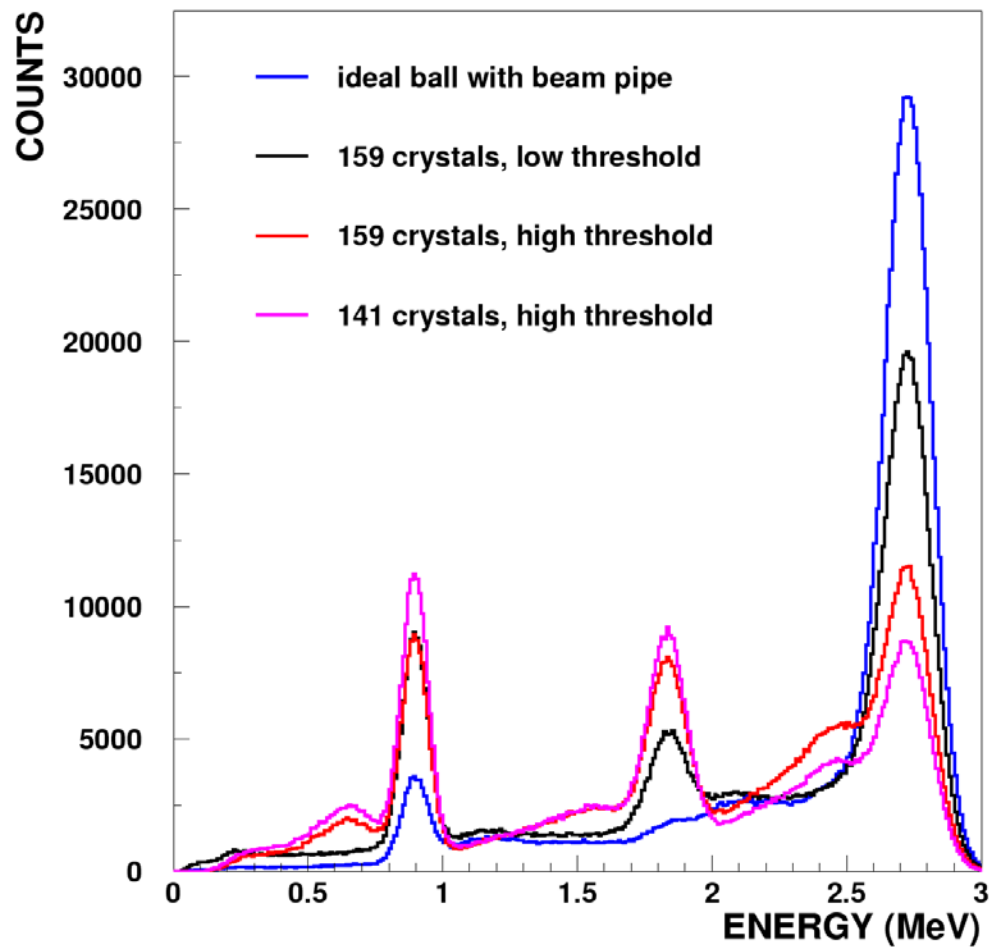


Figure 27: Response of the DANCE array with 141 and 159 crystals as well as low and high single detector thresholds to decay cascades of ^{88}Y . Additionally a configuration with 162 crystals is included.

Figure 28 shows the comparison of the setup with 159 crystals and low threshold with and without the ${}^6\text{LiH}$ moderator. The effect of the ${}^6\text{LiH}$ moderator on the full energy peak is about 40 % reduction.

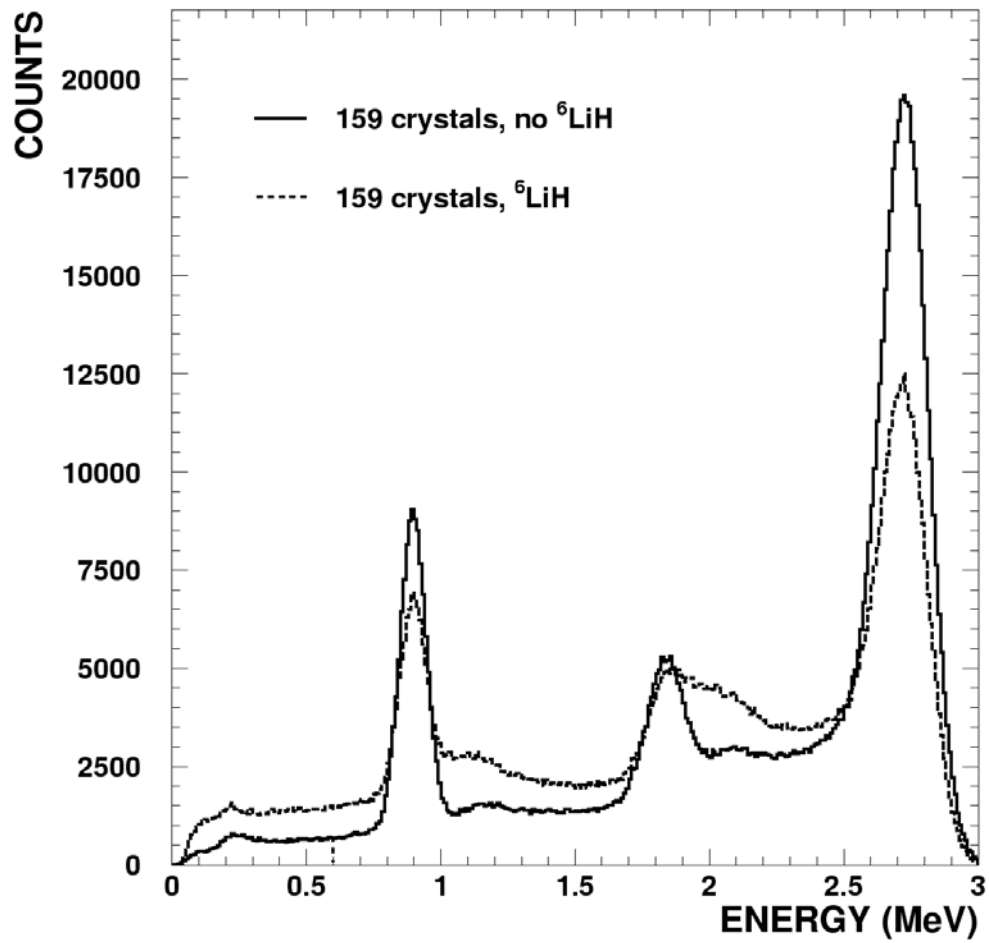


Figure 28: Response of the DANCE array with 159 crystals and low single detector thresholds with and without ${}^6\text{LiH}$ to decay cascades of ${}^{88}\text{Y}$.

4.2 Mono-energetic γ -rays

With the same threshold and energy resolution as in the previous chapter, the response to mono-energetic γ -rays of different energies has been simulated. At first the effect of different steps of improvements were investigated. Each spectrum shown in Figure 29 and Figure 30 correspond to 10^6 γ -rays, started isotropically in the center of the DANCE array. Figure 29 shows the total energy deposited in the BaF₂ crystals as a function of the primary γ -ray energy for the three different setups described in the previous section. The step from 141 to 159 crystals improves the peak efficiency significantly. For most energies the decreasing of the single detector thresholds would improve the measured spectra even more than the increasing of the crystal number. The effect on the γ -ray efficiency can be seen clearly in Figure 30 showing the integral of all counts above a given energy threshold.

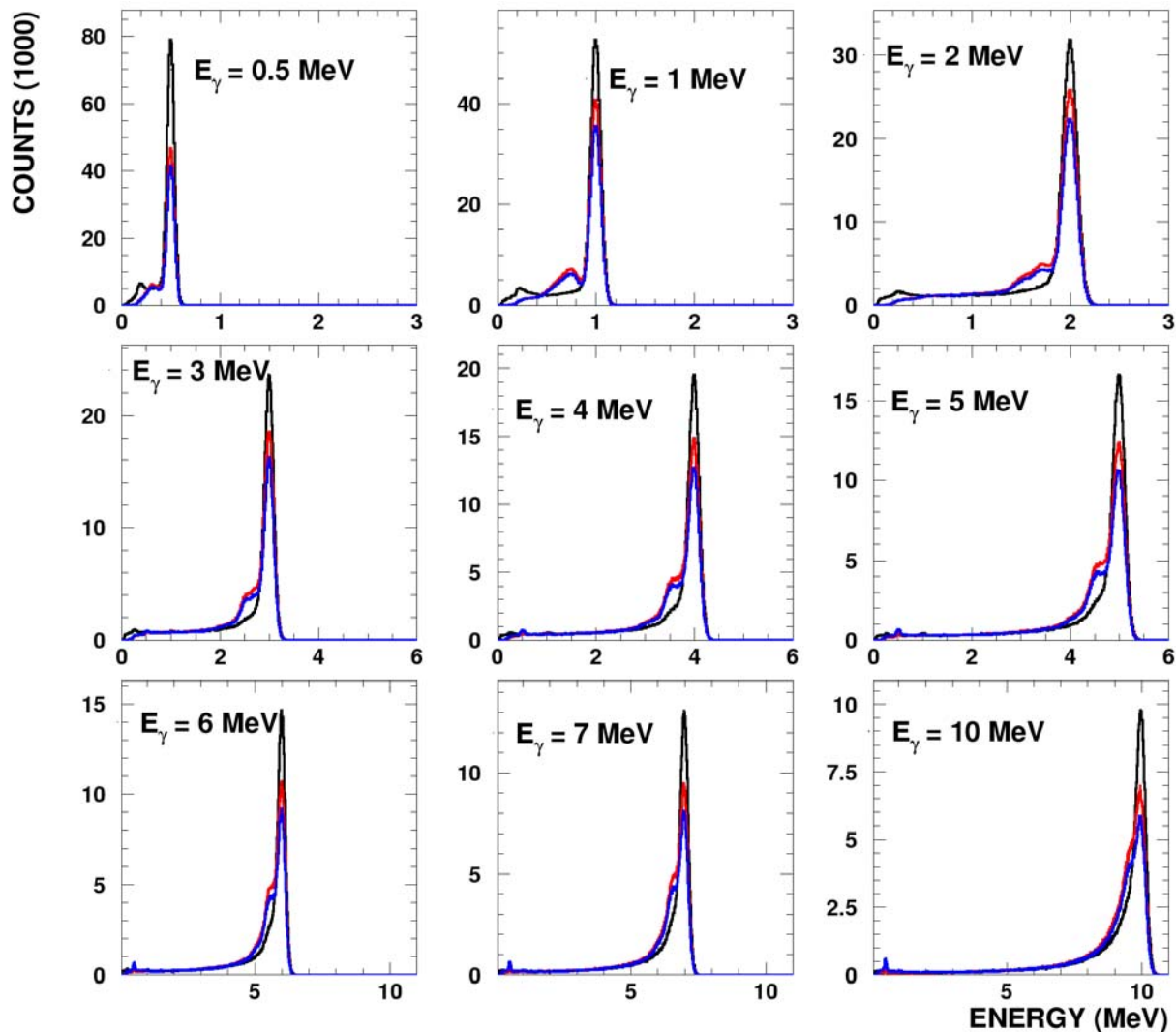


Figure 29: Energy deposit summed over all crystals for γ -energies from 0.5 MeV to 10 MeV. All spectra are without ⁶LiH absorber. The different colors correspond to spectra with 159 crystals with low threshold (**black**), 159 crystals with high threshold (**red**) and 141 crystals with high threshold (**blue**).

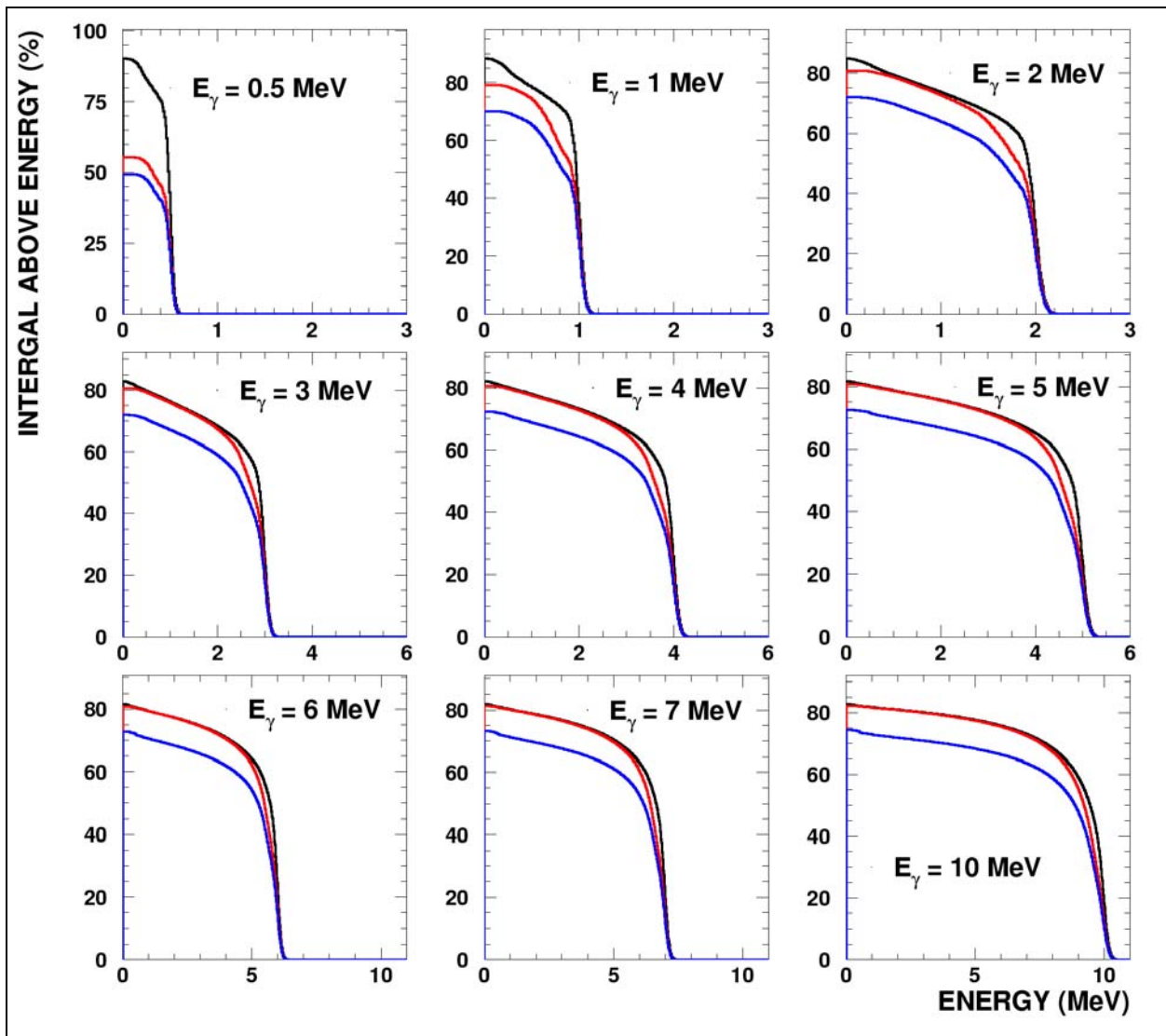


Figure 30: Percentage of counts above a given threshold energy for the spectra shown in Figure 29. The curves are normalized to the number of emitted γ -rays, which means, the value at $E = 0$ MeV reflects the total efficiency of the array.

In the next step the influence of the ${}^6\text{LiH}$ moderator within the optimized setup of 159 crystals and the low threshold was investigated. Figure 31 shows the total energy deposited in the BaF_2 crystals as a function of the primary γ -ray energy with and without the ${}^6\text{LiH}$ moderator in place. The ${}^6\text{LiH}$ moderator slightly reduces the full energy peak. The absorption effect of the ${}^6\text{LiH}$ shell on the γ -rays can be seen in Figure 32 showing the integral of all counts above a given energy threshold.

159 crystals, low threshold

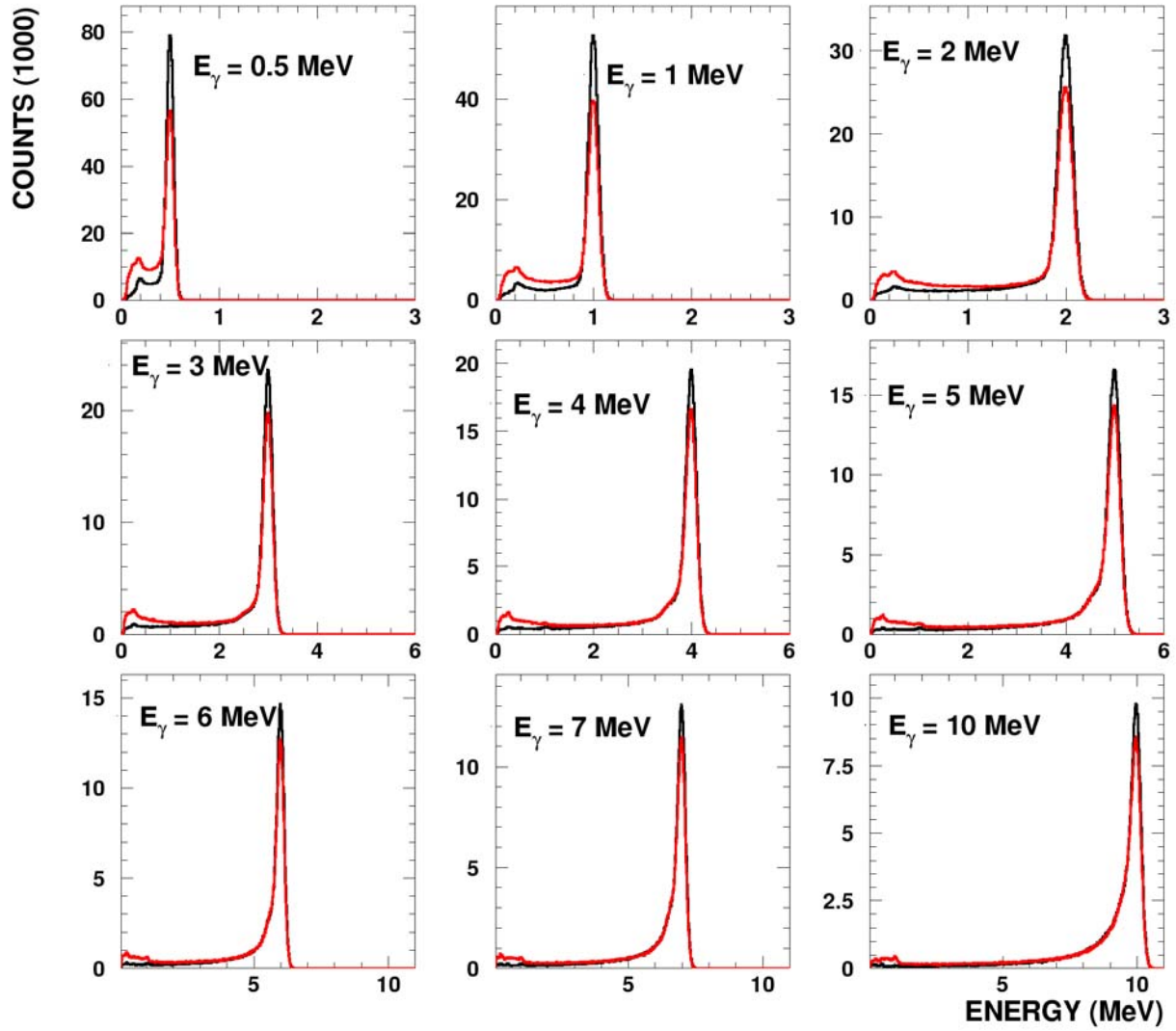


Figure 31: Energy deposit summed over all crystals for γ -energies from 0.5 MeV to 10 MeV. Spectra with (red) and without (black) the ${}^6\text{LiH}$ absorber for 159 crystals and low detector threshold are shown.

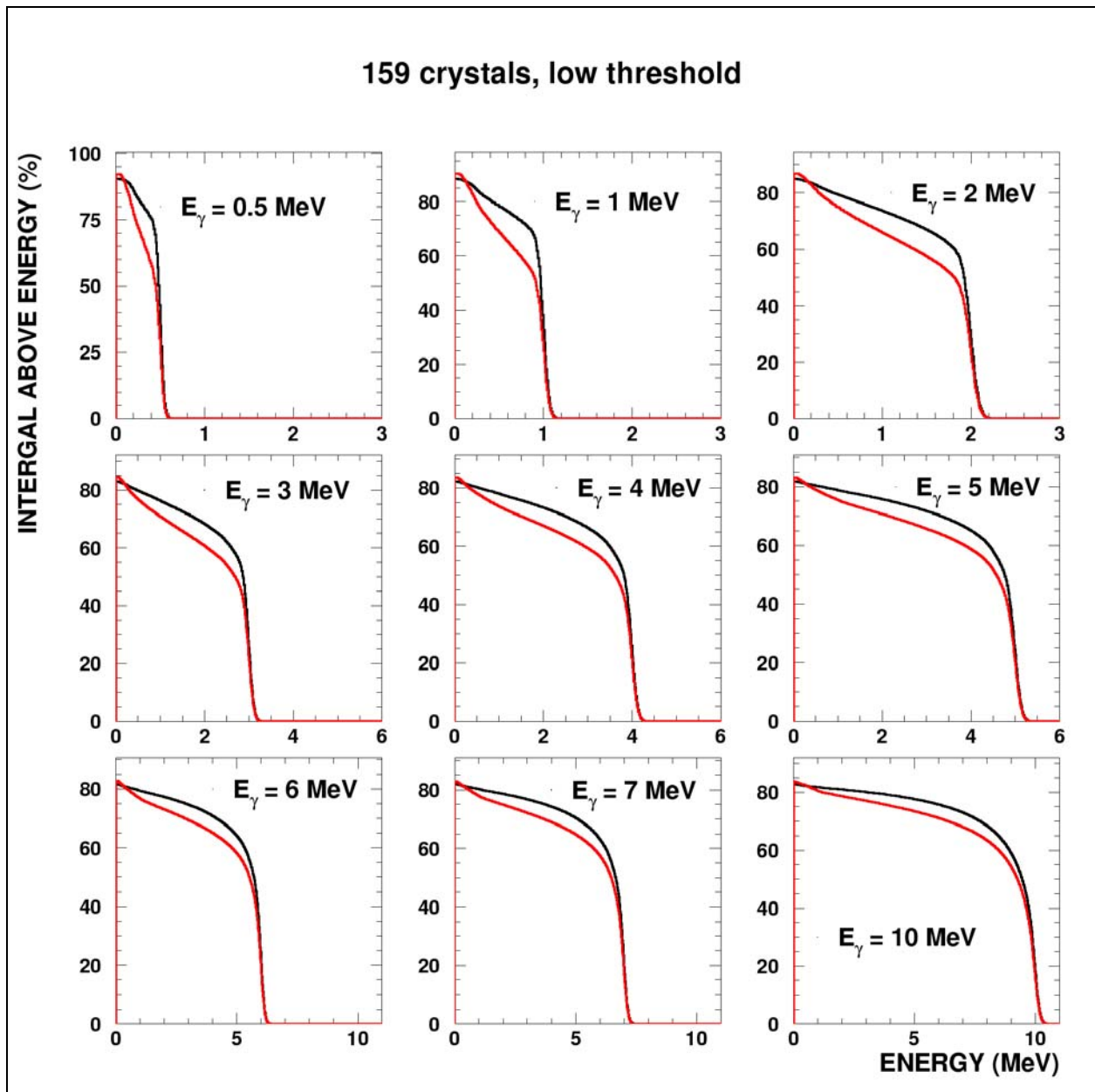


Figure 32: Percentage of counts above a given threshold energy for the spectra shown in Figure 31. The curves are normalized to the number of emitted γ -rays, which means, the value at $E = 0$ MeV reflects the total efficiency of the array.

As discussed in section 3.2, the number of clusters hit per event is much closer to the original γ -ray multiplicity than the number of fired crystals. This holds true also for the setup discussed in this section and is illustrated in Figure 33, showing the cluster multiplicity for single photons of different energies. One effect of the improved setup is a higher detection probability for low energy photons. This results in a higher number of crystals hit per photon and also in a slightly higher averaged cluster multiplicity. But even for the highest energies the probability for creating more than 1 cluster is below 30 %.

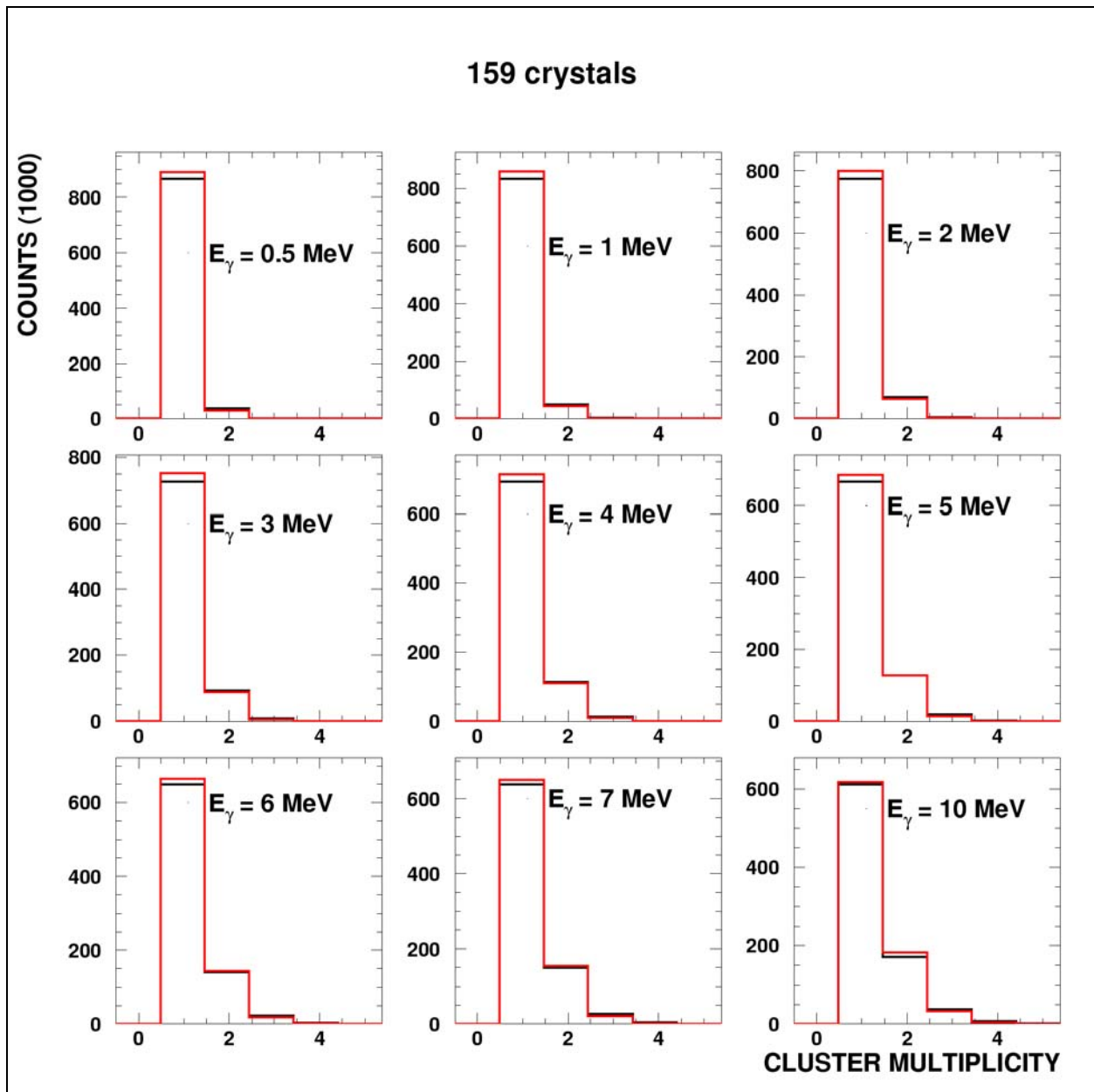


Figure 33: Number of clusters for mono-energetic g-rays of different energies with (red) and without (black) ${}^6\text{LiH}$ -absorber.

Table 3 contains total efficiency information for the 2 optimized setups – 159 crystals, low threshold, with and without ${}^6\text{LiH}$ ball – integrated over all cluster multiplicities as well as only for cluster multiplicity 2 and above.

Table 3: Total efficiency and part of events with cluster multiplicity 2 or higher as a function of energy. All the numbers are relative to the total number of emitted γ -rays.

E_γ (MeV)	total efficiency (%)		part (%) above cluster multiplicity 1	
	without ${}^6\text{LiH}$	with ${}^6\text{LiH}$	without ${}^6\text{LiH}$	with ${}^6\text{LiH}$
0.5	90.3	92.1	4.1	3.1
1	88.3	90.3	5.7	4.9
2	84.9	86.8	8.8	7.8
3	82.9	84.5	12.4	11.2
4	82.1	83.6	15.7	14.5
5	81.7	83.1	18.4	17.4

6	81.6	82.9	20.4	19.6
7	81.9	82.9	22.1	21.6
8	81.9	82.9	22.1	21.6
9	82.1	83.2	23.7	23.4
10	82.7	83.6	26.1	26.2

According to Table 3 the detection efficiency of the important 2.2 MeV background component of the commissioning could be reduced from 85 % to 10 % by applying a cluster multiplicity cut. This would mean, the number of detected events would be reduced by a factor of 8.5, while the reduction for true capture events is much less (see chapter 4.3.2, Figure 18).

4.3 Au(n,γ)

4.3.1 Au cascades

In this section the different steps of optimization will be checked with theoretical gold neutron capture cascades – the type of events the DANCE detector is designed for. Figure 34 shows the three steps of improvement discussed so far. The left part of the figure shows that the peak to valley ratio would be improved by a factor of 2. Taking into account that the peak of the isotope under investigation sits usually on top of background, represented by a valley of events due to captures on barium or other isotopes, this would mean that the signal to background ratio would be improved by a factor of 2. The improvement in detection efficiency above a given threshold is illustrated in the right part of the figure.

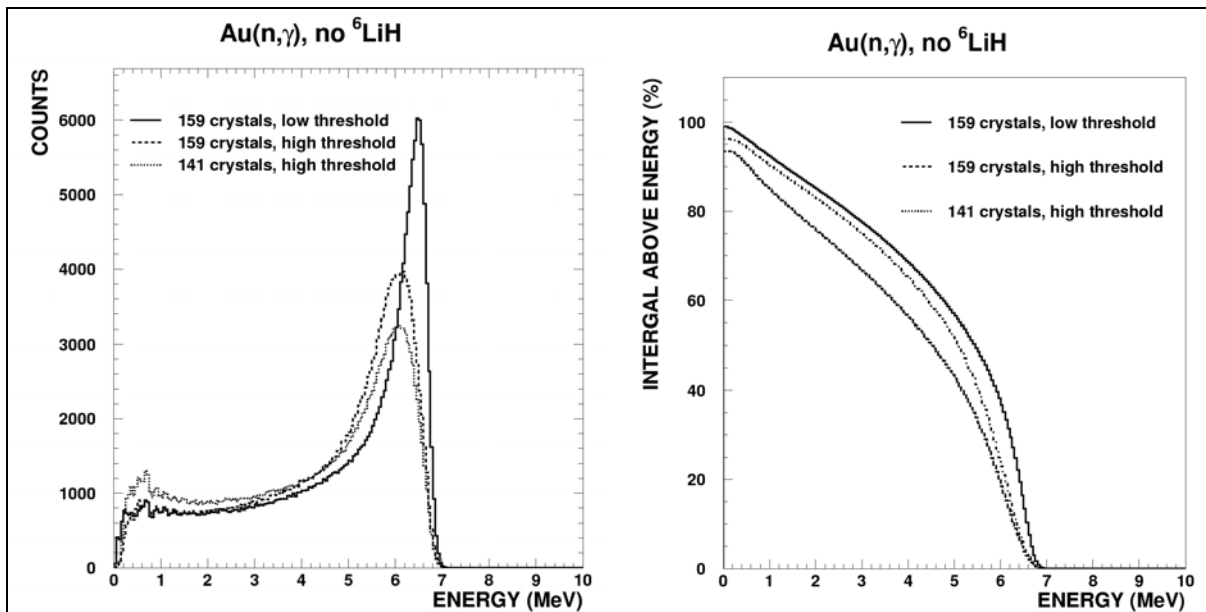


Figure 34: Left: Response of the DANCE array with 141 and 159 crystals as well as low and high single detector thresholds to theoretical gold capture cascades. Right: Percentage of counts above a given threshold energy for the spectra on the left. The curves are normalized to the number of emitted γ -cascades, which means, the value at $E = 0$ MeV reflects the total efficiency of the array.

In order to check the influence of the supporting pieces of the beam cross, a simulation without these pieces has been carried out (Figure 35). These pieces are mounted under 45 degrees to increase the mechanical stability of the beam cross. The cross section of those pieces is $2.55 \times 0.66 \text{ cm}^2$.

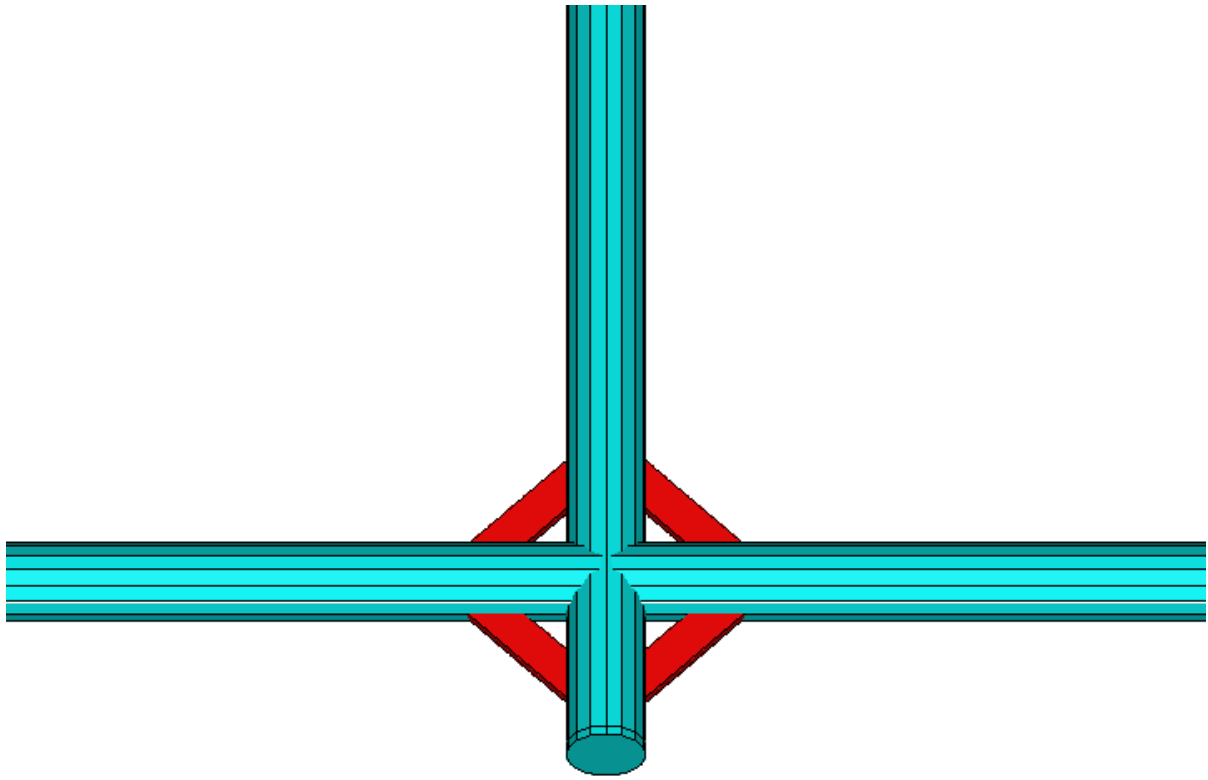


Figure 35: Beam pipe cross (light blue) as well as supporting pieces (red) as simulated. The surrounding DANCE ball is not shown. The sample position is in the middle of the cross. Neutrons are traveling horizontally.

The results are shown in Figure 36 and lead to the conclusion that there is only a minor effect on the peak to valley ratio due to the supporting pieces.

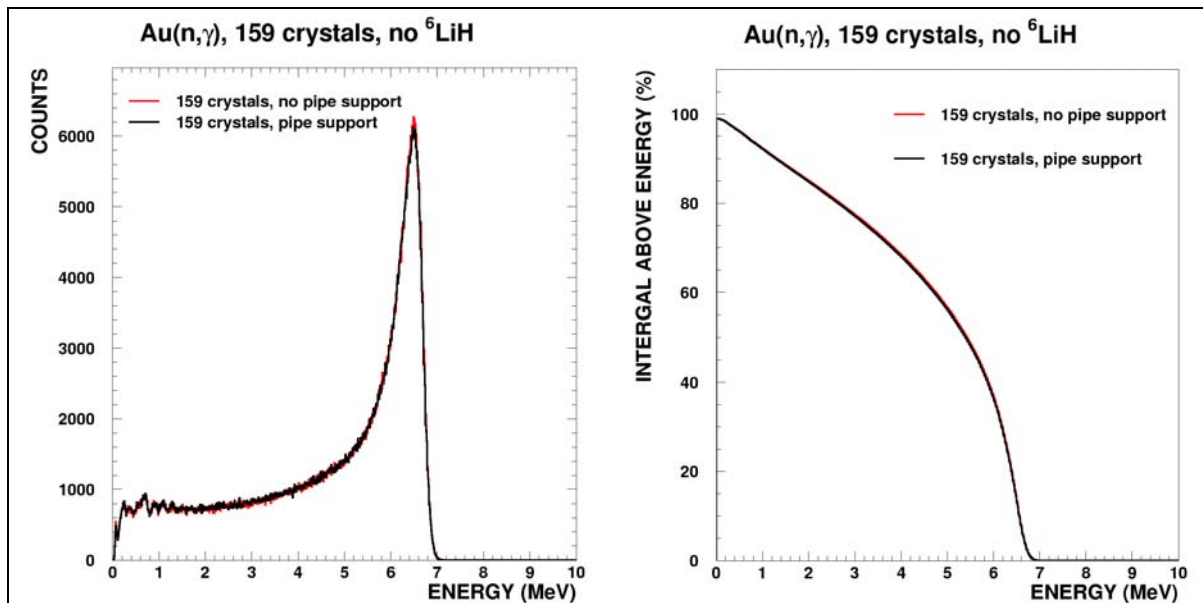


Figure 36: Left: Response of the DANCE array with 159 crystals and low single detector thresholds to theoretical gold capture cascades with and without additional supports for the beam pipe crossing. Right: Percentage of counts above a given threshold energy for the spectra on the left. The curves are normalized to the number of emitted γ -cascades, which means, the value at $E = 0$ MeV reflects the total efficiency of the array.

In order to show the potential of future improvements, an idealized setup has been simulated too. Figure 37 shows the comparison of the best realistic setup (see Figure 34) with a setup consisting of 162 crystals, no gap between the crystals and with and without a beam pipe. A geometry with

162 crystals does not leave space for a real beam pipe, the effect shown is only due to a small tube of aluminum in the center of the detector. This clearly shows that low-energy gammas are absorbed in the pipe

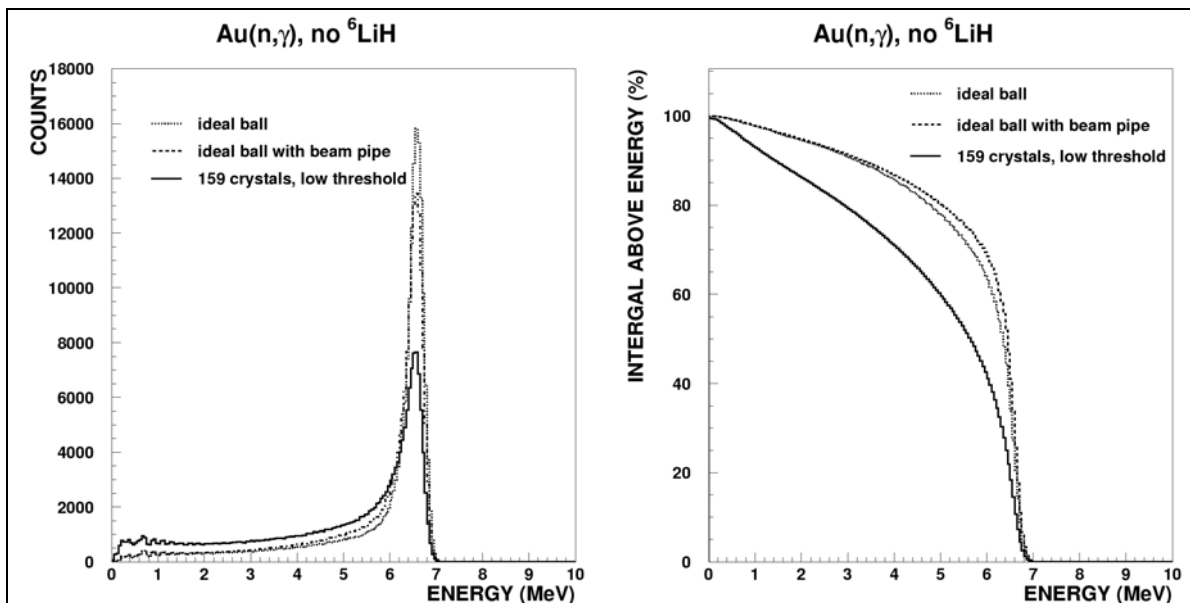


Figure 37: Left: Response of the DANCE array with 159 and 162 crystals with and without beam pipe to theoretical gold capture cascades. Right: Percentage of counts above a given threshold energy for the spectra on the left. The curves are normalized to the number of emitted γ -cascades, which means, the value at $E = 0$ MeV reflects the total efficiency of the array.

The last step was to investigate the influence of the ${}^6\text{LiH}$ moderator in the optimized setup. The left part of Figure 38 shows the resulting in a peak reduction of 30 %. This a slightly worse reduction than for the setup with 141 crystals (see Figure 16), but the setup discussed here has the same peak height *with* the ${}^6\text{LiH}$ moderator as the 141 crystal setup *without*.

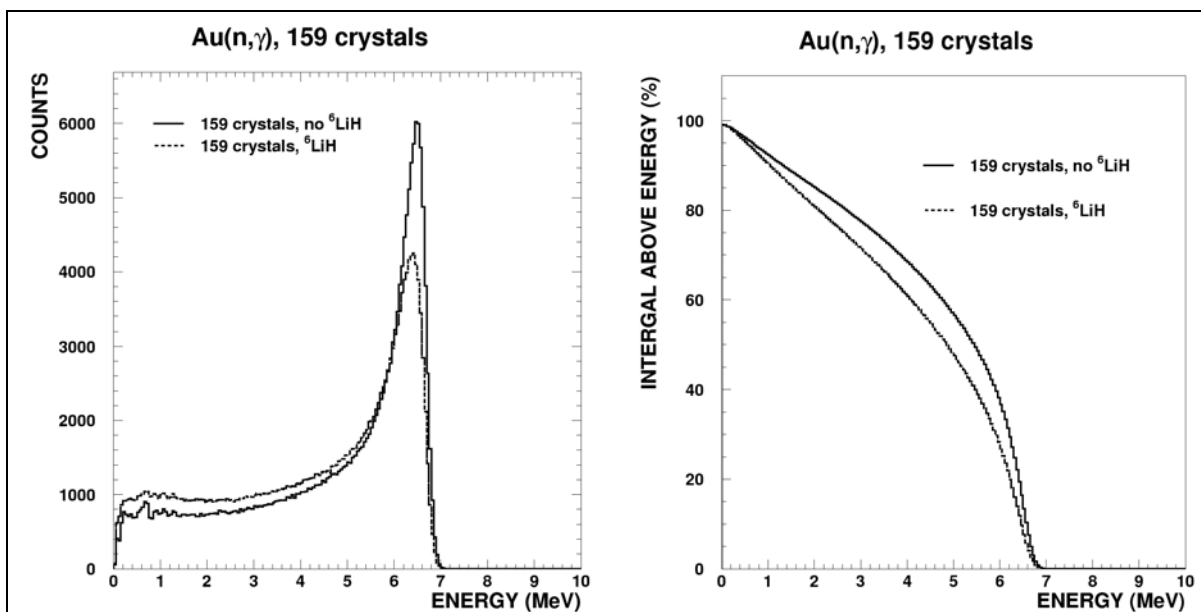


Figure 38: Left: Response of the DANCE array with 159 crystals and low single detector thresholds to theoretical gold capture cascades. Right: Percentage of counts above a given threshold energy for the spectra on the left. The curves are normalized to the number of emitted γ -cascades, which means, the value at $E = 0$ MeV reflects the total efficiency of the array.

4.3.2 Neutrons on Au

As illustrated in section 3.3.2 a significant reduction of the background due to scattered neutrons is the expected gain of using the ${}^6\text{LiH}$ moderator. The ${}^6\text{LiH}$ moderator results in a 30 % reduction of the full energy peak of the gold cascades as shown in the preceding section. Figure 39 corresponds to 10^7 simulated neutrons emitted 20 m away from the center of the ball towards the sample. The gold sample at the sample position was 1 cm in diameter and 0.2 mm thick. The emitted neutron spectrum was a typical $1/E$ moderated spallation spectrum. The simulations have been carried out for incident neutron energies from 1 eV up to 100 MeV. The left part of Figure 39 shows the results for neutrons between 10 and 100 keV without the ${}^6\text{LiH}$ moderator in place, while the right part shows the result for the same setup with the ${}^6\text{LiH}$ moderator in place. Obviously the signal to background ratio increased again significantly, even though the full energy peak of gold is broadened due to partial absorption of the emitted capture photons.

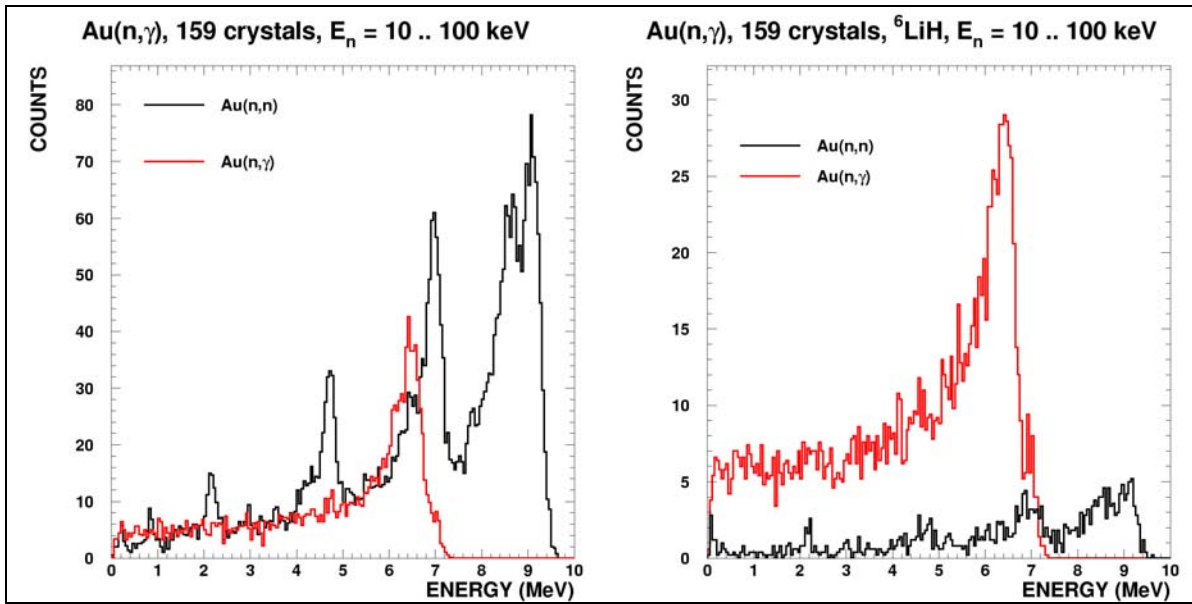


Figure 39: Response of the DANCE array with 159 crystals and low detector threshold to neutron reactions on a gold sample. The red line corresponds to events due to captures on a gold sample, the black curve to events due to neutrons scattered at the gold sample. The neutron energy 10 ..100 keV. The left picture shows the results without ${}^6\text{LiH}$ absorber, while the right picture corresponds to the standard ${}^6\text{LiH}$ absorber in place.

Table 4 contains the ratio of events due to neutron scatter on the sample to events due to neutron capture. According to these simulations, a significant background reduction is to be expected for lower energies, while for neutron energies of 100 keV or above the reduction is not as strong anymore. The reduction factor varies from 150 to 5 depending on the neutron energy.

Table 4: Ratio of events from scattered neutrons and capture events on the sample for different setups. The last column is for events with $E_{\text{tot}} > 1$ MeV only, while all other ratios correspond to the total number of detected events.

Setup	Ratio between scattered and captured events for different neutron energy regions.			
	0.1 .. 1 keV	1 ..10 keV	10 .. 100 keV	0.1 .. 1 MeV
159 crystals, low threshold, no ${}^6\text{LiH}$	0.52	1.45	2.7	11.5
159 crystals, low threshold, ${}^6\text{LiH}$	0.0035	0.024	0.20	2.3
159 crystals, ratio without/with ${}^6\text{LiH}$	149	60	13.5	5

As mentioned in previous sections, a cluster multiplicity cut would reduce background due to internal decays as well as from single γ -rays significantly. Figure 40 to Figure 44 illustrate that this holds true even for events due to scattered neutrons, which are eventually captured in the BaF₂ crystals. Since all the photons after a neutron capture in one of the crystals are emitted within this crystal, such an event tends to form only one big cluster, rather than 2 or more small clusters like capture events on the sample. The right part of Figure 40 shows that applying a cluster multiplicity threshold of 2 would reduce the number of background events by 50 %, while more than 85 % of the sample-captures would still be counted. This means that applying this kind of multiplicity cut is slightly more efficient with the optimized setup than with the 141 crystals setup. Especially in the higher neutron energy regime between 0.1 and 1 MeV, where the ratio between scatter and capture cross section is worst, a cluster multiplicity cut might be the only way of discriminating background due to scattered neutrons.

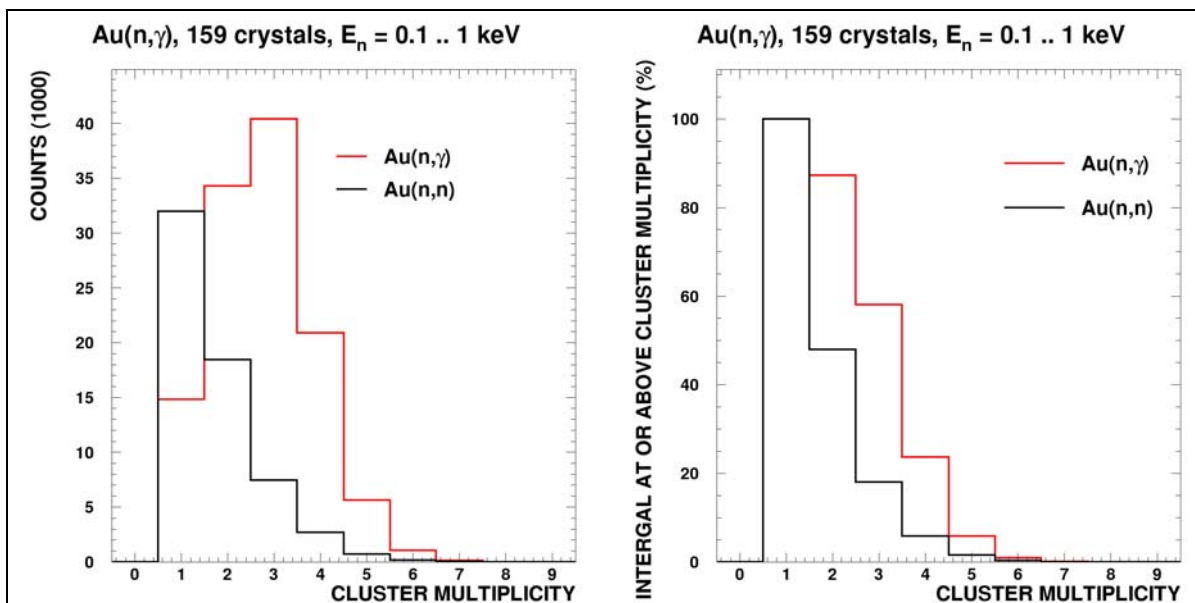


Figure 40: Left: Number of clusters for capture-events (red) and for scattered events (black) for neutron energies between 0.1 and 1 keV. Right: Corresponding percentage of counts for at least a given number of clusters.

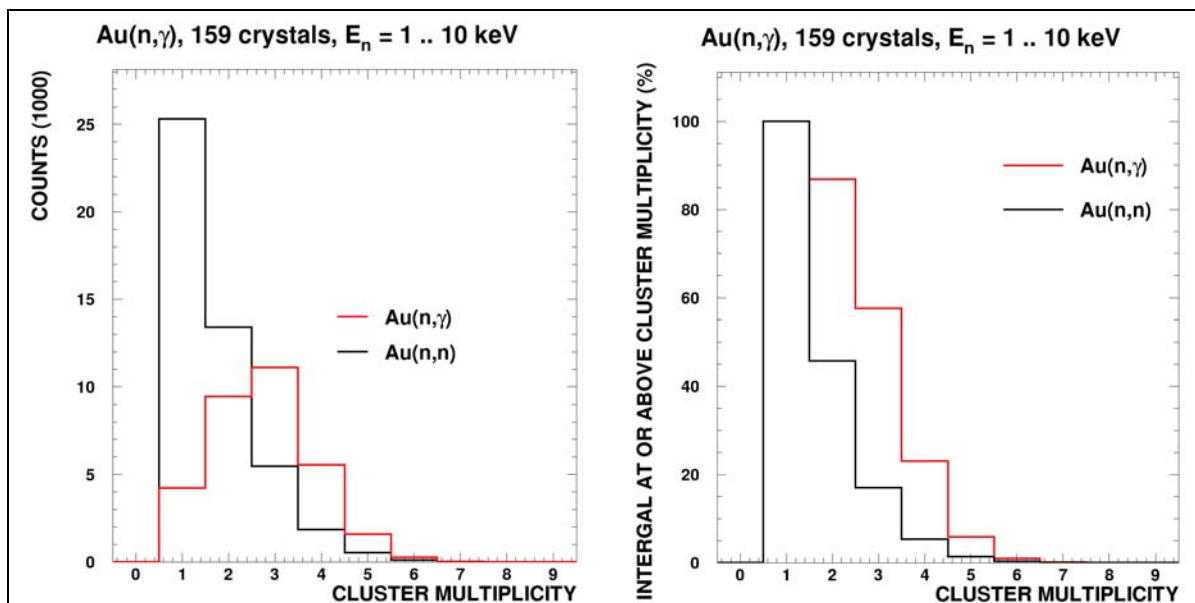


Figure 41: Left: Number of clusters for capture-events (red) and for scattered events (black) for neutron energies between 1 and 10 keV. Right: Corresponding percentage of counts for at least a given number of clusters.

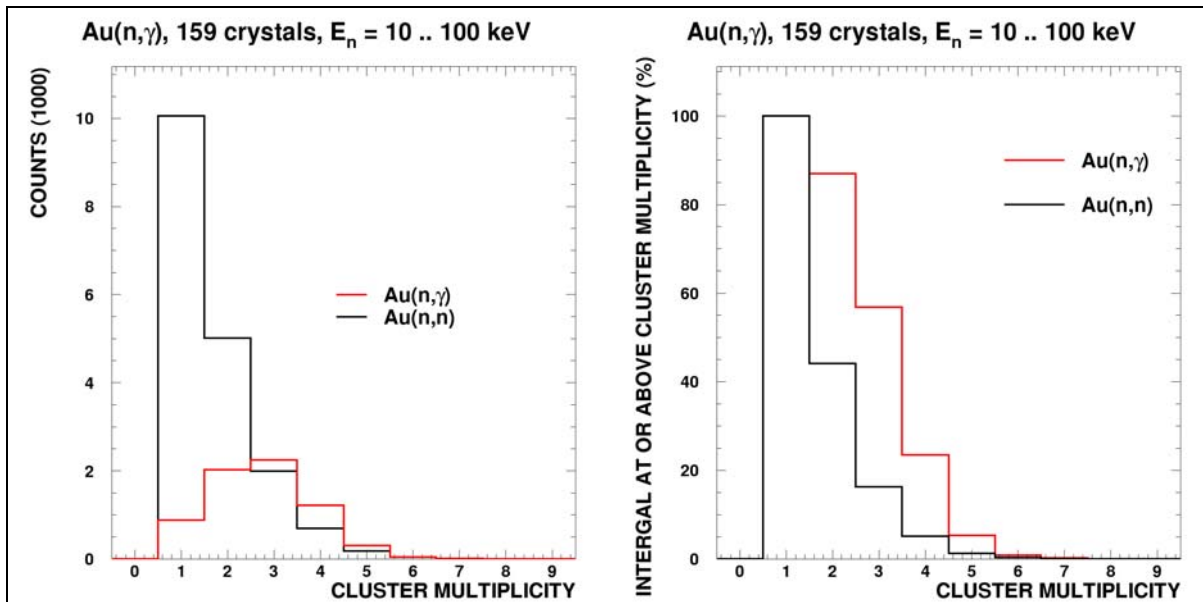


Figure 42: Left: Number of clusters for capture-events (**red**) and for scattered events (**black**) for neutron energies between 10 and 100 keV. Right: Corresponding percentage of counts for at least a given number of clusters.

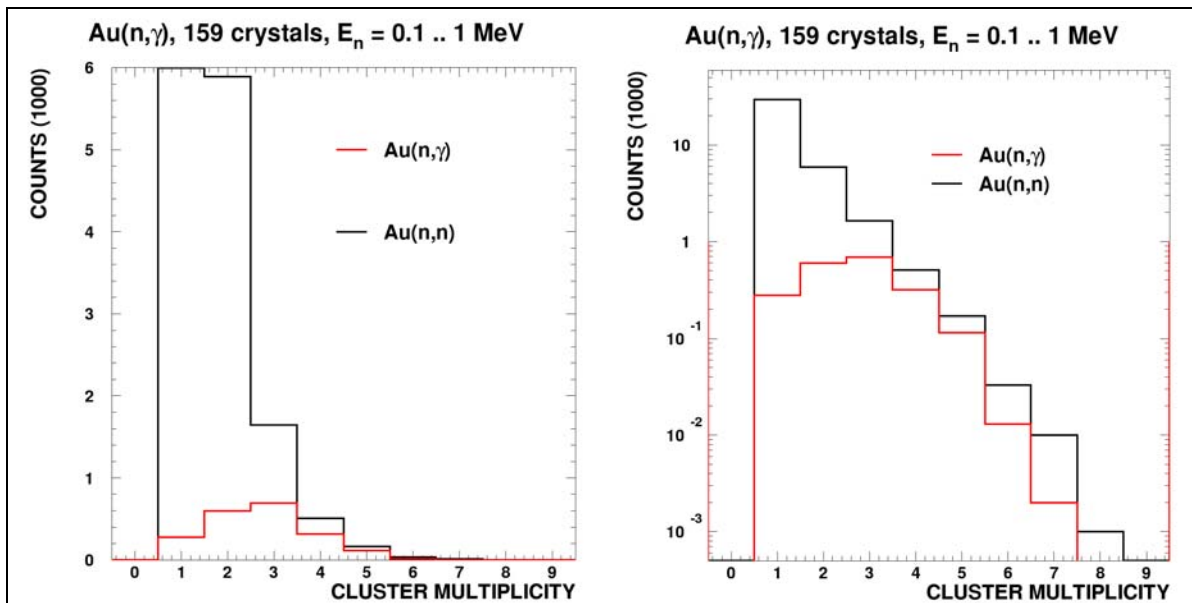


Figure 43: Left: Number of clusters for capture-events (**red**) and for scattered events (**black**) for neutron energies between 0.1 and 1 keV. The y-axis is expanded in order to increase the visibility. Right: Same as left, but without y-axis expansion and logarithmic y-axes.

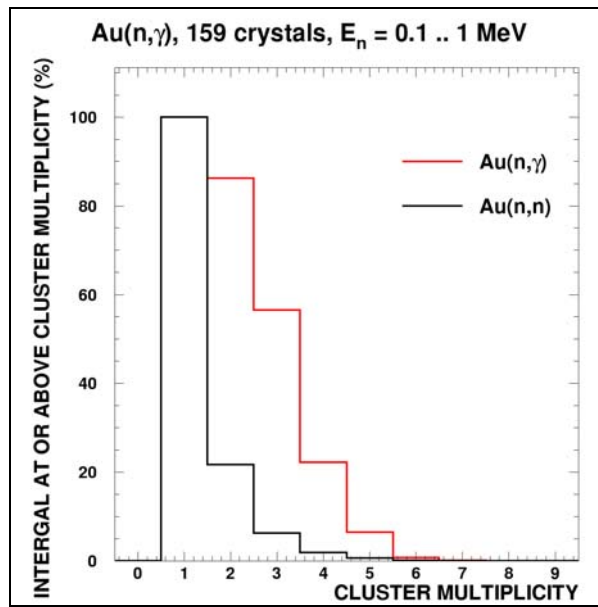


Figure 44: Percentage of counts equals or above a given number of clusters for the spectra shown in Figure 43. The numbers are normalized to the total number of detected events, respectively.

5 Neutron reactions with surrounding material

In order to determine the cause of the neutron induced background discovered during the commissioning runs 2002/2003 a set of simulations including a simplified housing around the detector has been carried out. The background observed turned out to be independent from the size of our generally small samples used during these experiments. This leads immediately to the idea that windows or other pieces of equipment in the beam might cause this background. The first set of simulations have been carried out with a symmetric housing consisting of walls and ceiling made of 5% borated polyethylene (BPE), a floor made of concrete, and a lead block at the entrance of the housing (see Figure 45). Three different window positions have been simulated:

- 1 m downstream of the sample; at approximately this position was a window of 10 mil (0.25 mm) aluminum in the beam
- 1 m upstream of the sample; a 1/8 inch (3.2 mm) aluminum window was just at the reduction of the beam pipe close to the walls of the housing
- 1.5 m upstream of the sample; this simulation has been carried out in order to check the effect of the possible shielding of the scattered neutrons by the combination of 5% BPE wall and the lead block.

All the simulations were carried out with 159 crystals and low thresholds. The reason for this was that the main conclusion should not depend strongly on those settings and the results gained in this way are probably valid also for future experiments, which will be carried out with the higher number of crystals etc. Furthermore, no ${}^6\text{LiH}$ moderator has been taken into account. The influence of this moderator on the background caused by neutron scattering on the sample was shown in the previous chapters. There is no influence of the moderator on the background caused by neutrons scattered on aluminum windows outside the ball expected.

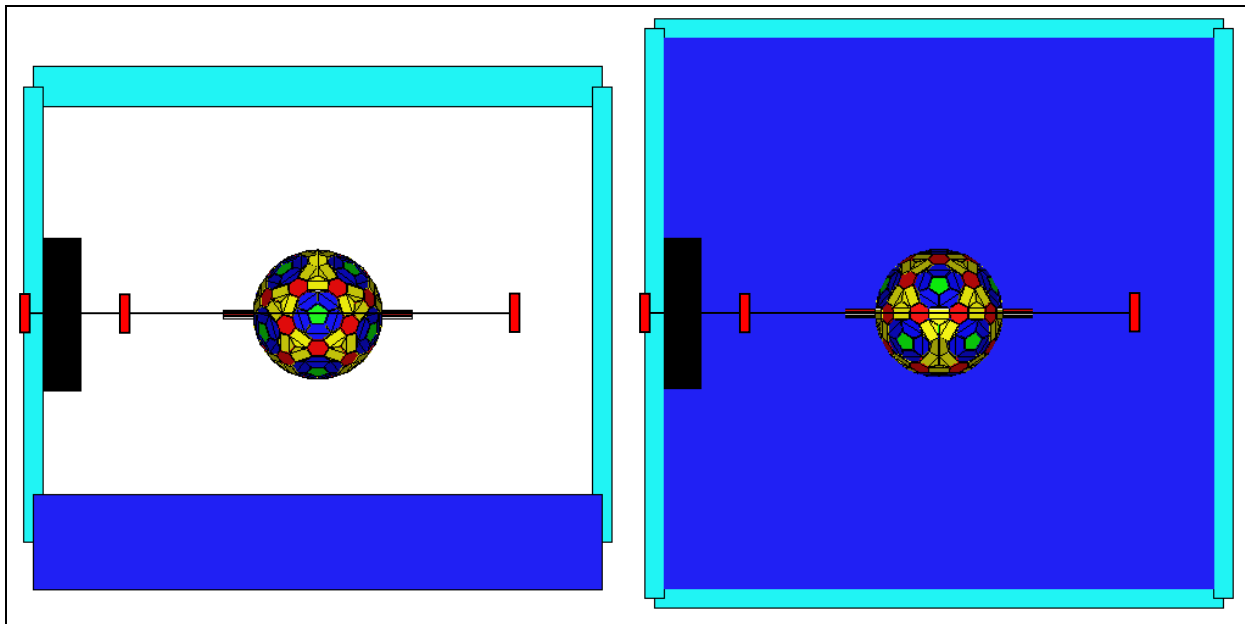


Figure 45: Schematic view of the simulated setup. The neutrons are coming from the left in both pictures. The left part shows a side view (side walls are not drawn) and the right part a view from the top. The light blue corresponds to 5% BPE walls, dark blue to the concrete floor and black to the lead shielding at the end of the beam pipe. The red rectangles mark the 3 different positions of the aluminum windows. The size of the windows is not to scale.

Figure 46 and Figure 47 show the result of simplified simulations. Since the observed experimental spectra show a peak around 2 MeV, a possible explanation would have been capture of scattered neutrons on hydrogen in the walls. The figures show the result of neutrons of different energies isotropically emitted 1 m downstream of the sample. Figure 46 shows the result for walls made of 5% BPE, while Figure 47 shows the same for 30 % BPE.

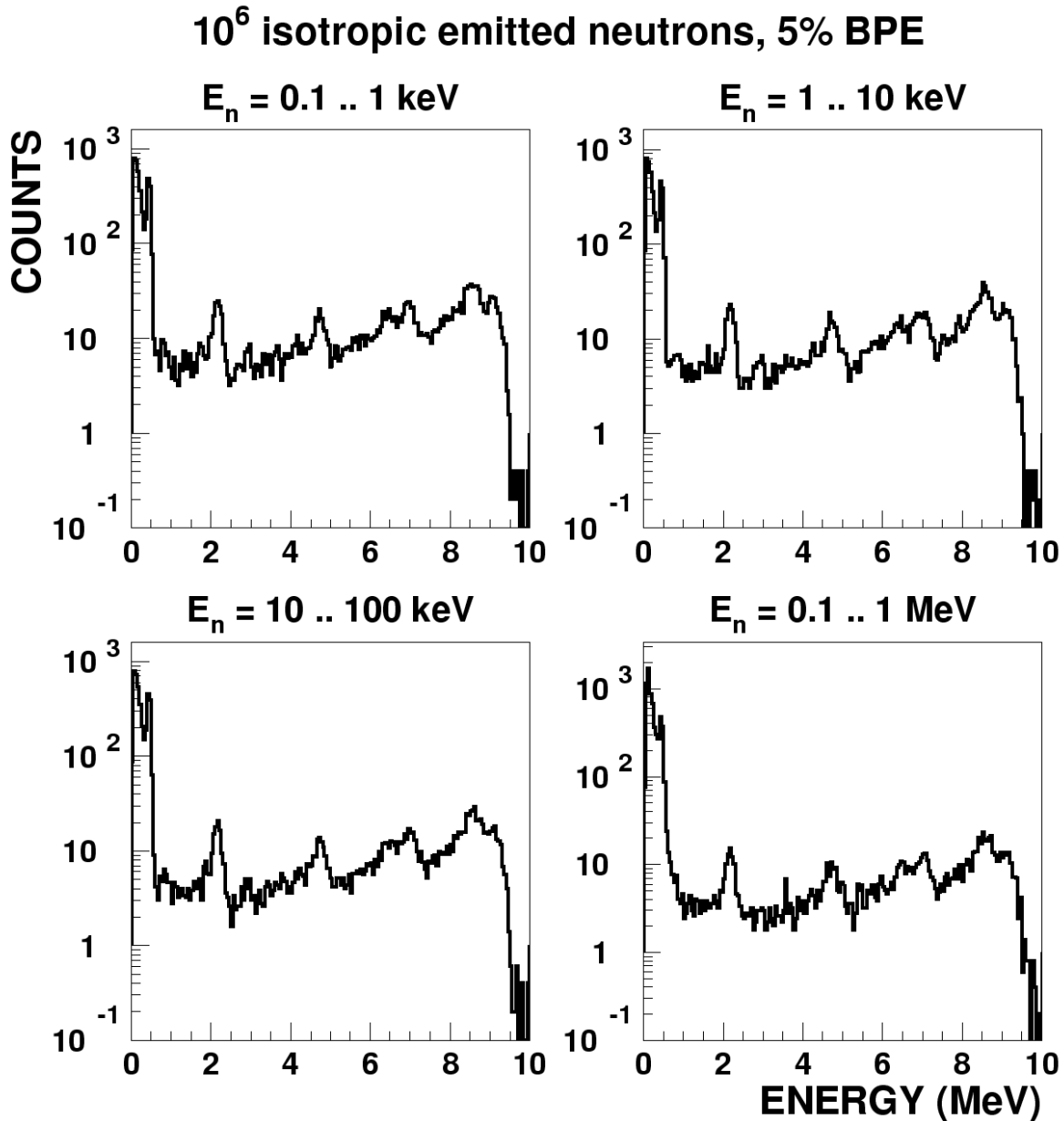


Figure 46: Background caused by 10^6 neutrons per energy interval, emitted 1 m downstream of the center of the crystal ball. The different peaks correspond to neutron captures on even, odd Ba isotopes, H, B (from right). The surrounding housing consists of 5% BPE.

Comparing the results for 5% BPE and 30% BPE one has to conclude that

- a) the 2.2 MeV peak due to neutron capture on hydrogen reduces slightly with increasing the boron content in the walls,
- b) the size of the 2.2 MeV peak compared to the peaks due to captures on barium, appearing at higher energies in the spectrum, is much smaller than experimentally observed.

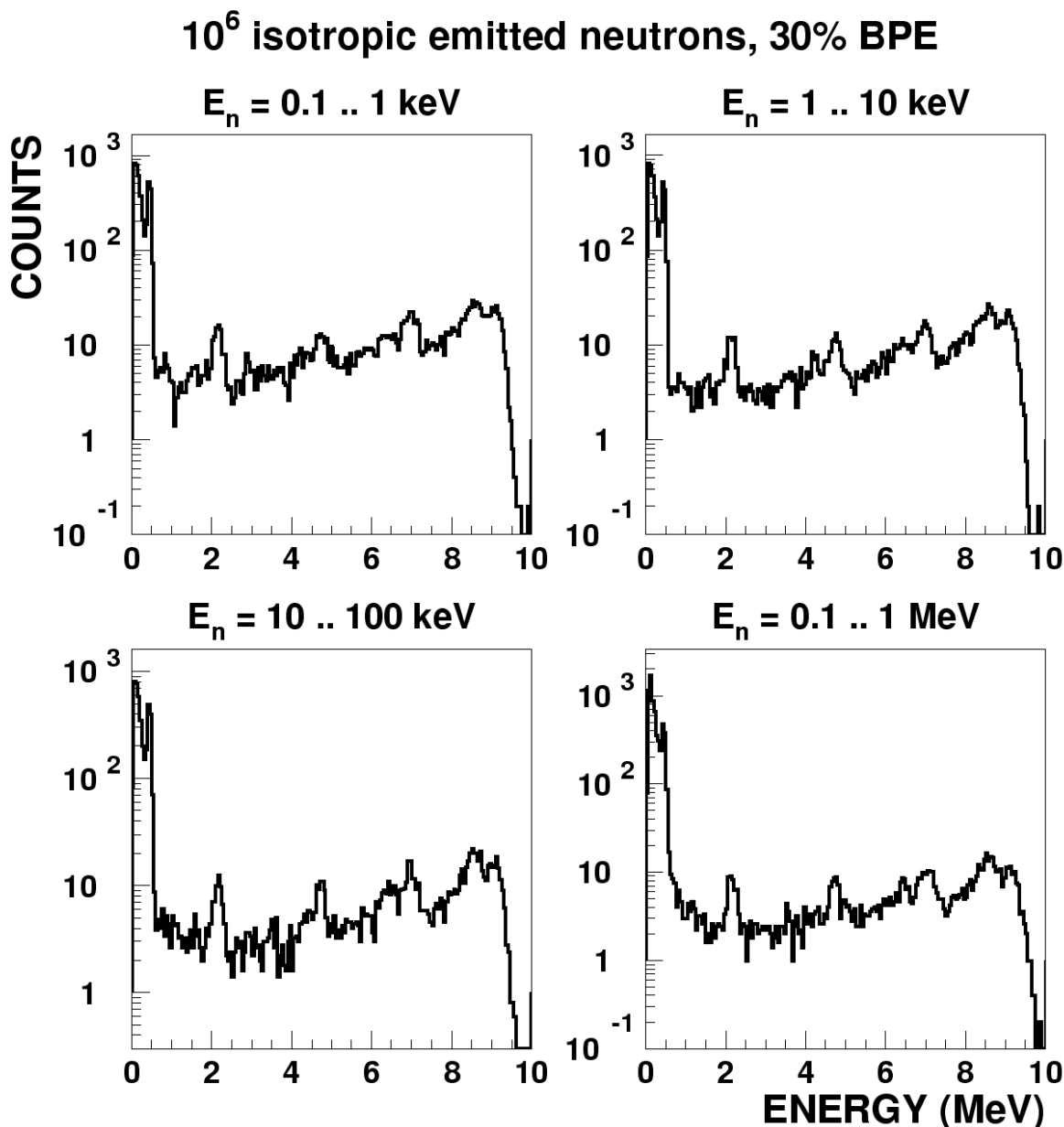


Figure 47: Background caused by 10^6 neutrons per energy interval, emitted 1 m downstream of the center of the crystal ball. The different peaks correspond to neutron captures on even, odd Ba isotopes, H, B (from right). The surrounding housing consists of 30% BPE.

Furthermore, the background region below 2.5 MeV depends on the sample size. This means, simulations as well as experimental data suggest a different origin of the background above and below 2.5 MeV.

Figure 48, and Figure 49 show the results for a 3.2 mm aluminum window and a 2 μ m gold sample. The window was 1 m and 1.5 m upstream of the sample, respectively. Figure 50 shows the results for a 0.25 mm aluminum window and a 2 μ m gold sample.

3.18 mm Al, 1 m upstream; 2 μm Au sample

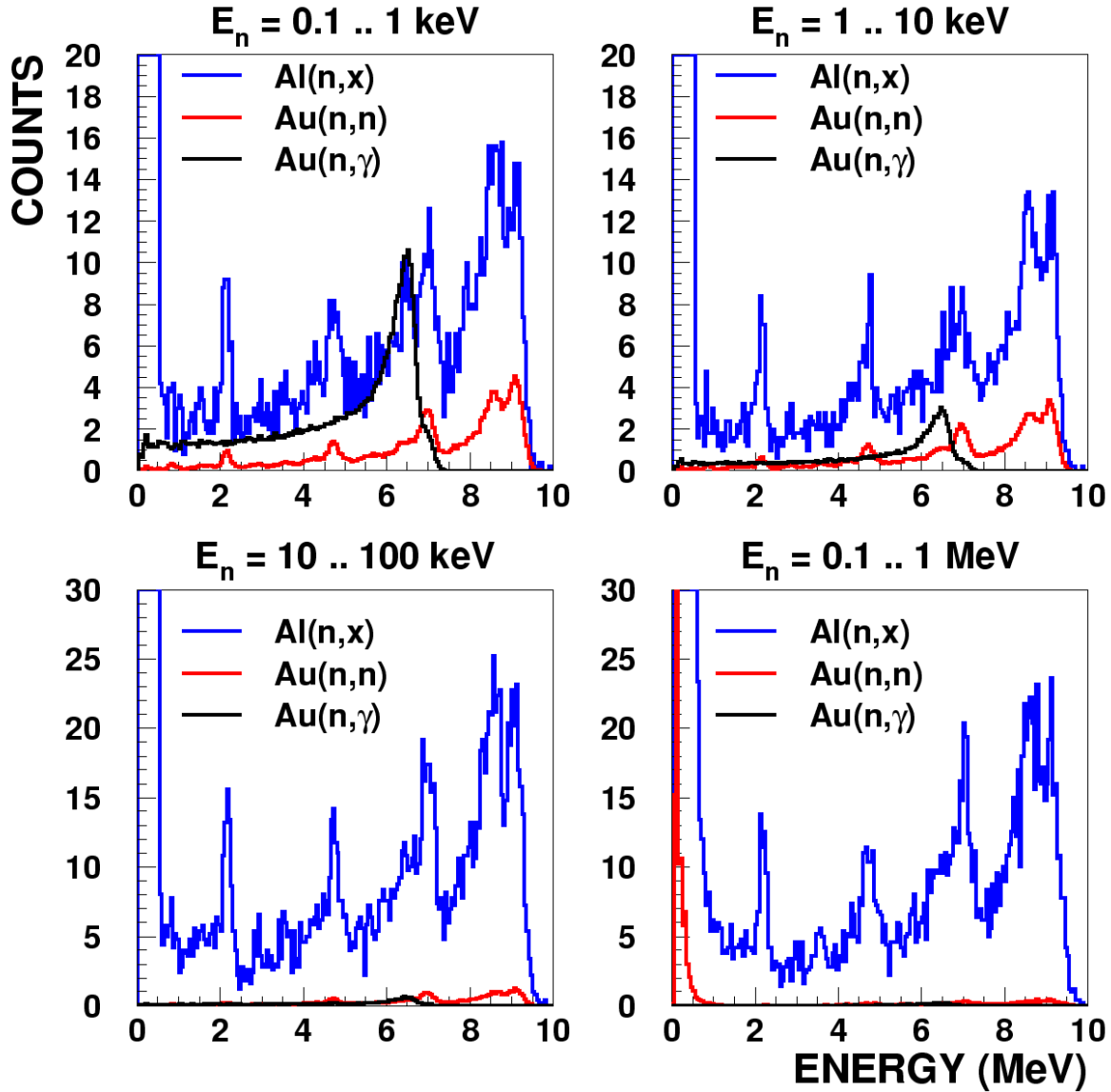


Figure 48: Comparison between a 3.18 mm (1/8 inch) aluminum window (blue) positioned 1 m upstream of the sample with neutron capture events (black) as well as neutron scatter events (red) on a 0.002 mm gold sample in the center of the crystal ball. Al(n,x) means that all reactions which eventually deposit energy in the BaF₂ crystals are included. These reactions are mainly Al(n, γ) and Al(n,n).

3.18 mm Al, 1.5 m upstream; 2 μm Au sample

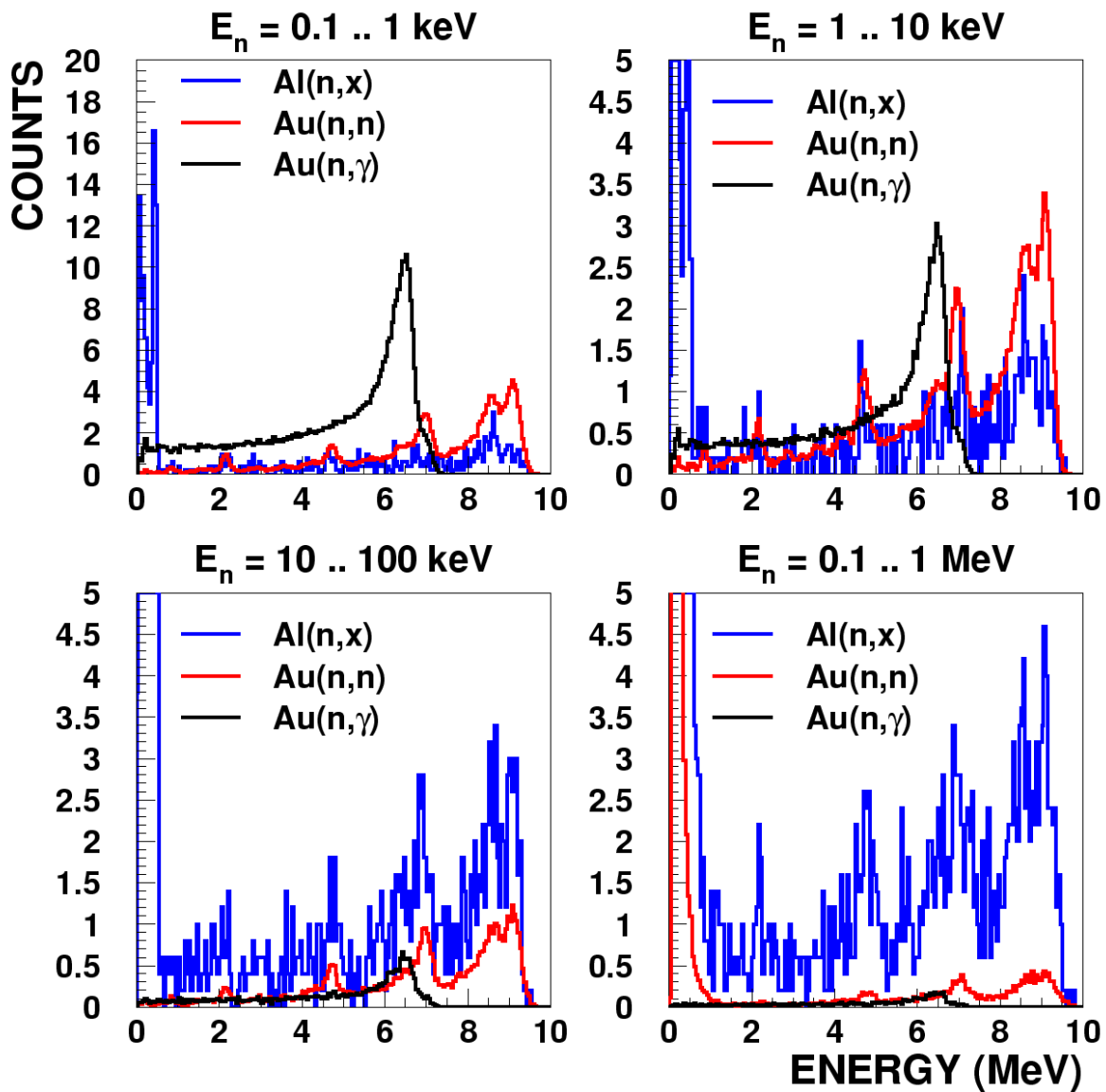


Figure 49: Comparison between 3.18 mm (1/8 inch) aluminum window (blue) positioned 1.5 m upstream of the sample with neutron capture events (black) as well as neutron scatter events (red) on a 0.002 mm gold sample in the center of the crystal ball.

0.25 mm Al, 1 m downstream; 2 μm Au sample

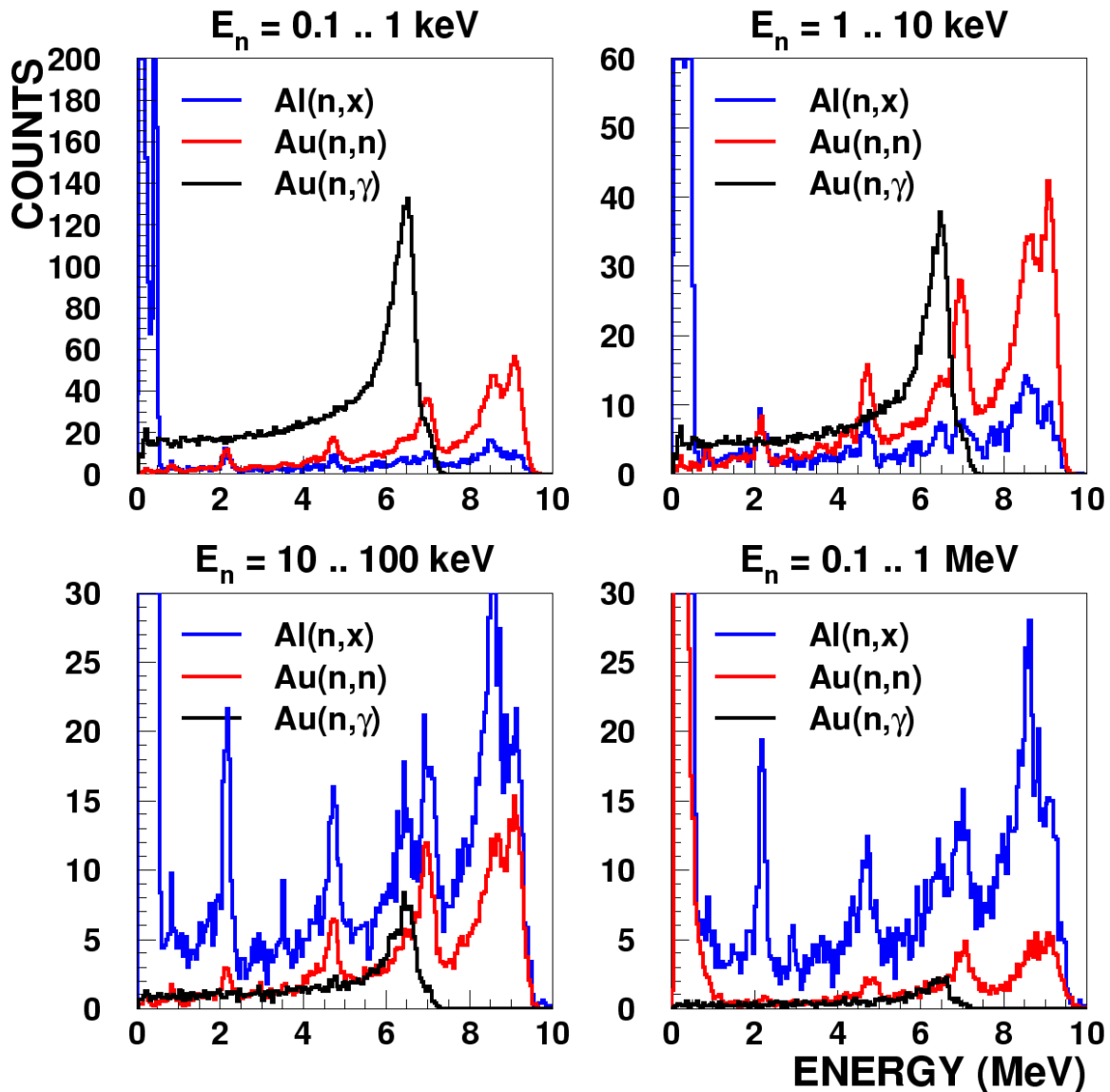


Figure 50: Comparison between a 0.25 mm (10 mil) aluminum window (blue) positioned 1 m downstream of the sample with neutron capture events (black) as well as neutron scatter events (red) on a 0.002 mm gold sample in the center of the crystal ball.

Moving the window from 1 m to 1.5 m upstream – which means from inside to outside the housing respectively – reduces the background caused by the aluminum window significantly. But even in the latter case, the background above 10 keV neutron energies is dominated by the aluminum window.

Since the downstream window is much thinner than the upstream one, the background is considerably less. But even this thin window dominates over the sample-related background for neutron energies above 10 keV neutron energy.

The real geometry in the shed is not symmetric as simulated above. In order to investigate the influence of a asymmetric position of the ball inside the housing a similar set of simulations as above has been carried out with a different position of the DANCE array inside the BPE-housing. The crystal ball has been moved 0.5 m upstream and 0.5 m to the left (looking in flight direction) relative to the center of the housing (see Figure 51). The following window positions have been investigated:

- 1 m downstream of the sample, and
- 0.7 m, 0.8 m, and 1 m upstream of the sample in order to investigate the influence of the wall and the lead block.

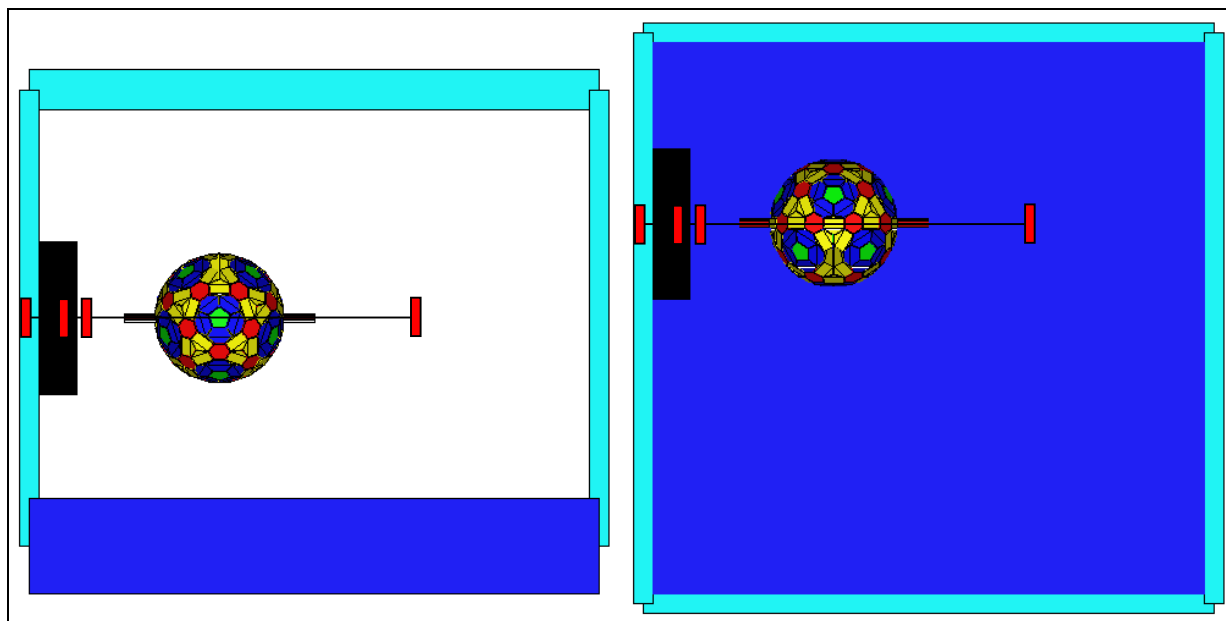


Figure 51: Schematic view of the simulated setup. The neutrons are coming from the left in both pictures. The left part shows a side view (side walls are not drawn) and the right part a view from the top. The light blue corresponds to 5% BPE walls, dark blue to the concrete floor and black to the lead collimator at the end of the beam pipe. The red rectangles mark the 4 different positions of the aluminum windows. The size of the windows is not on scale for visibility reasons.

A first test was again a set of simulations with isotropically emitted neutrons 1 m downstream of the sample (Figure 52) . Comparing the results with the symmetric case (Figure 46 and Figure 47) shows no significant change.

10^6 isotropic emitted neutrons, 5% BPE, asymmetric

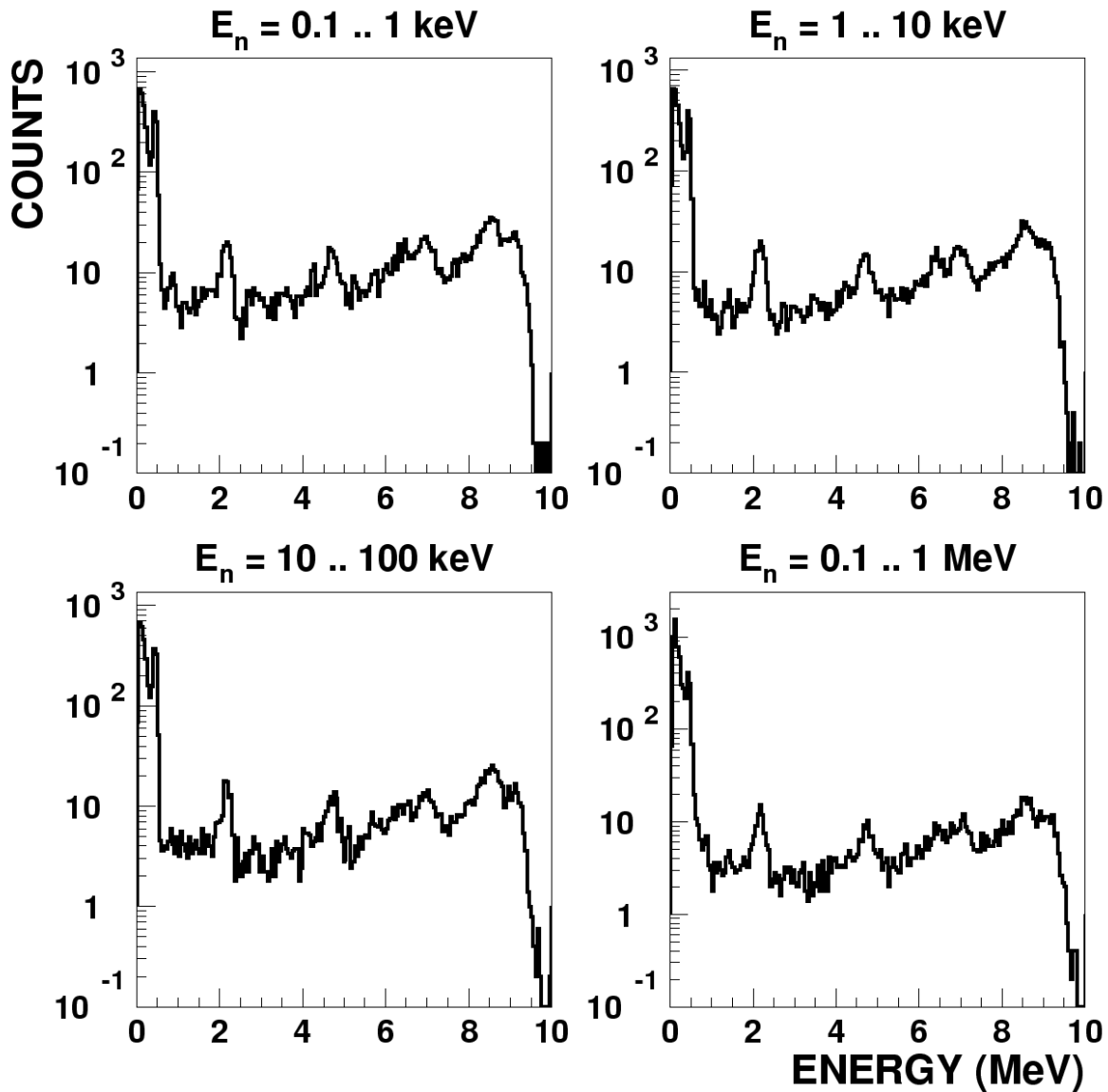


Figure 52: Background caused by 10^6 neutrons per energy interval, emitted 1 m downstream of the center of the crystal ball. The different peaks correspond to neutron captures on even, odd Ba isotopes, H, B (from right). The surrounding housing consists of 5% BPE. The ball is asymmetrically positioned inside the shed.

Figure 53, Figure 54, and Figure 55 show the results for a 3.2 mm aluminum window and a $2 \mu\text{m}$ gold sample. The window was 1 m, 0.8 m, and 0.7 m upstream of the sample, respectively. Figure 56 shows the results for a 0.25 mm aluminum window and a $2 \mu\text{m}$ gold sample.

3.18 mm Al, 1 m upstream; 2 μ m Au sample; asymmetric

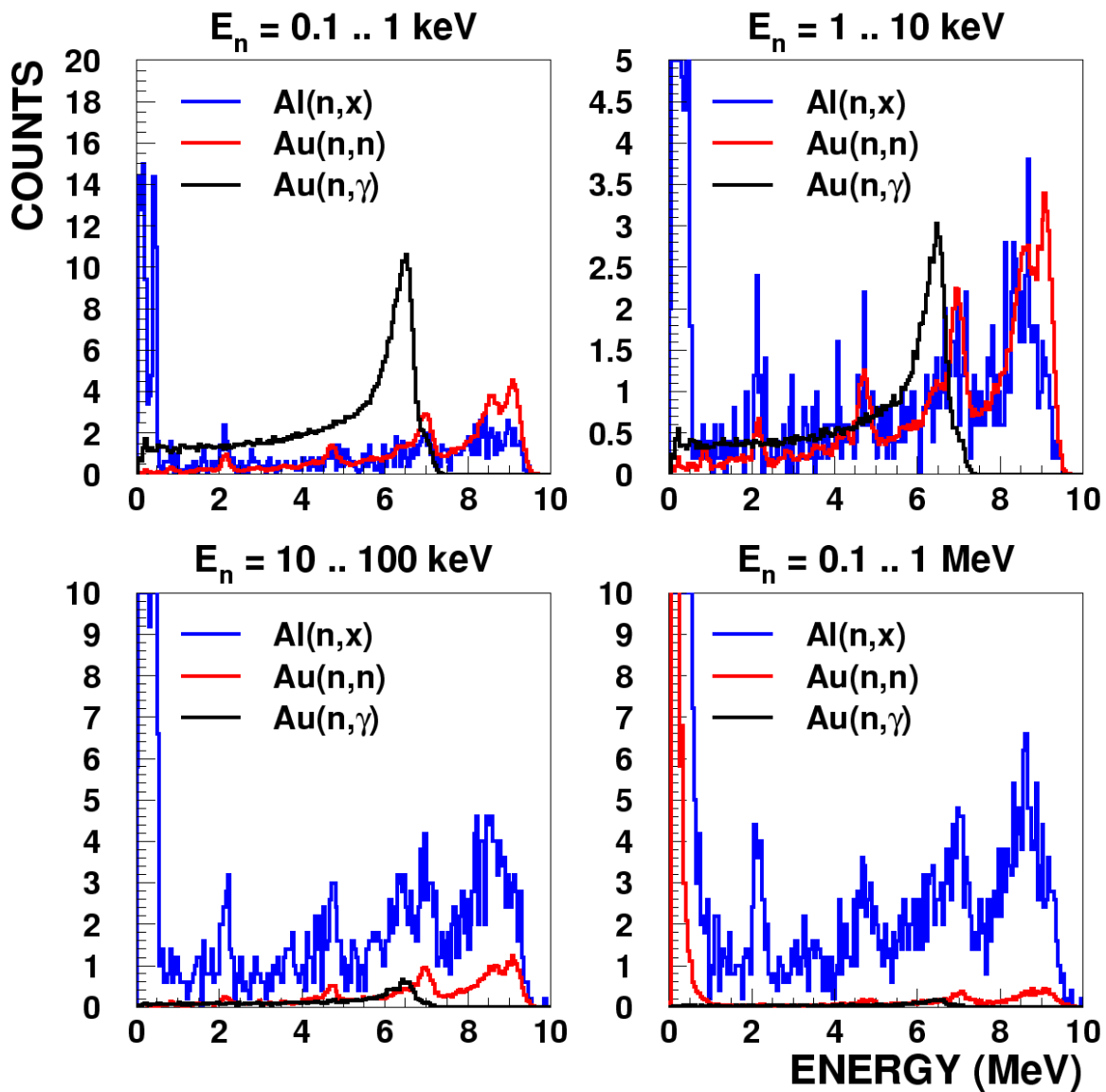


Figure 53: Comparison between a 3.18 mm (1/8 inch) aluminum window (blue) positioned 1 m upstream of the sample with neutron capture events (black) as well as neutron scatter events (red) on a 0.002 mm gold sample in the center of the crystal ball. The ball is asymmetrically positioned inside the shed.

3.18 mm Al, 0.8 m upstream; 2 μm Au sample; asymmetric

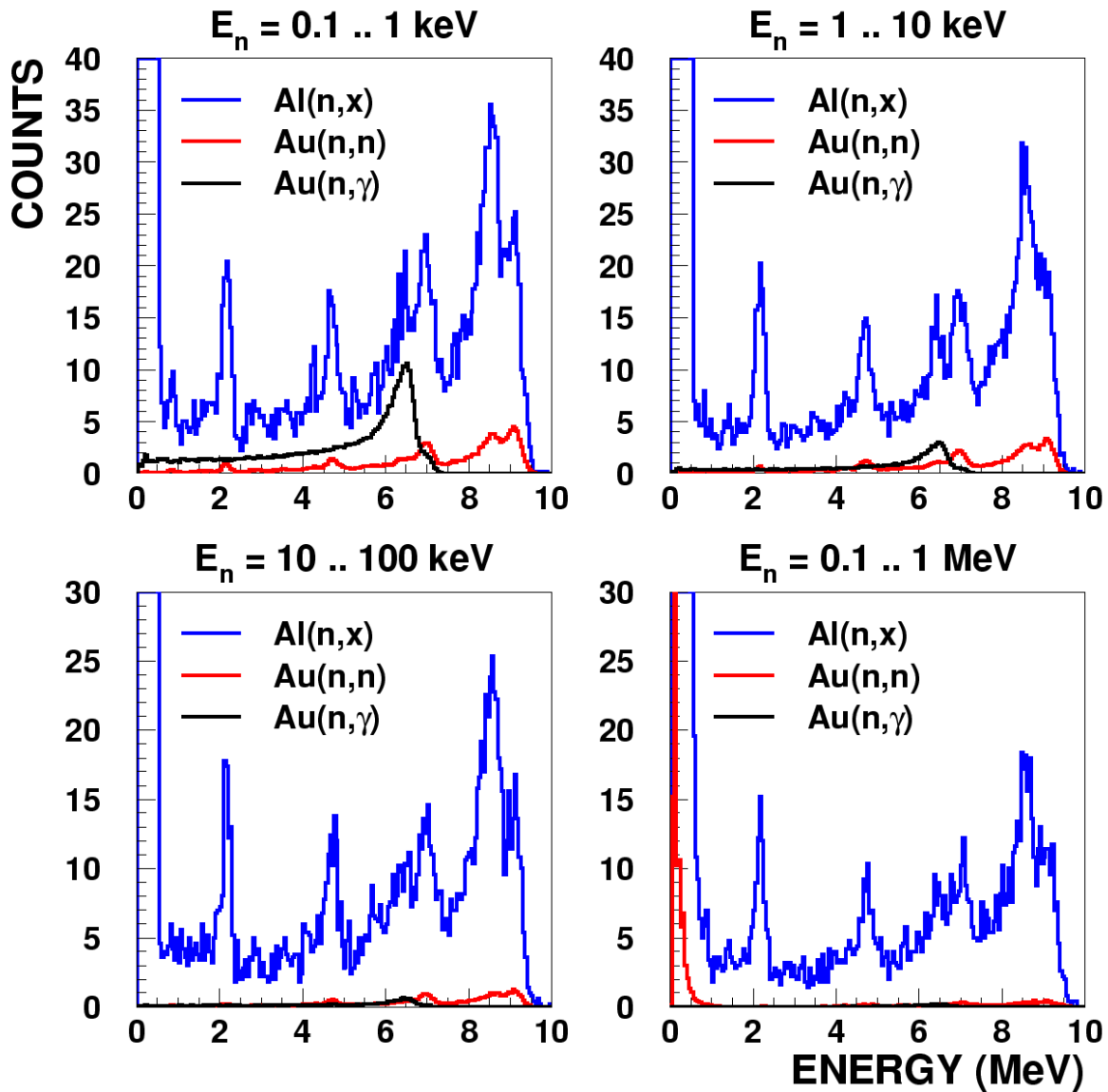


Figure 54: Comparison between a 3.18 mm (1/8 inch) aluminum window (blue) positioned 0.8 m upstream of the sample with neutron capture events (black) as well as neutron scatter events (red) on a 0.002 mm gold sample in the center of the crystal ball. The ball is asymmetrically positioned inside the shed.

3.18 mm Al, 0.7 m upstream; 2 μ m Au sample; asymmetric

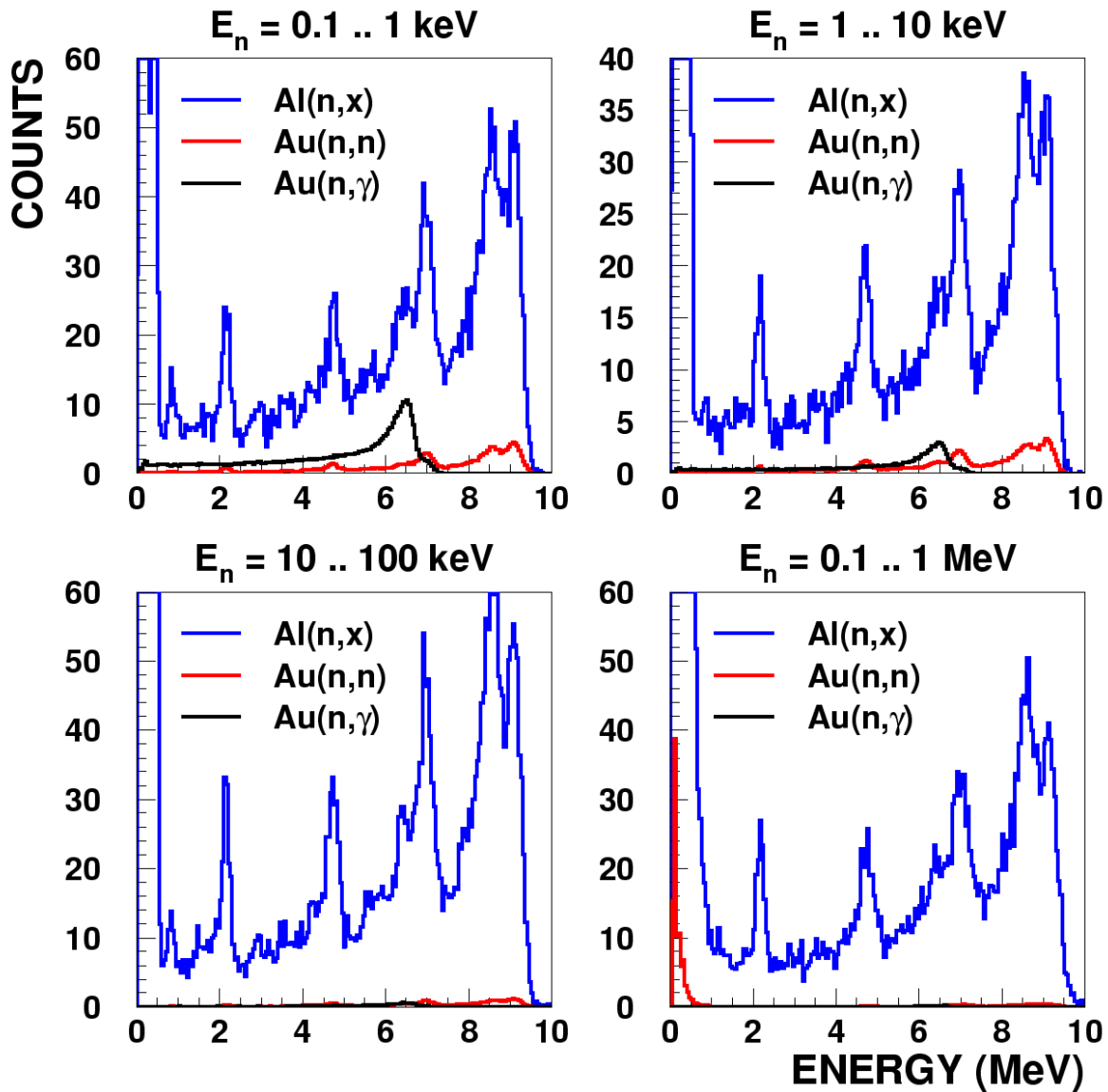


Figure 55: Comparison between a 3.18 mm (1/8 inch) aluminum window (blue) positioned 0.7 m upstream of the sample with neutron capture events (black) as well as neutron scatter events (red) on a 0.002 mm gold sample in the center of the crystal ball. The ball is asymmetrically positioned inside the shed.

0.25 mm Al, 1 m downstream; 2 μm Au sample; asymmetric

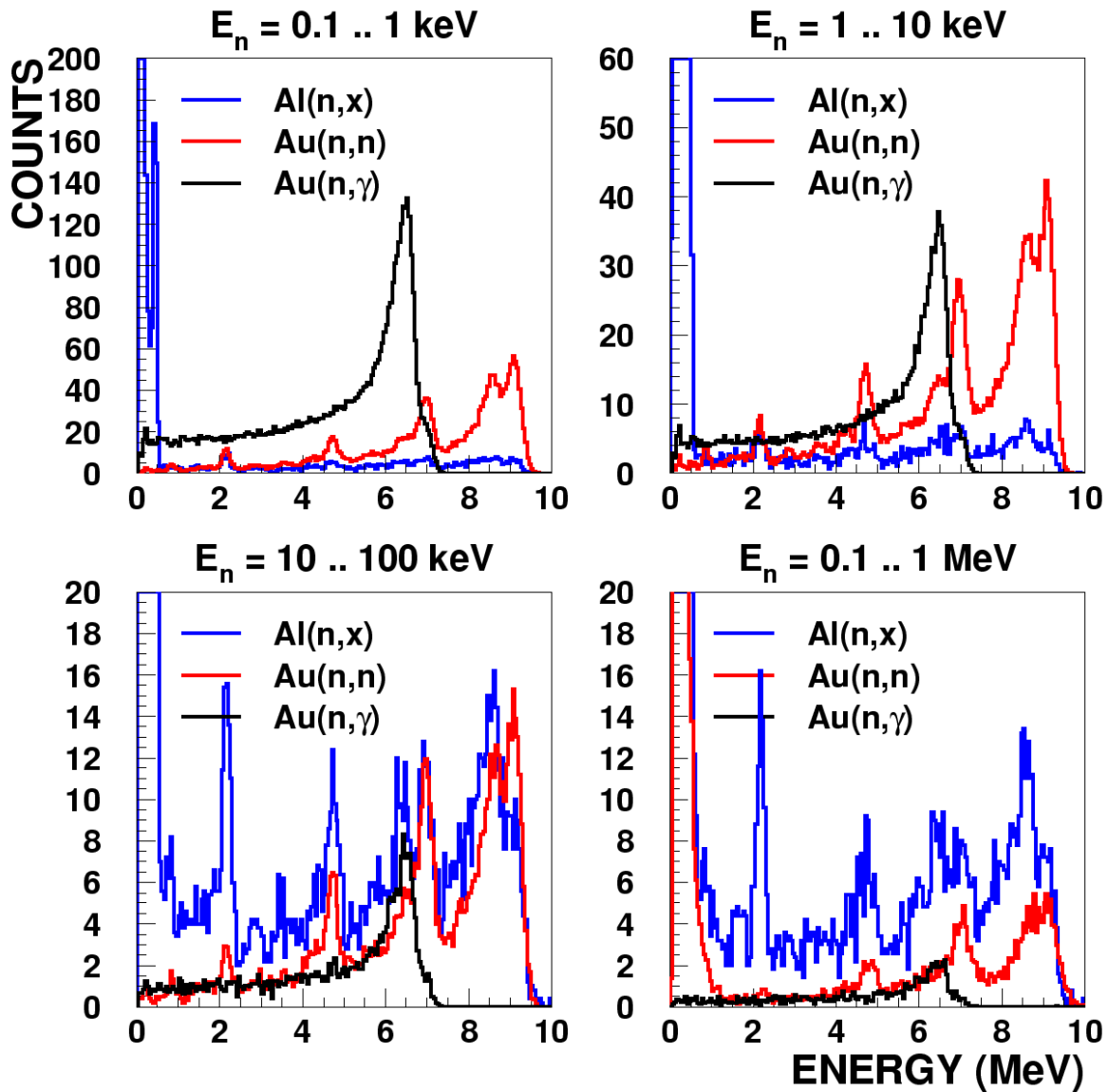


Figure 56: Comparison between a 0.25 mm (10 mil) aluminum window (blue) positioned 1 m downstream of the sample with neutron capture events (black) as well as neutron scatter events (red) on a 0.002 mm gold sample in the center of the crystal ball. The ball is asymmetrically positioned inside the shed.

The trends found for the symmetric case were found to be true for the asymmetric case too. No matter where the window actually is, the thicknesses used during the commissioning phase were sufficient to dominate the background above 10 keV neutron energy for a 2 μm (3.8 mg/cm^2) gold sample.

6 Conclusions

The set of simulations described in this report provides some intuition to understand the results gained during the commissioning phase 2002/2003. There are two major improvements, which have to be done before the next run cycle. At first the number of crystals has to be increased to the nominal number of 159. Secondly the single detector thresholds have to be decreased significantly. Even with these improvements done, there is still potential for further optimization. Especially the gaps between the crystals are a parameter, which could be changed realistically in the real detector.

The effect of the ${}^6\text{LiH}$ moderator shell has been studied in detail. It was found that there is a significant reduction of the peak efficiency with the moderator in place, while there is an overwhelming reduction of the background caused by scattered neutrons. For most of the isotopes planned to be investigated with DANCE the moderator would therefore improve the signal to background ratio.

The main source of the background during the commissioning phase above 2.5 MeV are probably neutrons scattered at the aluminum windows, while late γ -rays interacting with the sample could cause the background below 2.5 MeV. The most likely interaction mechanism of such gamma rays with a heavy metal sample is pair production. Each such process would produce at least two photons with 511 keV. If two such events happen at the same time, a peak around $4 \times 0.511 \text{ MeV} = 2.044 \text{ MeV}$ could be explained. A more comprehensive investigation of this possibility will be addressed in an upcoming report.

References

1. Lisowski P.W., et al., *Nucl. Sci. Engineering* **106** (1990) 208.
2. Heil M., et al., *LANL Report*, **LA-UR-99-4046** (1999).
3. Reifarth R., et al., *LANL Report*, **LA-UR-01-4185** (2001).
4. Heil M., et al., *Nucl. Instr. Meth. A* **459** (2001) 229.
5. Firestone R.B., Chu S.Y.F., *Table of Isotopes, CD-ROM Edition*. 8th ed, ed. J. Zipkin. 1996, New York: Wiley Interscience.
6. Uhl M., *private communication*. 1993.
7. Uhl M., Kopecky J., in *Nuclei in the Cosmos 1992*, K. Wisshak, Editor. 1993: Bristol. p. 259.